Mechanical and Electrical Properties of 3D Printed Wearable Structures

by

Jose Gonzalez-Garcia

Submitted in Partial Fulfillment of the Requirements

for the Degree of

Master of Science in Engineering

in the

Chemical Engineering

Program

YOUNGSTOWN STATE UNIVERSITY

December, 2023

Mechanical and Electrical Properties of 3D Printed Wearable Structures

Jose Gonzalez-Garcia

I hereby release this thesis to the public. I understand that this thesis will be made available from the OhioLINK ETD Center and the Maag Library Circulation Desk for public access. I also authorize the University or other individuals to make copies of this thesis as needed for scholarly research.

Signature:

Jose Gonzalez-Garcia Date

Approvals:

Dr. Pedro Cortes, Thesis Advisor Date

Dr. Frank X. Li, Committee Member Date

Dr. Eric MacDonald, Committee Member Date

Dr. Salvatore A. Sanders, Dean of Graduate Studies Date

Abstract

The transformational impact of incorporating new 3D-printing technologies and manufacturing methods, particularly in the field of printed electronics, can be observed in various areas such as flexible electronics, wearable sensors, wireless communications, and solid-state display technologies. Particularly, the utilization of soft and flexible electronic devices for extended periods in health monitoring has the potential to significantly revolutionize customized healthcare. However, despite the potential benefits that wearable electronics have demonstrated, their application in long-term health monitoring has proven to be hard due to the requirement for consistent operation under diverse conditions of mechanics, temperature, and hydration. Specifically, investigation about their mechanical and electrical properties under prolonged fatigue conditions needs to be assessed in order to allow them to be useful in applications such as wearable sensors and flexible electronics. Therefore, the objective of this research is to evaluate the structural and electrical characteristics of a 3D printed flexible electronic platform capable of withstand bending fatigue over long periods of time. Currently, there is a noticeable change occurring in the field of flexible and wearable electronics, primarily attributed to the utilization of developing materials and advancements in structure design, specially 3D printing being such technology that holds immense potential in revolutionizing the production of these. Lastly, this work will provide comprehension of flexible structures that could be employed as a potential substrate for a nitrogen dioxide (NO_2) gas sensor.

Acknowledgments

I would like to thank for all the support and strength that **my father** gave me through all my master's degree. Without his advice, I would not have accomplished any goal.

To my **my mother** that she has always been there with me through any difficulty, for her constant encouragement for completing my goals the best way possible.

To my thesis advisor, **Dr. Pedro Cortes** for giving me the incredible opportunity to work with him in different scientific projects. For his constant advice that helped me solving diverse difficulties.

To my committee members, **Dr. Frank X. Li** and **Dr. Eric MacDonald** for providing me with their invaluable feedback regarding my research.

To my great **friends** that supported me through all this journey and making the laboratory my second home. Moreover, I would like to thank to **Dr. Byung-Wook Park** for his insightful suggestions about my research.

Table of Contents

List of Figures

List of Tables

Nomenclature

PCBs Printed Circuit Boards

ICs Integrated Circuits

AM Additive Manufacturing

STL Stereolithography

DIW Direct Ink Writing

NO_2 Nitrogen Dioxide

PE Printed Electronics

LEDs Light Emitting Devices

R2R Roll-to-Roll

DOD Drop-On-Demand Inkjet Printing

CIJ Continuous Inkjet Printing

AJP Aerosol Jet Printing

e-3DP Embedded-3D Printing

NPs Nanoparticles

PI Polyimide

PET Polyethylene Terephthalate

PEN Polyethylene Naphthalate

TPU Thermoplastic Polyurethane

FPI Fibrous Polyimide

PDMS Polydimethylsiloxane

CAD Computer-aided Design

ME Material Extrusion

BI Binder Jetting

MJ Material Jetting

DED Directed Energy Deposition

PBF Powder Bed Fusion

VP Vat Photopolymerization

SL Sheet Lamination

FDM Fused Deposition Modeling

DLP Digital Light Processing

LOM Lamination

SLS Selective Laser Sintering

SLM Selective Laser Melting

SLA Stereolithography

UV Ultraviolet Light

PEM Precise Extrusion Manufacturing

PED Precise Extrusion Deposition

MJS Multi-Phase Jet Solidification

PAM Pressure-Assisted Microsyringe

LDM Low-Temperature Deposition Manufacturing

FETs Field-Effect Transistors

HNO_3 Nitric Acid

Introduction

1.1 Flexible Electronics

Electronic devices are compact modular components that could be connected to each other in order to regulate the flow of electrical current during the processing of information. Nowadays, the traditional approach to modeling and designing electronics is subtractive in nature, with the normal procedure being the selective removal of materials patterned from a master template. This involves electronic designs for printed circuit boards (PCBs), integrated circuits (ICs), and chips that have been preprogrammed [1]. These electronics devices, however, are made up of large, inflexible components such as hard-silicon based chips, integrated circuits, capacitors, and resistors that prevent them from maintaining electrical continuity in both their initial condition and when deformed. In this sense, flexible electronics devices are capable of withstand electrical continuity while experiencing sophisticated mechanical deformation such as bending, twisting and stretching [2]. In Figure 1.1 is showed an example of a flexible electronic switch.

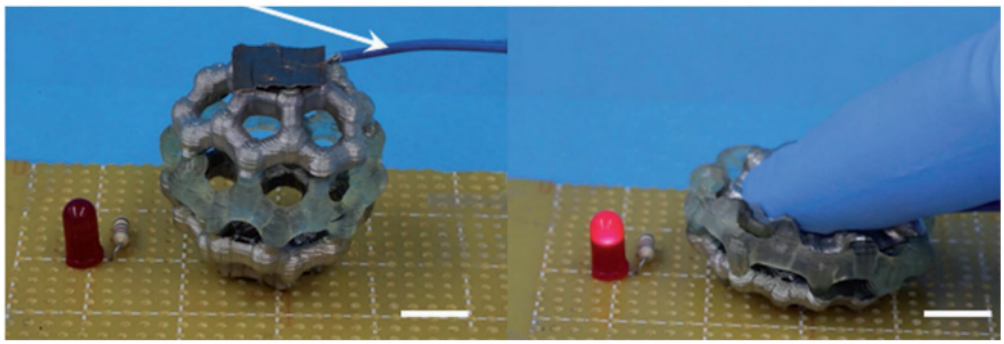

Figure 1.1. A 3D printed ball coated with silver nanoparticles in order to fabricate a 3D printed flexible switch [2].

Flexible electronics have a variety of uses, particularly for long-term health monitoring, application in which these devices are also called wearable electronics due to their facile interaction with humans, for example, for uses like portable screens, human activity monitoring sensors, and self-powered devices, they can be installed directly onto human skin or even connected to clothing, [3]. Specially, wearable electronics have a significant potential to transform personalized healthcare when they are sufficiently soft and flexible.

Even though wearable electronics have showed considerable promise in these types of applications, developing them has been difficult due to the necessity for consistent performance across a broad range of mechanical, environmental, and physiological conditions. Therefore, compatibility with all of these factors is the ultimate objective for soft and wearable electronics for long-term health monitoring even though, in practice, environmental changes can cause a device's structural and functional deterioration, [4], [5]. Figure 1.2 shows some different applications for flexible electronics devices as biosensors for the collection of typical physiological data.

Figure 1.2. Measurement of typical physiological data using flexible electronic devices as biosensors [5].

1.2 Additive Manufacturing

Additive manufacturing, often known as 3D printing, has received an unprecedented level of interest and consideration from the academic and business sectors since it was first developed in the 1980s. In this instance, 3D printing is a technique for creating three-dimensional things based on the digitally controlled deposition of successive layers of material until a final structure is produced, [6]. 3D printing is the opposite of subtractive manufacturing, which creates three-dimensional items using material-removal procedures like drilling, milling, sawing, broaching, etc. One important aspect is that rapid prototyping is nearly unlimited thanks to 3D printing.

Nevertheless, both subtractive and additive manufacturing processes are appropriate for rapid prototyping. The decision will be based on the complexity of the products to be produced, the material used, the required number of copies, and, of course, the cost. The main distinction between the two approaches may be seen in the object's geometric complexity, [6]. Figure 1.3 shows these two different manufacturing processes.

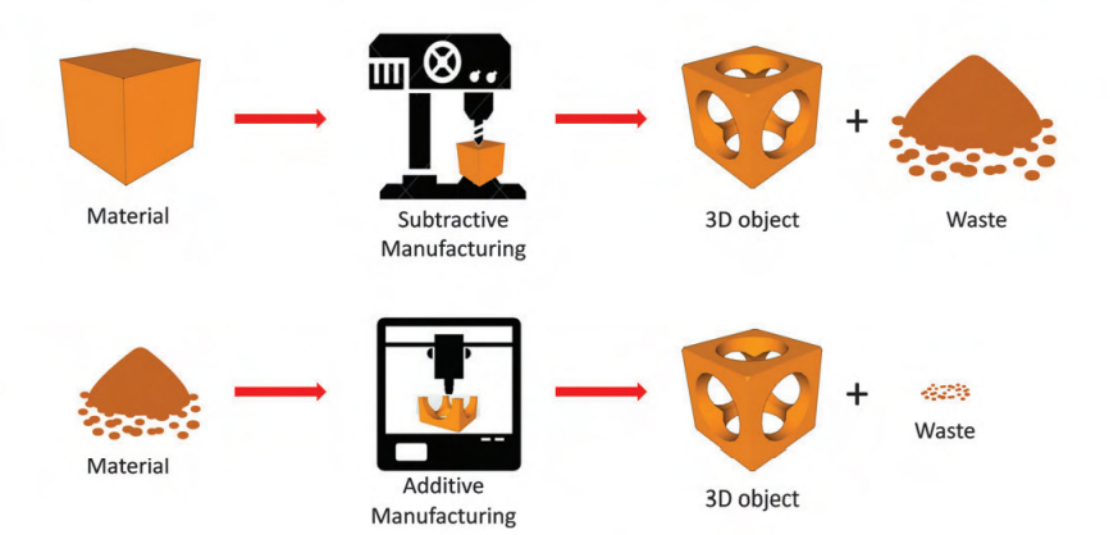

Figure 1.3. Both manufacturing processes, additive and subtractive, produce the same 3D object. However, it can be seen that the waste produced in the subtractive process is much more than the one produced in the additive process, leading to a less efficient use of resources in this technique [6].

In this regard, the utilization of 3D printing extends beyond the production of mechanical parts, including the fabrication of electronic components and sensors as well. Indeed, various types of sensors have been manufactured based on their specific areas of application. The development of sensors has been subject to meticulous attention over the years due to their significant impact on both quantity and quality where various manufacturing procedures are employed for their creation. However, among the various contemporary manufacturing techniques employed globally, additive manufacturing (AM) has demonstrated its capabilities and exhibits significant potential for revolutionizing the manufacture of sensors.

1.3 Wearable Sensors

Nowadays, the need for personal healthcare systems that can identify users' bio-signals at any given location and time has been rising as the population becomes older. The creation of these systems makes it easier to provide medical care for the elderly, monitor chronic diseases in real-time, regulate the activities of elite athletes, and generally promote public health. Nevertheless, due to the complicated integration of stiff and huge components such as bulk power supplies and rigid circuit boards to sensors, these personal healthcare systems are typically bulky, rigid, and incompatible with skin, [7].

Moreover, research has been conducted on the creation of more skin-attachable, miniaturized, and customizable health monitoring devices. Properties like great flexibility, lightness, and ultra-thinness for unnoticeable usage in medical devices can be generated by manipulating the morphologies of organic, inorganic, and hybrid materials on either the nano or micro-scale, [7]. One important aspect is that wearable sensors can be firmly mounted to the skin in a conformal way to monitor the thermal, electrical, mechanical, or chemical changes of specific targets, [8]. However, the ability to integrate the appropriate sensing functionality with a reasonable level of body integration is one of the major issues for wearable sensors. Therefore, it is frequently necessary for flexible devices to make smooth contact with the body in order to prevent slippage and guarantee operation, [9].

Specifically, for the development of wearable chemical sensors, the objective is to create non-invasive sensors for precise and accurate biomarker analysis in human bodily fluids, avoiding the discomfort and risks associated with invasive diagnostic procedures like blood draws and finger sticks, [10]. Figure 1.4 shows several non-invasive wearable chemical sensor systems.

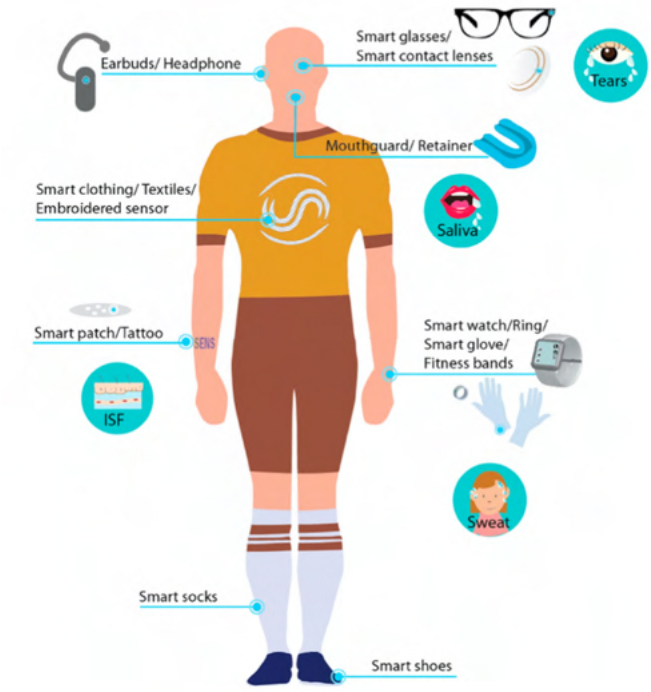

Figure 1.4. An overview of several wearable chemical sensor technologies that are non-invasive [10].

With this being said, wearable sensors, emerging as advanced diagnostic tools, have the potential to significantly advance the healthcare system through the integration of novel technology. The widespread use of these technologies depends on the utilization of novel manufacturing methods that possess crucial attributes such stretchability, enhanced flexibility, ultra-thinness, lightweightness, and rapid responsiveness, hence facilitating the development of more effective wearable platforms. Particularly, for the development of wearable sensors, the utilization of 3D printing technologies has emerged as a significant contributor. Specifically, these technologies facilitate the fabrication of innovative flexible 3D structures by utilizing the capabilities of printable soft materials. This advancement holds promise for the advancement of next-generation wearable sensors.

1.4 Motivation for Thesis

Nowadays, due to advantages in fast production and adaptability in terms of material support and system process, printed electronics presently occupies an important part of the electronics manufacturing industry. Due to the relationship that the printed electronics have with the additive manufacturing technology, new 3D printing technologies and production techniques, especially for printed electronics, have the potential to revolutionize flexible electronics, wearable sensors, wireless communications, effective batteries, solid-state display technologies, and other fields.

It is important to mention that aspects like the establishment of the substrate, the printing of conductive tracks, the process of pick-and-place or embedding of electronic components, and the interconnection of these components are essential fabrication protocols that should be incorporated into these novel 3D-printing technologies to achieve a more integrated fabrication approach. Therefore, in the present work, a new alternative has been explored for the development of a 3D printed flexible electronic platform capable of withstand mechanical fatigue. This new alternative combines two different additive manufacturing technologies such as stereolithography (STL) and direct ink writing (DIW) capable of fabricating a flexible platform with embedded electronics. This 3D printed flexible platform will be able to show the proof of concept of 3D printed electronics highly capable of withstand bending movements while the electrical properties remained constant under this fatigue.

1.5 Objectives

Wearable sensors emerging from 3D printing technologies are becoming the next generation of integrate platforms for different applications in the health field such as sweat sensing and tactile sensing among others. However, more studies about their mechanical and electrical properties need to be addressed in order to evaluate their response under fatigue conditions over long periods of time. This with the purpose of evaluate their integrity. Indeed, modifications in their manufacturing process including different conductive pastes and different polymeric substrates will affect their performance. Therefore, the aim of this study is to evaluate the structural and electrical properties of 3D printed wearable platform where the paste conductivity, as well as the paste-substrate interaction are evaluated. This study will provide the fundamental understanding of flexible printed structures to act as supporting platform for a nitrogen dioxide (NO_2) gas sensor being investigated.

The specific goals for the present work are:

- Evaluate the electrical resistance of a 3D printed conductive silver line onto a flexible platform under bending fatigue for an embedded and not embedded system.
- Analyze the voltage behavior for an embedded 3D printed electronic circuit onto a flexible platform.
- Characterize the effects of the bending movement for the embedded and not embedded system.
- Conduct an adhesion test for the evaluation of the interaction between the 3D printed conductive silver line with the flexible substrate used as a platform.
- Perform experiments in order to evaluate the sensibility of an embedded gas sensor capable of detecting nitrogen dioxide (NO_2) under different polluted environments.

1.6 Organization

This thesis will be presented in the following order:

1. Chapter 1. This chapter will briefly review what flexible electronics are, their applications as well as their current barriers that they present in order to be used under a broad range of mechanical as well as environmental conditions. Moreover, the additive manufacturing technology, also called 3D printing, is briefly discussed in order to give the reader an insight of this technology and its relationship for the development of flexible and wearable electronics which are involved in the manufacturing process of wearable sensors.
2. Chapter 2. This chapter will present a literature review of the background of what flexible electronics are, their relationship with additive manufacturing, the different type of processes that exist in order to develop flexible electronics, their applications in wearable sensors as well as their current disadvantages.
3. Chapter 3. A discussion of the experimental methodology followed in the present work.
4. Chapter 4. The chapter discusses the results which were obtained in the present work.
5. Chapter 5. Conclusions of the present thesis are presented in this chapter.

Literature Review

2.1 Printed Electronics

Printed electronics (PE) is a broad term that refers to the printing technique employed in the fabrication of electrical devices through the process of printing on various substrate materials. In a general sense, the term generally describes the methodologies employed for the production of electrical circuits, components, and devices using traditional printing techniques [11]. Printed electronics offer several significant benefits, including cost-effective production at a high rate, compatibility with flexible systems such as large-area electronics, and the ability to fabricate hybrid systems on flexible or stretchable substrates using inorganic, organic, and bioinspired materials. Additionally, the integration of printed electronics with flexible substrates is relatively simple [12]. Due to the increasing demand for wearable devices and the need for thinner electronics, printed electronics have emerged as a viable solution for fabricating a diverse range of electronic structures. These structures include keyboards, electronic skin patches, sensors, actuators, antennas, biochips, microfluidics, flexible electronics, electronic components, embedded circuits, and various other applications [11].

2.1.1 Drawbacks of the Conventional Manufacturing Methods of Electronics

One notable distinction between printed electronics and traditional electronics production lies in their respective fabrication methods. Printed electronics utilize an additive approach, where materials are deposited to build the electronic circuitry. In contrast, traditional electronics manufacturing, which utilizes lithography, employs subtractive procedures to create the circuitry by removing excess material [13]. Indeed, the usual approach for modeling and designing electronics follows a subtractive methodology, where the selective elimination of materials, based on a master template, is a commonly employed procedure. Examples of this type of methodology are applied in preprogrammed electronics designs such as printed circuit boards (PCBs) and integrated circuits (ICs). However, this substrative method suffers a considerable cost due to the necessary equipment and substantial material waste, including the disposal requirements for wasted water resulting from washing and cleaning. The technique is considered to be ecologically unfriendly due to its dependence on many chemical-processing phases. Furthermore, designing and patterning each layer in its entirety is a process that is both time-consuming and iterative [1]. In this regard, lithography and etching are two techniques that both use specific chemicals for the removal of conducting materials that are not needed.

Nonetheless, another important technology has become more popular in the field of electronics fabrication recently, being this one known as additive manufacturing (AM) or also called 3D printing. One of the important aspects of this technology is that it holds significant promise in revolutionizing the electronics fabrication sector, leading to a more dynamic and intelligent approach for their manufacturing. These both manufacturing technologies are shown in Figure 2.1 while Figure 2.2 shows in a more detailed view both manufacturing approaches [14, 15, 16].

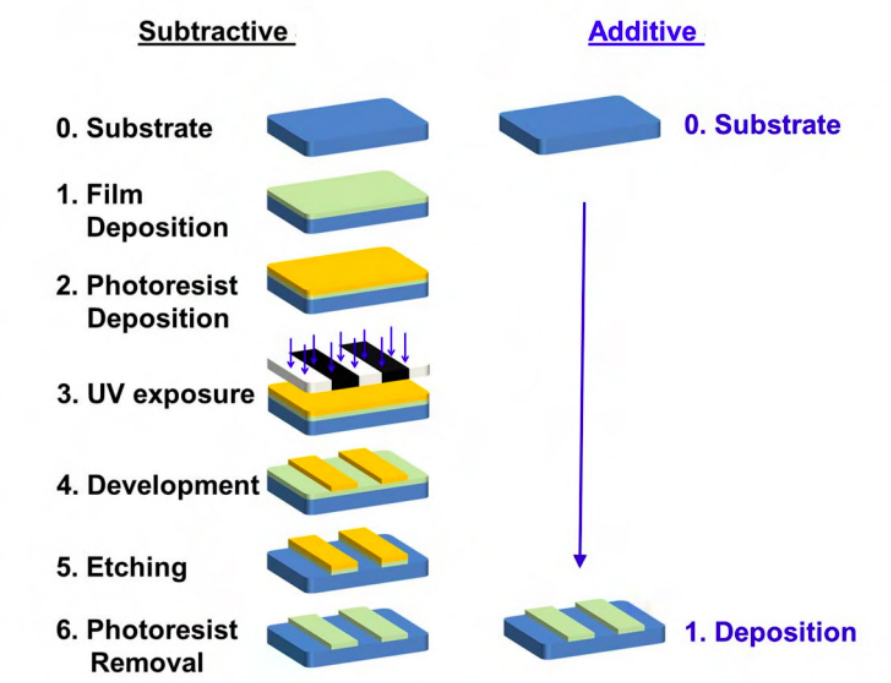

Figure 2.1. Overall distinction between subtractive and additive manufacturing technologies [14-16].

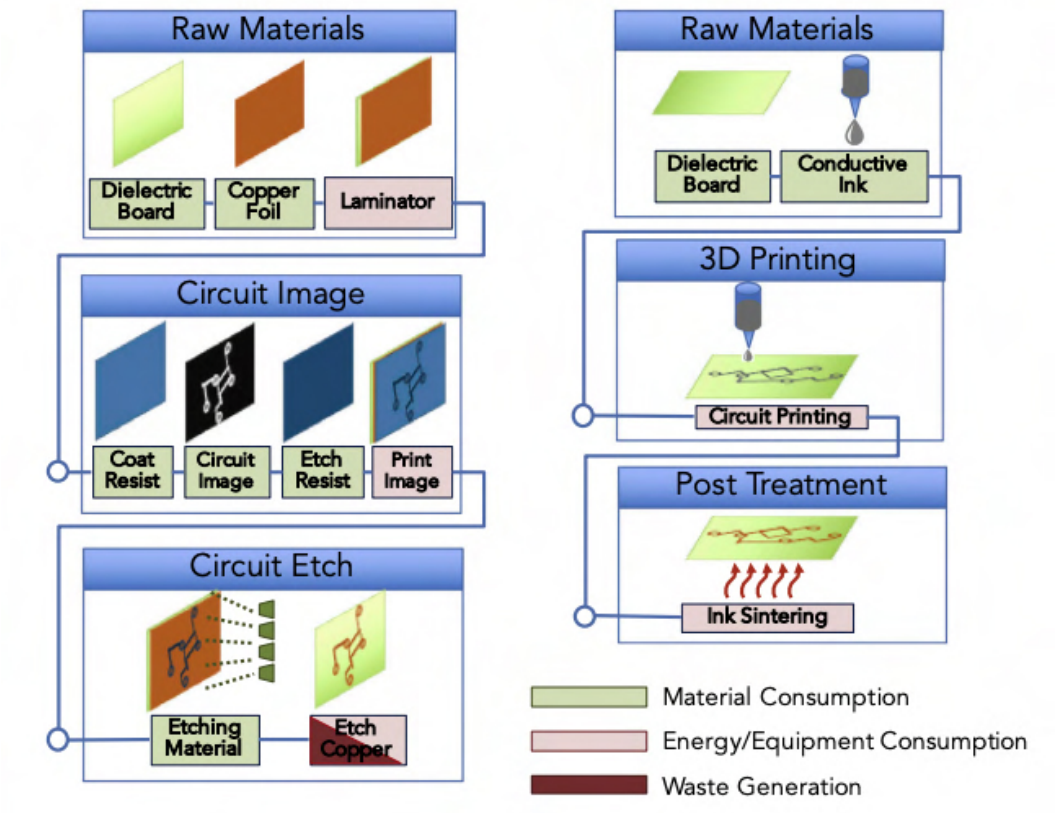

Figure 2.2. Detailed view of both manufacturing process, being the subtractive one on the left side and additive one on the right side [14-16].

Considering the information mentioned above, the field of additively manufactured printed electronics, which combines electronics manufacturing with graphic fabrication, is rapidly gaining recognition as a viable substitute for conventional electronics. This approach offers the advantage of avoiding traditional subtractive fabrication techniques, thus removing the requirement for costly specialized equipment and complicated manufacturing procedures. Printed electrical components frequently consist on just base substrates and functional ink coatings which are applied onto the substrates and then experience a sintering process. The significant advantage of reducing the number of process steps is evident when comparing this approach to subtractive fabrication processes that include many stages [14]. However, despite all these advantages that the additive manufacturing could represent to the electronics fabrication sector, many electronic manufacturing companies continue to rely on PCB designs as a result of the difficulties associated with incorporating emerging 3D-printing technology into both machinery and materials [17].

Focusing in the advantages that the additive manufacturing fabrication presents, additively manufactured printed electronics are produced using a diverse range of printing processes which can generally be classified into two main categories: non-contact printing, often known as nozzle-based patterning, and contact printing. The contact printing technique involves the physical contact between patterned components that have inked surfaces and the substrate. In a non-contact procedure, the solution is distributed via apertures or nozzles, while the formation of structures is achieved by manipulating the stage (substrate holder) in a predetermined pattern [18]. In this case, the non-contact techniques involve aerosol jet printing, inkjet printing and slot die coating, whereas gravure printing, screen printing and flexographic printing serve as illustrations of the contact techniques [12]. The authors Khan et. al. [18] schematically showed the conventional methodologies employed in the fabrication of printed electronics and sensors in Figure 2.3.

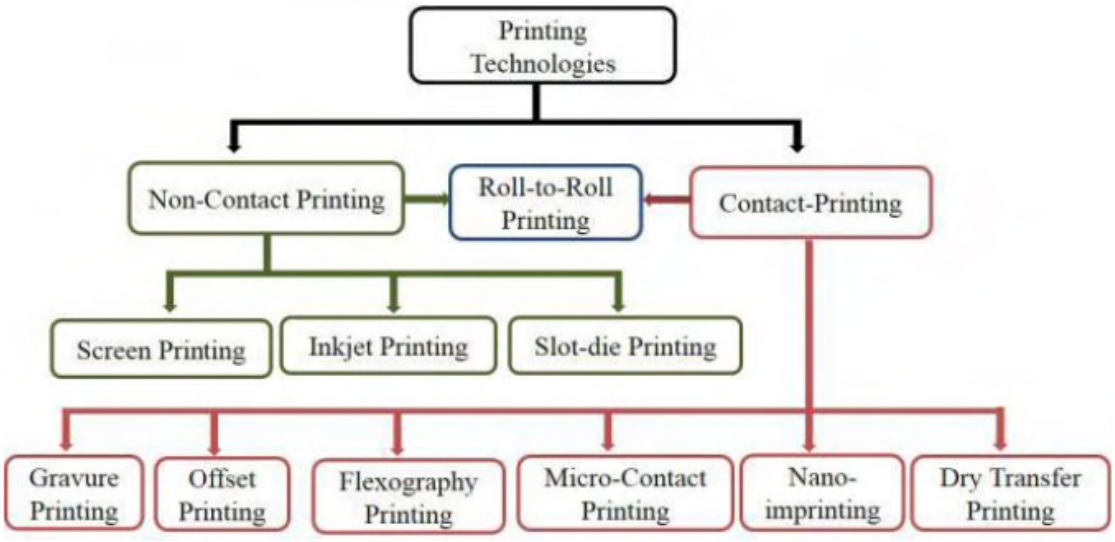

Figure 2.3. The categorization of popular printing technologies for electronics and sensors [18].

Each of these methods presents specific advantages and disadvantages, however, they all depend on the fundamental concept of transferring inks onto a substrate. As an example, various printing techniques, including screen printing, flexographic printing, gravure printing, and inkjet printing, have been effectively utilized in the production of diverse electronic components.

These structures include sensors [19], light emitting devices (LEDs) [20], displays [21], and solar cells [22]. Moreover, the utilization of printed electronics technology has proven to be effective in the production of printed circuit boards (PCBs) using a diverse range of flexible dielectric materials, such as various types of paper, plastic, and textiles, through standard manufacturing processes [11]. In particular, the utilization of polymer substrates in printed electronics has provided novel opportunities for cost-effective production of electronics on bigger surfaces compared to commercially available conventional wafers. In this sense, one important application of printed electronics onto flexible substrates is the development of conformable and responsive electronic systems, such as electronic skin, which has the capability to be wrapped around the body [23]. Figure 2.4 shows, for instance, an application for electronic skin.

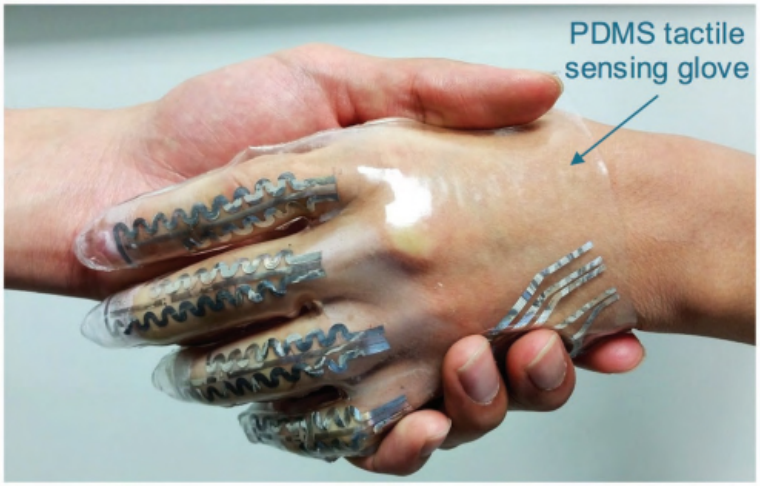

Figure 2.4. A photograph demonstrating a hand-shaking gesture while utilizing a PDMS tactile sensing glove [23].

It is also important to mention that additive manufacturing (AM) is an emerging technological advancement that facilitates the design and production of electronic products. This technology offers several significant advantages in the field of electronics manufacturing, including enhanced design flexibility, reduced costs for customization, shorter production timelines, adaptable digital manufacturing capabilities, decreased waste generation, reduced initial investment requirements, and the potential for decentralized manufacturing [11].

Nevertheless, the selection of the best fabrication process for printed electronics is determined by the characteristics of the electronic components involved, taking into account factors such as weight, size, flexibility, volume, disposability and production cost. The printed electronic device is influenced by several notable characteristics, including the simplicity of processing, the performance of the finished product, and the long-term consistency of the organic and inorganic components utilized in the form of inks, pastes or coatings [11].

2.1.2 Contact Printing Methods for Printed Electronics

2.1.2.1 Screen Printing

Screen printing is a widely employed technique for mass printing, where ink is forced through a stencil with a squeegee to create a desired pattern. The squeegee is employed to exert pressure against the screen, so facilitating the passage of ink through it. The screen printer consists of a basic setup that includes a screen frame, screen mesh, base plate, squeegee, substrate, and spacer, as shown in Figure 2.5.

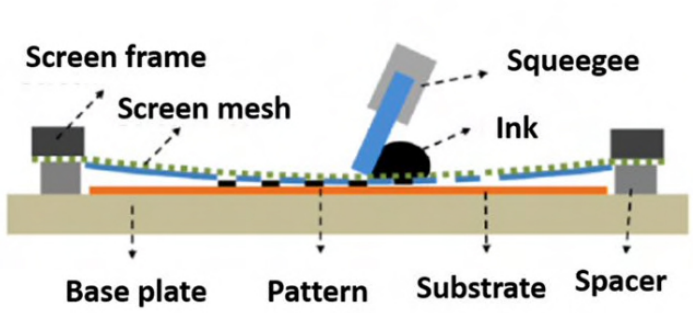

Figure 2.5. The present diagram illustrates a cross-sectional perspective of the screen-printing process [11].

One notable characteristic that differentiate screen printing apart from other printing techniques is the considerable aspect ratio exhibited by the produced patterns. The wet layer thicknesses commonly lie within the range of 10–500 μm, making them advantageous for applications in printed electronics that require high conductivity.

Nowadays, two distinct types of screen printers, namely flatbed and rotary, are utilized for roll-to-roll (R2R) manufacturing, as illustrated in Figure 2.6. Particularly, in the flatbed technique, the ink is applied onto the screen and then manipulated using a squeegee to go through the screen, so facilitating its passage through the stencil apertures onto the underlying substrate. Even though this technique might be the most common one for screen printing, the rotary printing technique has the potential to serve as a viable alternative to this last technique for continuous processing applications. This technique involves folding the web of the screen while keeping the squeegee and ink within the tube as it can be seen in Figure 2.6.

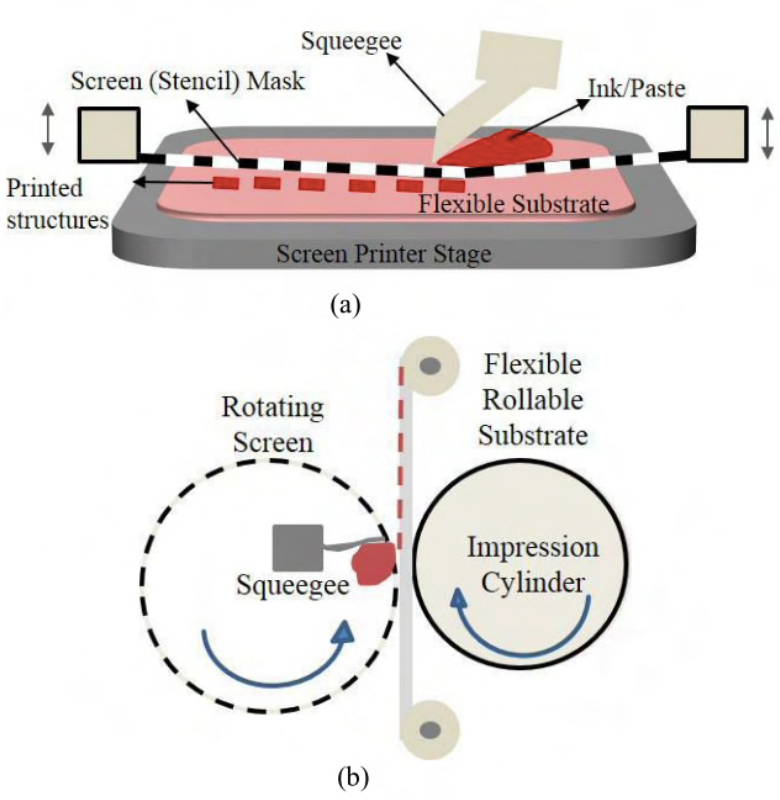

Figure 2.6. Part a) The process of flatbed screen printing involves the use of planar surfaces, where a screen and squeegee are employed for the dispensing of a solution. Part b) The rotary screen printer employs a dynamic substrate (web) that moves between a cylindrical mask and an impression cylinder [18].

Moreover, the viability of screen-printing as a technique for fabricating flexible electronics has been supported by many examples of successfully printed sensors, electrical devices, and circuits. For instance, according to the findings of Cao et. al. [24], the utilization of screen printing as a technology for the production of separated single-wall carbon nanotubes in both rigid and flexible thin-film transistors is considered viable due to its simplicity, scalability, and cost-effectiveness. Hong et. al. [25] describe the fabrication of textile-based conductive circuits that are both flexible and washable. This was achieved using a screen-printing process and a newly created UV-curing conductive ink that possesses characteristics of low temperature and fast cure. Nevertheless, the print quality and advantages of screen printing are influenced by several aspects, including solution viscosity, printing speed, squeegee angle and geometry, snap off between the screen and substrate, mesh size, and material [18], [26].

2.1.2.2 Gravure Printing

The process of gravure printing involves the direct transfer of functional inks to the substrate through physical contact with engraved structures. The technique shows the ability to generate patterns of superior quality in a cost-efficient manner, as is characteristic of a roll-to-roll (R2R) process. The printing roller, commonly referred to as a cylinder, is covered with engraved cells that are arranged in a certain pattern on its surface. The printing roller undergoes a motion in opposition to the doctor blade, resulting in the removal of excessive ink from the printing roller's surface. The process of ink transfer onto a rollable substrate occurs by capillary action when the substrate is positioned between the engraved and impression cylinders. Moreover, the characteristics that determine the quality of printed results on flexible substrates include ink receptivity, viscosity, drying, smoothness, wettability, doctor blade angle and pressure, printing speed and uniformity of the gravure cylinder diameter [18].

Figure 2.1.2.2 illustrates the configuration of a gravure printing system.

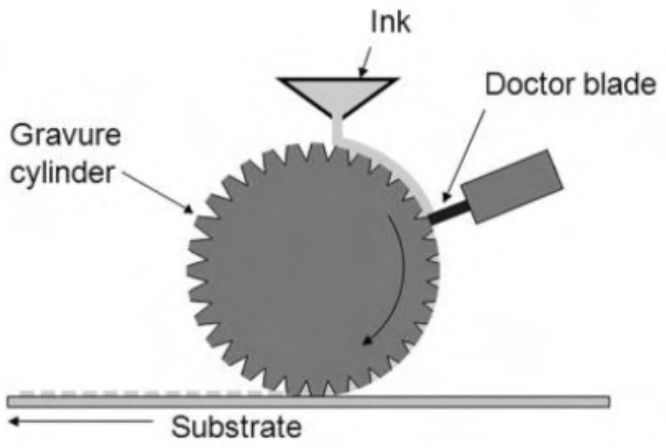

Figure 2.7. Configuration of a gravure printing system [18] .

Moreover, Figure 2.8 shows the alternative form of gravure printing known as inverse direct gravure printing. Instead of employing a printing roller for pattern transfer, the inverse direct gravure printing technique utilizes a flat plate to transfer patterns onto the substrate located on the impression roll [12].

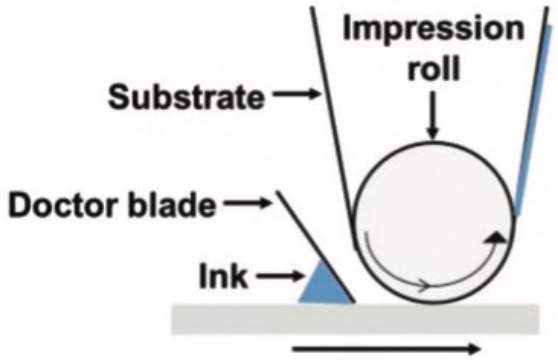

Figure 2.8. Configuration of the inverse gravure printing technique [12].

2.1.2.3 Flexographic Printing

Flexographic printing is commonly employed for the production of printed electronics in large quantities and at high speeds. It is considered to be more attractive compared to gravure and offset printing methods, particularly when it comes to achieving high-resolution patterns [27], [18]. In this technique, printing occurs when the inked sections of the higher surfaces make contact with the substrate in motion, after the transfer of ink from the reservoir by the anilox cylinder. This printing technique is illustrated in Figure 2.9.

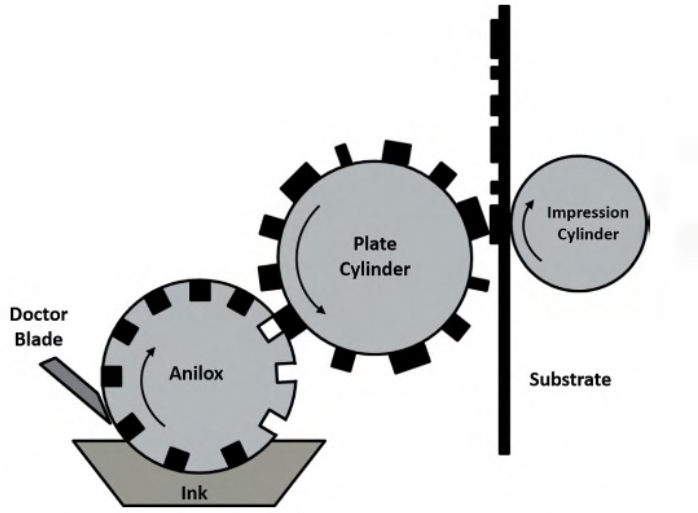

Figure 2.9. Illustration of flexographic printing [11].

One important aspect of this technique is that the printed results using this technique present consistent and thin layers, which leads to improved reliability of patterns and more precise distinction of edges compared to gravure printing. However, the deposition of a thick film requires multiple printing cycles with similar parameter settings which is one the challenges of this technique that comes from the need to repeat a similar procedure for printing subsequent layers while ensuring the correct placement of the flexographic equipment during each pass.

2.1.3 Non-Contact Printing Methods for Printed Electronics

2.1.3.1 Inkjet Printing

Inkjet printing is a form of additive manufacturing that involves the deposition of liquid materials or solid suspensions at low temperatures and pressures. The deposition of these materials, which are in the form of colloidal or chemical solutions, occurs via a micrometer-sized inkjet nozzle head. For this technique, several systems have been created for the actuation of inkjet nozzle heads. Among these options, the thermal, piezoelectric, and electrohydrodynamic inkjet systems are the most notable approaches. Droplets, commonly referred to as drop-on-demand (DOD), are released in response to a pulse created by thermal or piezoelectric actuators employed in the inkjet nozzle head [18]. This technique has several notable benefits, such as the precise and efficient application of diverse functional materials across a wide surface area, all at a very reasonable expense. Additionally, it allows for the deposition of small amounts of materials and facilitates the simple incorporation of several materials onto a single substrate. Furthermore, due to its non-contact and maskless nature, the potential for substrate contamination is significantly reduced [12]. Figure 2.10 shows a schematic illustration of inkjet printing [28] .

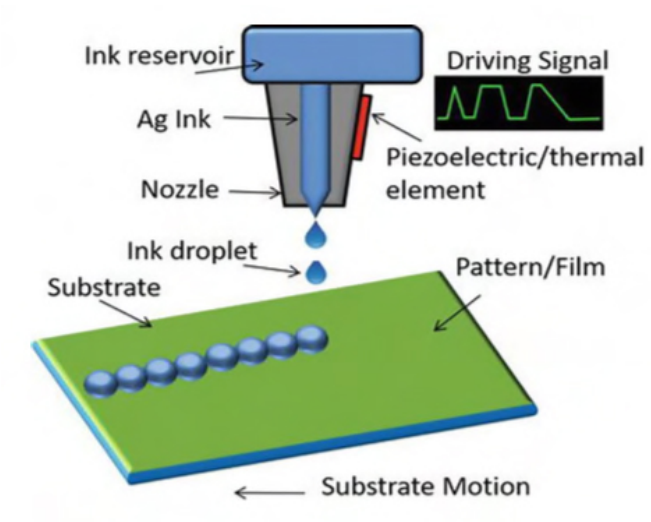

Figure 2.10. Illustration of the inkjet printing process [28].

Currently, two primary methods are employed for the generation of these droplets in this technique which are called continuous inkjet printing (CIJ) and drop-on-demand inkjet (DOD) printing [29]. In the context of continuous inkjet (CIJ) printing, an uninterrupted flow of pre-formed ink droplets travels between charging plates, enabling them to acquire an electrical charge. Subsequently, these charged droplets are guided towards the substrate through the manipulation of an electric field. Within the context of drop-on-demand (DOD) printing, the production of ink droplets occurs only in instances when their usage is considered necessary. This approach provides a more efficient utilization of energy, however, the probability of nozzle blockage increases as a result of solvent evaporation during periods of print head inactivity. These two methods are showed in Figure 2.11.

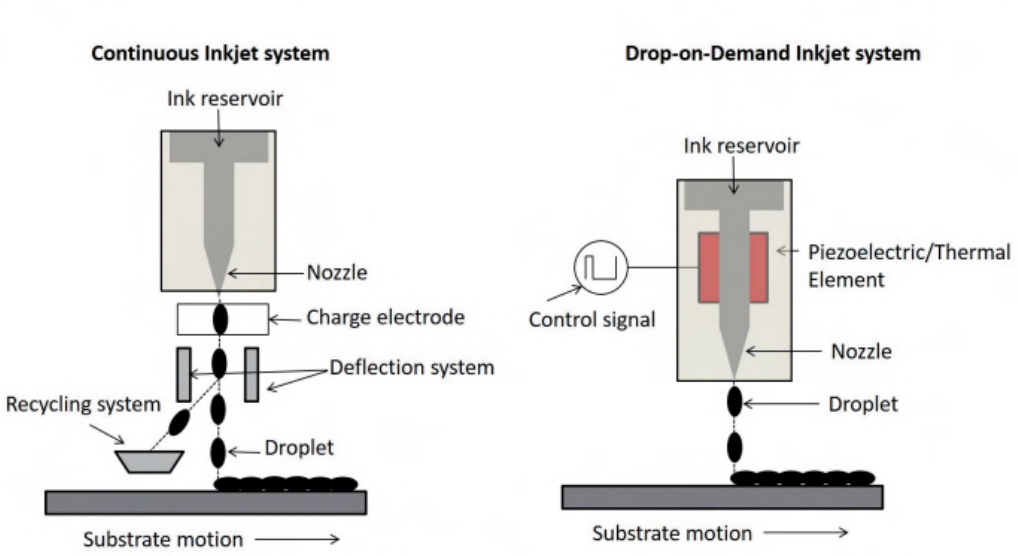

Figure 2.11. Illustration of the two primary methods used in a inkjet printing process [28].

2.1.3.2 Aerosol Jet Printing

Aerosol jet printing (AJP) is an increasingly popular non-contact direct writing technique utilized for the fabrication of small-scale features on various types of substrate materials. The present methodology employs aerodynamic focusing as a way to achieve precise deposition of colloidal suspensions or chemical precursor solutions, resulting in high-resolution results. In aerosol jet printing, the jet consists of several droplets with a diameter ranging from 2 to 5 μm, as opposed to inkjet printing where a single droplet is utilized [30]. It is important to mention that as a result of the significant nozzle-to-substrate distance, aerosol jet printing demonstrates compatibility with nonplanar substrates. This allows for the printing of complicated patterns and structures on surfaces that exhibit texture, steps, or curvature, while maintaining nearly consistent linewidths [31]. In addition, this technique is also employed to print high-resolution transmission lines, sensors, and antennas on a diverse range of substrate materials, encompassing various glass, polymers, FR4 (glass-epoxy), ceramics, and certain metals.

Currently, AJP can be generally categorized into two distinct classifications, namely pneumatic and ultrasonic, based on their respective operational techniques, as depicted in Figure 2.12 and Figure 2.13, respectively.

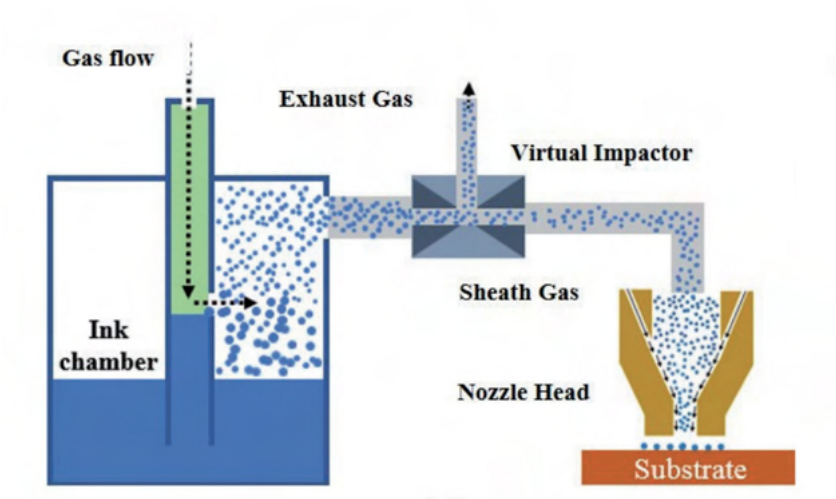

Figure 2.12. Illustration of the pneumatic aerosol jet printing process [28].

The production of aerosol mist in a pneumatic atomizer involves the injection of pressurized air or gas into a confined chamber containing the ink. This process leads to the creation of small droplets in close proximity to the interface between the ink and the air. On the contrary, for the aerosol method, the ink contained inside a vessel experiences ultrasonication, leading to the generation of micro-droplets through the application of ultrasonic pressure waves. Consequently, the micro-droplets that are formed are subsequently captured within the aerosol gas and propelled towards the print head through acceleration. The size of the design printed on the desired substrate is determined by both the nozzle orifice size and the flow velocity of the sheath gas. It is notable to point out that pneumatic atomizers are frequently employed in the context of large-scale printing and consume a greater amount of resources. However, ultrasonic aerosol systems possess the capability to produce highly intricate designs with a minimum size of 10 μm and require around 0.5 mL of solution [11].

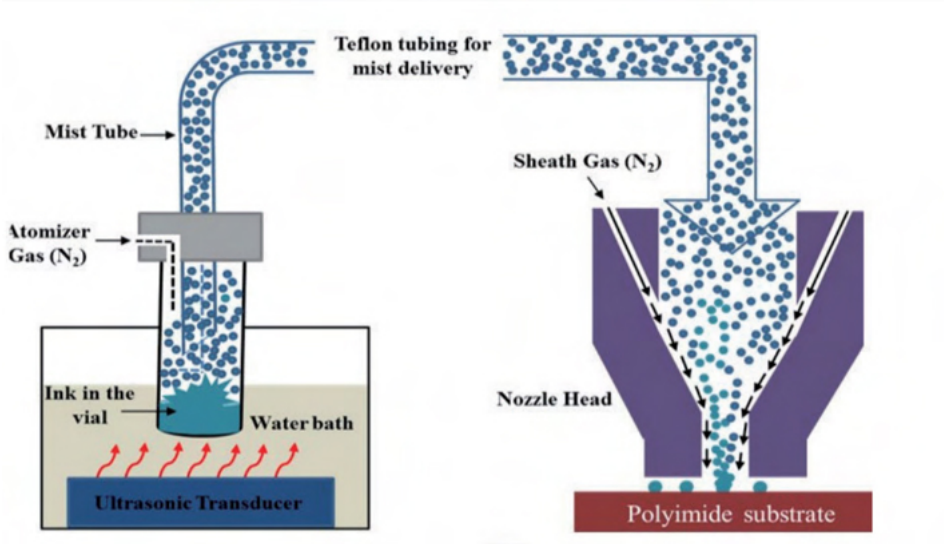

Figure 2.13. Illustration of the ultrasonic aerosol jet printing process [28].

2.1.3.3 Slot Die Coating

Slot die coating is a non-contact technique used for the deposition of wet films over vast areas. This method ensures the formation of homogenous films with a high level of uniformity in the cross-direction [32]. Moreover, this technique is capable of allowing a large variety of viscosities, ranging from less than 1 $mPa \cdot s$ to several thousand $Pa \cdot s$. Similarly, the coating speed exhibits a broad spectrum, ranging from less than 1 $m\,min^{-1}$ to over 600 $m\,min^{-1}$ [12].

As it can be seen in Figure 2.14, in slot die coating, the ink passes through a narrow opening located within the coating head, which is positioned in close distance to the web. Following the formation of a meniscus, which is sustained through ongoing pumping, the motion of the substrate results in the deposition of a uniform layer along the surface [33]. The use of this particular coating demonstrates advantages when used on wide surfaces, while achieving precise patterns of complex designs presents challenges. Hence, this methodology is commonly employed for devices with extensive surface areas, such as solar cells and light-emitting diodes [34].

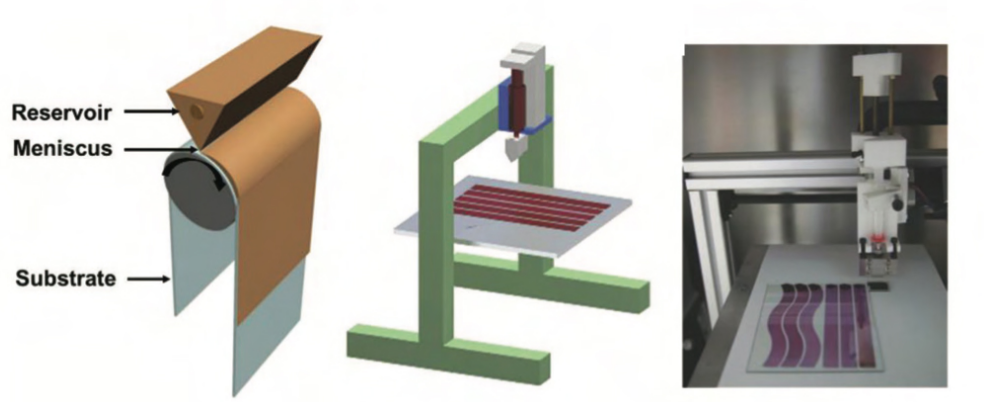

Figure 2.14. Schematic diagram illustrating the slot die coating process and also a modified 3D printer equipped with a slot die head [33].

Nevertheless, the efficiency of this technique is influenced by a variety of coating problems, including but not limited to air entrainment, dripping, ribbing, and the start-up and shut-down times of the coating cycle. The lack of effective control over the printing process leads to the inefficient utilization of the coating solution, resulting in wastage. Additionally, this lack of control also has a negative effect on the quality of the patterns formed on the substrate, as it introduces unwanted edge effects [35]. Therefore, the inherent stability concerns associated with this particular technology present significant challenges in terms of its applicability for the fabrication of printed electronics on flexible surfaces. Figure 2.15 presents a photograph capturing the roll coater in operation during the process of depositing the active layer as well as a detailed photograph showing the slot-die head in close proximity while applying a coating to a stripe of the active layer [35].

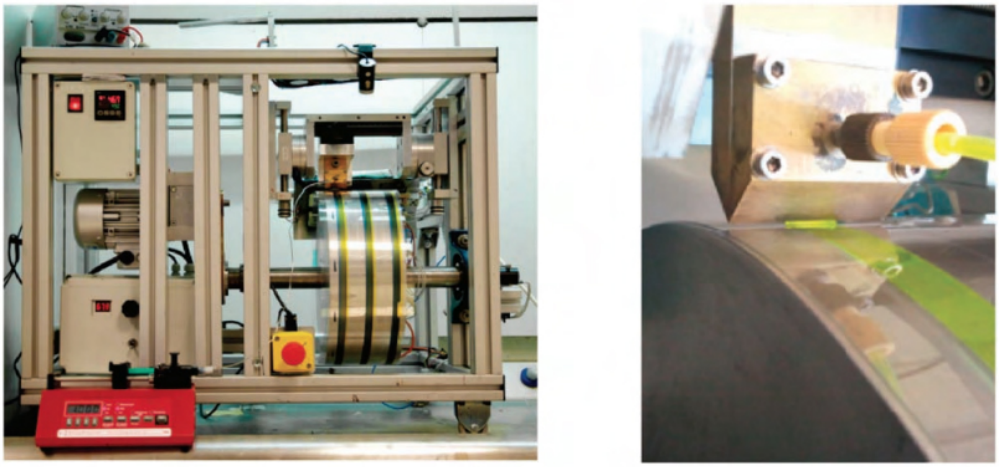

Figure 2.15. The photograph of a roll coater depositing an active layer (left side) and a photograph of the slot-die head during coating of an active layer stripe (right side) [35].

2.2 Flexible Electronics

The idea of flexible electronics has been in existence for numerous decades. In general, objects that possess a slim or extended form have the potential to exhibit flexibility. However, it was during the era of the space race when silicon wafers, employed in the construction of solar cells for satellites, faced reduction processes to enhance their power-to-weight ratio. This development consequently facilitated a certain level of deformability. The introduction of this concept in the 1960s facilitated the development of the initial flexible solar cells. The subsequent years witnessed significant advancements in the field of conductive polymers, organic semiconductors, and amorphous silicon. These developments brought about substantial improvements in flexibility and processability, making these materials the base for electronic devices used in various applications that necessitate characteristics such as bending, rolling, folding, and stretching which are properties beyond the capabilities of conventional electronics [36]. In this sense, Figure 2.16 presents a comprehensive chronology outlining the key advancements in materials, processing techniques, and applications in the field of flexible electronics.

Currently, the process of reduction in size, particularly through the utilization of integrated circuits, has been an impulse for the worldwide development of modern electronics. The global electronics components organizations are expected to have sustained growth of 7.7%, resulting in a predicted increase in market value from 5.41 million US dollars in 2017 to 7.86 million US dollars by 2022, driven by the current growth in modern electronics [1].

Therefore, different authors have been interested in this topic. For example, Nathan et. al. [37] critically evaluate the present state of flexible electronics and seeks to foresee their potential advancements in several domains such as healthcare, environmental monitoring, displays and human-machine interaction, energy conversion, management and storage, as well as communication and wireless networks.

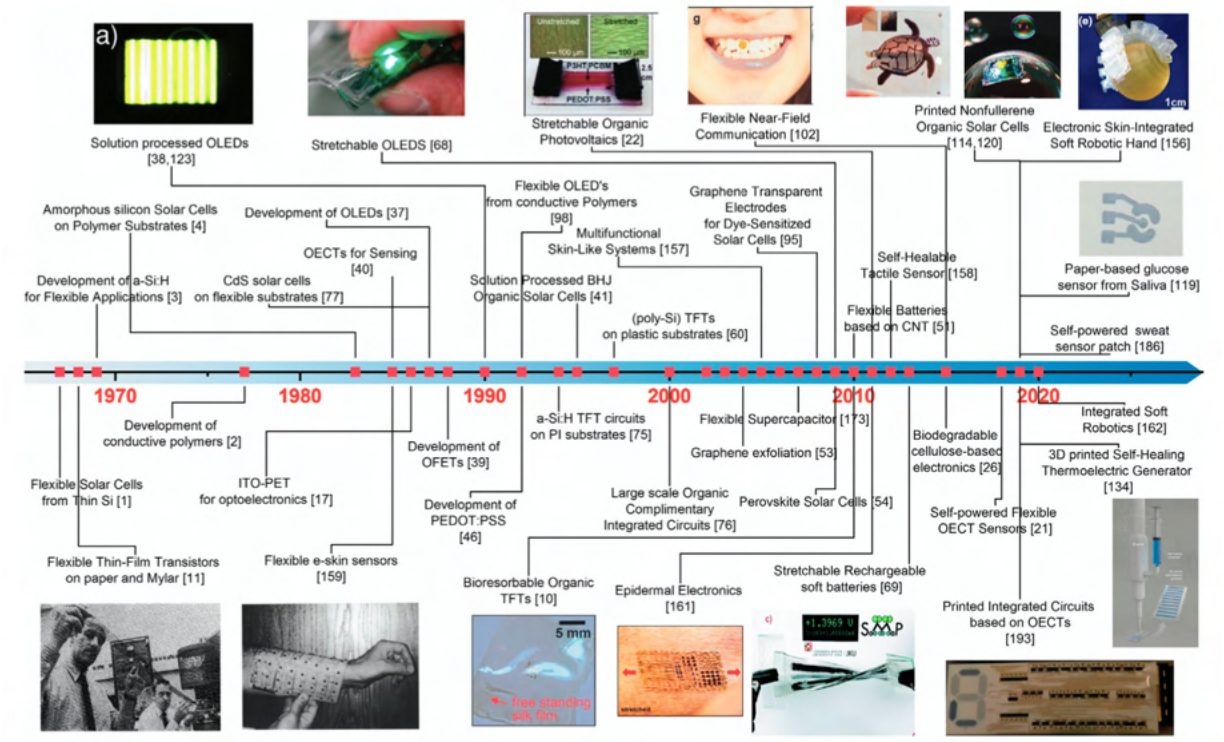

Figure 2.16. Comprehensive timeline outlining the key advancements in materials, processing techniques, and applications within the field of flexible electronics [36].

In the case of the applications of flexible electronics in healthcare monitoring, the integration of intelligent and flexible sensing electronic devices plays a crucial role in the development and implementation of wearable health monitoring systems. Over the recent years, a variety of flexible sensors have been developed and studied for their potential in monitoring human physiological signals, such as heart rate, wrist pulse, and blood/intraocular pressure. These sensors involve different configurations, including piezo-electrical devices, capacitive sensors, piezo-resistive sensors, and field effect transistor based devices. Particularly, these configurations have exhibited a notable capacity for high sensitivity in capturing such physiological signals [38].

For instance, Gao et. al. [39] present a sensor array that is both mechanically flexible and fully integrated, eliminating the need for external analysis. This sensor array allows multiplexed in situ perspiration analysis, allowing for simultaneous and selective measurement of sweat metabolites (e.g., glucose and lactate) and electrolytes (e.g., sodium and potassium ions). Additionally, the array includes a skin temperature sensor to calibrate the response of the sensors. The flexible electronic device as well as the integrated sensor are presented in Figure 2.17 and Figure 2.18, respectively.

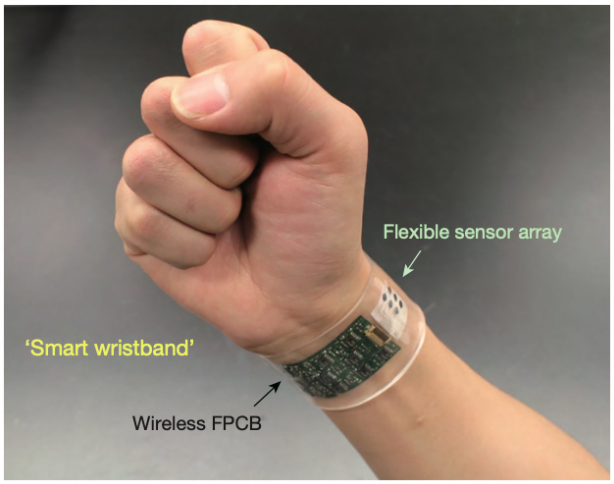

Figure 2.17. Photograph of a wearable and flexible integrated sensing array positioned on the wrist of an individual. [39].

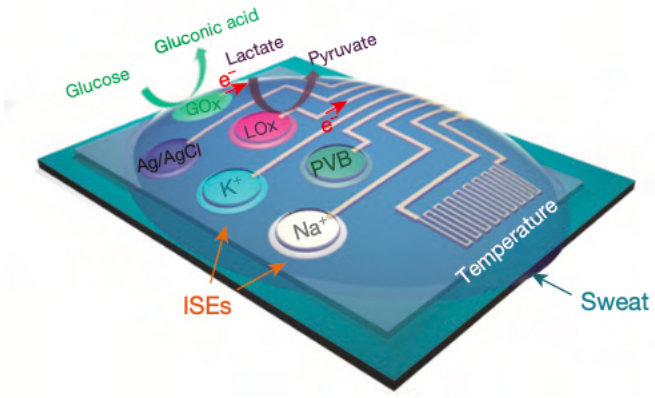

Figure 2.18. Schematic view of the multiplexed sweat sensor array [39].

Muth et. al. [40] present an application of an embedded 3D printed strain sensor using highly stretchable elastomers. This study introduces a novel technique called embedded-3D printing (e-3DP) for the production of strain sensors incorporated inside elastomeric matrices that possess great conformability and extensibility. This sensor is shown in Figure 2.19. Moreover, another interesting application for flexible electronics includes the development of batteries. Gaikwad et. al. present this application with a novel battery architecture that incorporates a mesh-embedded Zn-MnO_2 system. This design effectively overcomes the limitations in thickness and capacity commonly observed in thin-film flexible batteries, while maintaining the power performance requirements of conventional batteries [41].

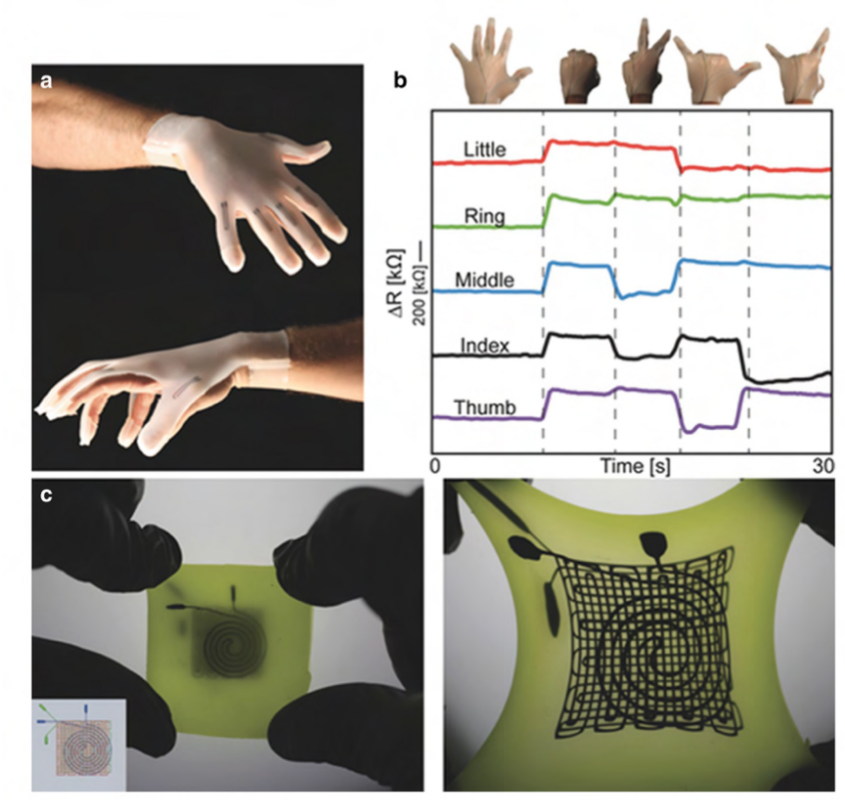

Figure 2.19. a) Photograph of a glove that has been equipped with strain sensors, which has been manufactured using the e-3DP technique. b) The effect of electrical resistance variation in response to distinct hand motions. c) A three-layer strain and pressure sensor in both the unstrained condition (left) and the stretched state (right) [40].

2.2.1 Strategies for the Development of Flexible Electronic Devices

For over four decades, the microelectronics industry has extensively employed inorganic semiconductors like silicon, germanium, and gallium arsenide [42]. Silicon dioxide insulators, along with metals such as aluminum and copper, have been serving as the fundamental components for the development of this sector. Nevertheless, there is a growing trend towards the substitution of conventional inorganic materials with organic-based materials and metals. The change is mainly caused by the multiple benefits associated with these alternatives, including their facilitation of device fabrication, suitability for large area applications, compatibility with lightweight and mechanically flexible substrates, as well as their ability to manipulate electrical, optical, and magnetic properties. Therefore, the field of electronics that refers to these substances is commonly referred to as organic or plastic electronics.

These organic materials include polymers, oligomers, and hybrid composites which exhibit considerable potential in several domains such as aerospace, military applications, and everyday life. Moreover, these materials provide excellent prospects for the development of flexible and cost-effective electronic circuits [43]. Therefore, they can be utilized in the production of smart sensors, wearable electronics and plastic-based full-color displays as previously discussed. Table 2.1 presents the best particular characteristics for each material for its application in electronics [44].

Table 2.1. Differences between the organic electronics and silicon electronics [44].

Silicon Electronics	**Organic Electronics**
Economic Difference	
High price per unit area	Low price per unit area
Hight cost in dedicated plant	Low capital in flexible plant
Technological Difference	
Small area for final products	Big area for final products
Hard substrates	Flexible substrates
Breakable	Robust

Nowadays, there are two different strategies employed in the production of flexible electronic devices. One approach involves the deliberate placement of functional elements, such as conductive semiconductors or nanomaterials, onto organic polymer substrates using techniques such as coating, photoetching or depositions [45].

The second approach involves the development and production of polymers that possess intrinsic flexibility and functionality, namely organic conjugated polymers that exhibit semiconductor or conductive characteristics [46]. For instance, designing materials that combine unique structural characteristics, including helix, serpentine and various micro/nanostructures is the best way for the fabrication of flexible electronics using this second strategy. These both strategies are presented in Figure 2.20 where it can be seen different materials and structures of each approach for the development of flexible electronics [38].

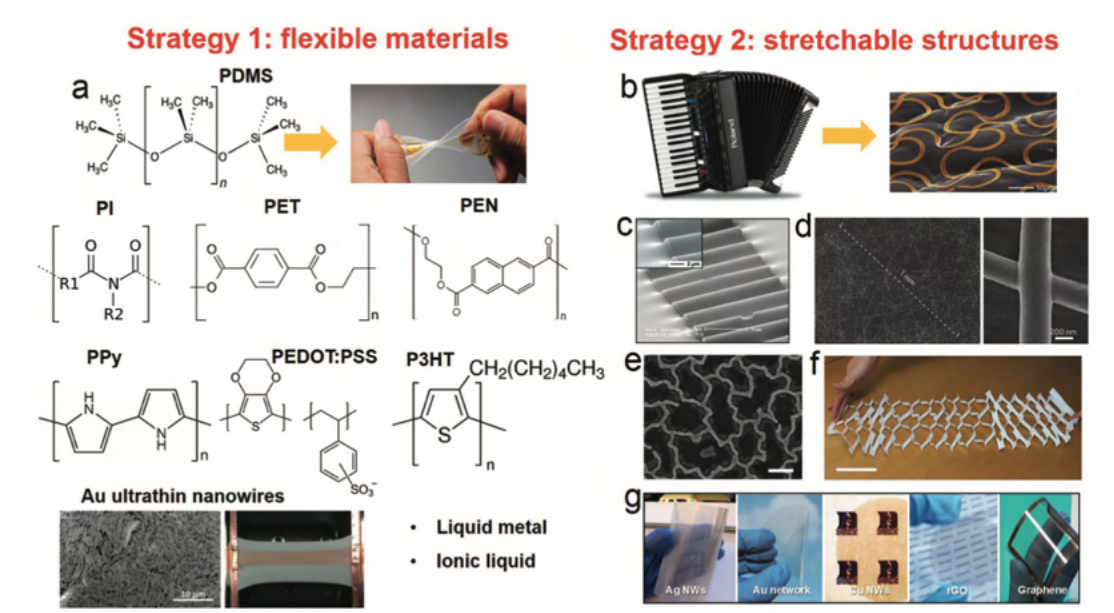

Figure 2.20. Conventional approaches and materials employed in the fabrication of mechanical flexible structures. a) The primary materials with inherent flexibility and stretchability for the development of flexible devices. The use of electrical insulating polymers, such as PDMS, PI, PET, and PEN, as substrates is a viable option. b) The geometric design of inorganic materials, such as Si wavy structures (c) and network films (d-g) composed of Ag nanowires, Au nanowires, and Cu nanowires, can result in stable electric output even when subjected to significant deformations. In figure (e), the scale bar is set at 500 nm [38].

Figure 2.21 also illustrates the application of these two approaches in order to achieve stretchability in flexible electronics also called soft electronics. Particularly, this figure presents the two main strategies that are used in order to fabricate flexible electronics despite the substrate material that is being used. In this sense, these two strategies are divided as: 1) material innovation and 2) structural design. The first area involves the development of new materials that have the ability to stretch either individually or when combined while the second area involves modifying nonstretchable materials to create specialized structures that can withstand applied strain without breaking. For instance, the material method includes liquid metals, hydrogels, nanomaterials and conductive polymers. On the other hand, the structural approach involves island-bridges, waves and wrinkles, textiles, kirigami, origami, interlocks and fissures [47].

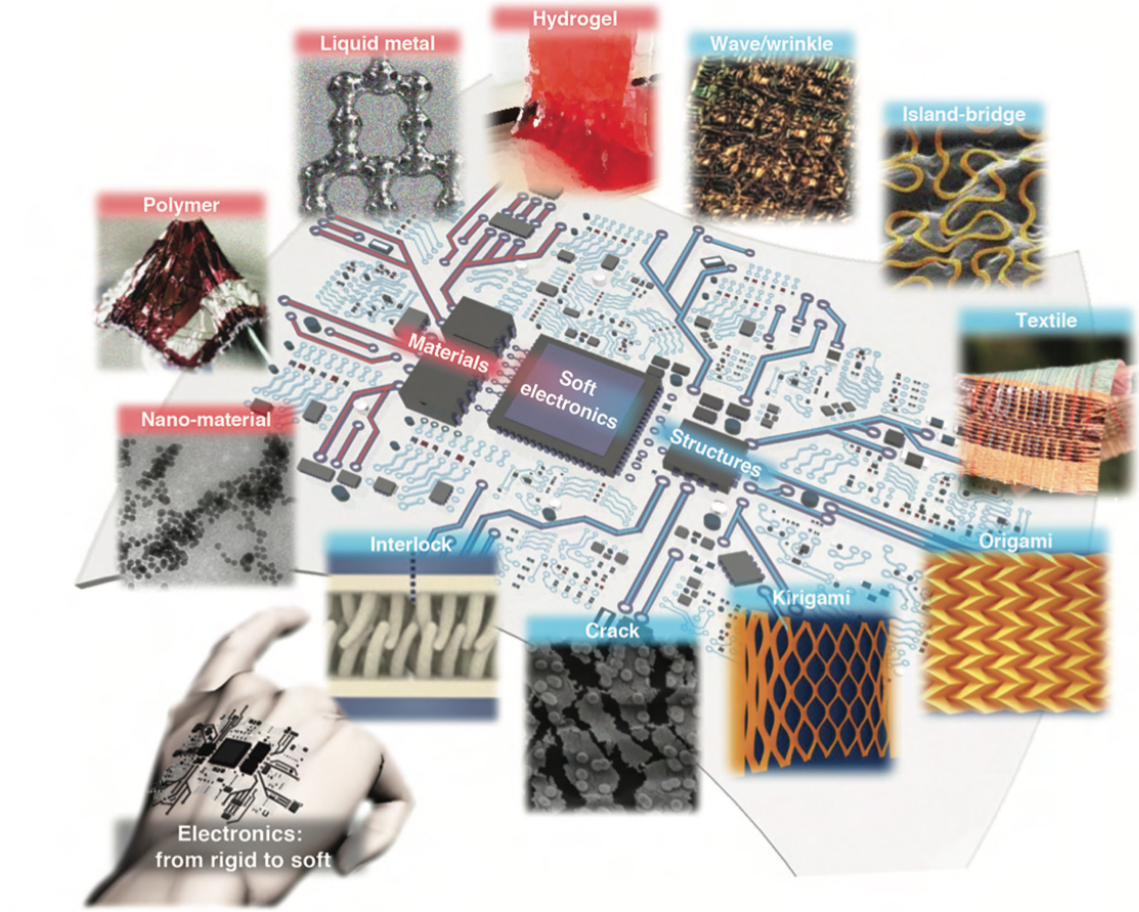

Figure 2.21. Schematic view of the two strategies that can be employed to achieve soft electronics: materials innovation and structural design [47].

2.2.1.1 Flexible Substrates

The substrate serves as the base material for a printed electronic component, requiring compatibility and strong adhesion with the ink. Additionally, it should possess desirable qualities such as low thermal expansion coefficient, flexibility, resistance to chemicals, gases, and water, controllable optical transparency, as well as appropriate dielectric permittivity and dielectric loss [48, 49]. The most widely utilized substrates in the field of printed electronics are polymers and paper. For instance, talking about polymers, these ones provide several desirable characteristics that make them a highly attractive choice as a substrate for printed electronics. These include their adaptability, flexibility, and capacity to easily be incorporated into sophisticated configurations.

Due to the fact that in order to fabricate flexible electronics by an additively manufactured process it is necessary the use of conductive inks which the majority of the time they present nanoparticles (NPs), the dispersion of nanoparticles in inks is commonly achieved through the utilization of insulating organic additives [50]. Subsequently, a process of thermal sintering at elevated temperatures is necessary post-printing to eliminate these dispersants. Therefore, the primary factor to be taken into account when choosing a suitable material is the thermal stability of the substrate. This is because extended exposure to high temperatures has the potential to cause harm and distortion to the device [14]. Polymer films made from Polyimide (PI), Polyethylene Terephthalate (PET), Polyethylene Naphthalate (PEN), and Thermoplastic Polyurethane (TPU) are the most widely utilized substrates in the production of printed electronics. The mechanical and physical properties of these materials towards their application in flexible electronics are presented by Wang et. al. [38] in Figure 2.22.

Materials	Stretchable/ bendable	Transparency/Dielectric constant	Thermal stability/Coefficient of thermal expansion	Chemical Resistance
PI	Bendable	Low transparency (yellow color)	Resist temperature (<450 °C)	Weak acids and alkali
		2.8–3.5	$\approx 5 \times 10^{-5}$/K	Ethanol and acetone
PET	Bendable	High transparency (>85%)	Resist temperature (<100 °C)	Dissolvable in acetone
		2.5–3.5	$\approx 7 \times 10^{-5}$/K	
PEN	Bendable	High transparency (>85%)	Resist temperature (<180 °C)	Easily permeated by oxygen and water
		2.9–3.2	$\approx 2 \times 10^{-5}$/K	
Silicone (PDMS,Ecoflex)	Stretchable	High transparency (>95%)	Resist temperature (<100 °C)	Ethanol and acetone (in short time)
		2.3–2.8	Thermal expansion	
			$\approx 30 \times 10^{-5}$/K	
Metal foil	Bendable	No	Resist temperature (≈250 °C)	Ethanol and acetone
		Good conductivity	Thermal stable	Moisture and oxygen
Paper	Bendable	No	Resist temperature (<100 °C)	No
		2.3–3.0		
Self-healing	Stretchable	Low transparency (92%)	Thermal healing	Moisture and oxygen
		Ionic conductivity	Thermal expansion	Ethanol and acetone (in short time)

Figure 2.22. Overview of the chemical and physical properties of commonly used flexible substrates [38].

Among these flexible substrates, PI is a polymer substrate that possesses notable characteristics such as exceptional flexibility, minimal creep, and high tensile strength. These properties remain intact even when the material is exposed to continual use at temperatures as high as 452 °C [51]. In addition, it also exhibits resistance to weak acids and alkalis, as well as regularly employed organic solvents such as ethanol and acetone. For instance, Yang et. al. [52] presents an application of this polymer which consists in the fabrication of a Cu/Ni interconnector that is air-permeable and machine-washable made of a flexible fibrous polyimide (FPI) membrane. This example of interconnector is shown in Figure 2.23.

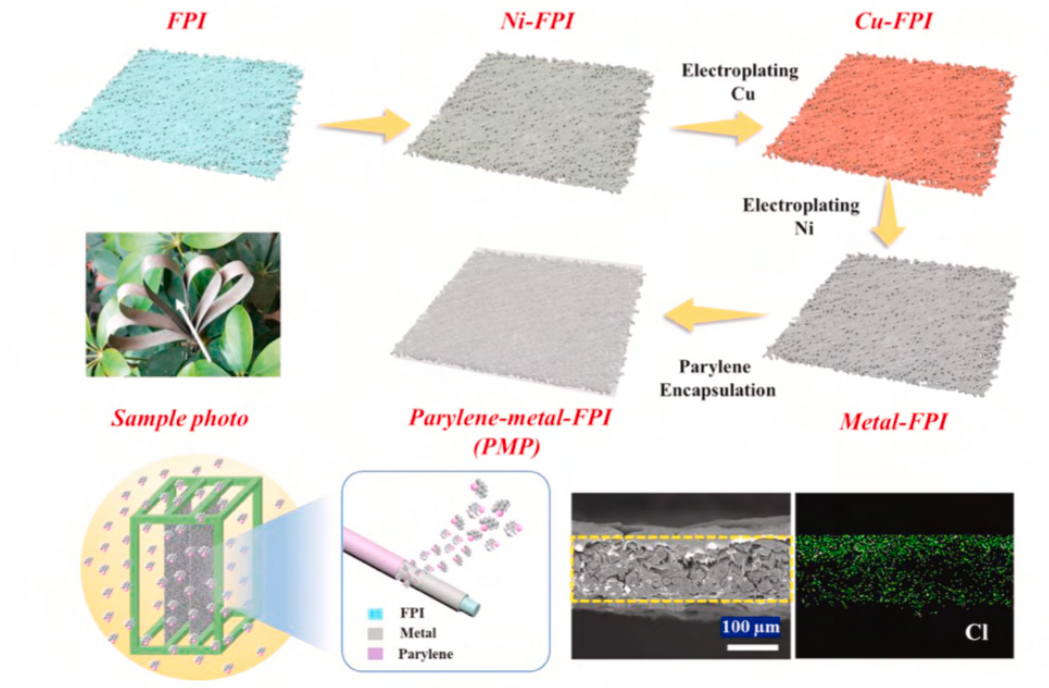

Figure 2.23. Schematic illustration of the fabrication process for a Cu/Ni interconnector that is air-permeable and machine-washable made of a flexible fibrous polyimide (FPI) membrane [52].

Nevertheless, due to PI is a yellow colored material, its application results in reduced levels of transparency in flexible electronics. In fact, this characteristic is important in applications that may require a substrate that exhibits high transparency such as solars cells or flexible transparent displays.

On the contrary, polyethylene naphthalate (PEN) and polyethylene terephthalate (PET) exhibit optical clarity, allowing for the transmission of more than 85% of visible light in the wavelength range [53]. Nevertheless, it should be noted that these materials exhibit worse thermal stability compared to polyimide (PI). Additionally, they are susceptible to permeation by oxygen and water, with a water absorption rate of approximately 0.14% and their limited stretchability can be attributed to their relatively high modulus of elasticity, which falls within the range of 2-3 GPa [38], [14].

Another important polymer that it is specially utilized as a biocompatible and intrinsic high stretchable material is Polydimethylsiloxane (PDMS). In fact, the microstructured polydimethylsiloxane (PDMS) film is widely recognized as the most preferred flexible substrate for the integration of sensitive nanomaterials in flexible sensors as it can been seen in Figure 2.24 [54]. This preference derives from its exceptional elasticity and biocompatibility. It is important to note that PDMS exhibits inherent hydrophobicity, presenting challenges in its application for printing purposes. Nevertheless, studies have indicated that modifying the surface of PDMS can significantly improve its wettability [55].

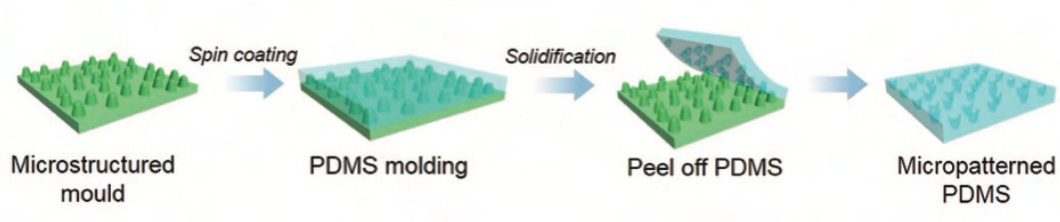

Figure 2.24. Schematic representation of the manufacturing technique employed for the production of micro-patterned polydimethylsiloxane (PDMS) films [54].

Lastly, another important material that is used in flexible electronics is paper. In this sense, cellulosic papers are extensively utilized in the field of printed paper electronics [56]. The material exhibits a low cost, possesses flexibility, possesses wide availability, demonstrates environmental friendliness, and is capable of being composted [57]. Nevertheless, the material exhibits a significant level of moisture absorption, leading to alterations in dimensions and adverse effects on the functionality of printed devices. Also, the presence of a high degree of surface roughness can lead to ink penetration, which in turn has the potential to negatively impact the conductive traces and contribute to an increase in resistance. Despite all these drawbacks that this material may present, the addition of particular substances can lead to modifications in its properties, hence increasing its flexibility. These modifications can include improvements in water repellency, electrical conductivity, transparency, fire retardancy, and various other characteristics [58].

2.2.2 Importance of Stretchable Conductors for the Fabrication of Flexible Electronics

The stretchable conductors play an important role for the fabrication and functionality of flexible electronics. Their importance in this field comes from the fact that these are able to keep electrical conductivity as well as their mechanical integrity when they are exposed to mechanical deformation such as bending, stretching or twisting movements. This feature enables a flexible electronic device to be capable of stretch while providing reliable communication and functionality between the components on the device. Moreover, they can be applied onto different types of surfaces and shapes which is one important characteristic in the development of wearable sensors. It is also important to mention that their cost-effectiveness and scalability are increasing. Figure 2.25 presents the most common hybrid materials as well as geometric designs for the development of stretchable conductors [7].

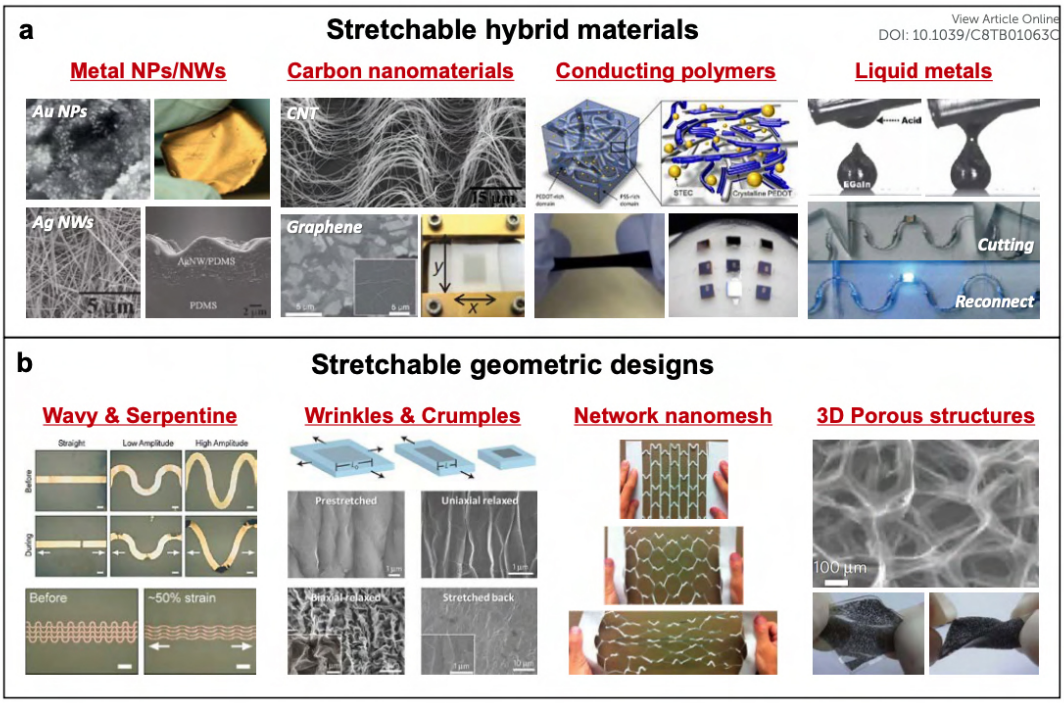

Figure 2.25. Examples of the most common hybrid materials and geometric designs for the fabrication of stretchable conductors [7].

2.2.2.1 Stretchable Metallic Inks

Ink is formulated by combining specific elements in precise proportions in order to get the desired characteristics of the printed electronic device. The successful creation of printed electronics depends primarily on the compliance of the substrate and the printing process itself [59]. Particularly, metal nanoparticles and carbon nanomaterials are commonly utilized for the printing of conductive layers in various applications. However, in multi-material printed electronic applications, additional types of nanomaterials such as semiconductor nanomaterials, reactive inks, dielectric materials, and others may also be employed [60]. Regarding the use of nanoparticles inks, the primary factors to be taken into account when choosing them are bulk conductivity, cost, and simplicity of handling. Currently, gold and silver are considered the most appropriate noble metals for use as conductive nanoparticle inks in the field of printed electronics. Silver exhibits chemical stability against oxidation, possesses a lower cost compared to gold, and demonstrates superior electrical and thermal conductivity [61].

2.2.2.2 Stretchable Silver Paste

Conventional inflexible materials commonly employed for integrating and interfacing purposes, such as metal thin films and solder tin cream, are inadequate for flexible and stretchable systems. A significant disadvantage of these materials is their toxicity, mostly attributed to the inclusion of lead (Pb) components. Consequently, these type of traditional interconnecting conductive materials have been substituted with novel alternatives such as silver paste and copper paste. These materials exhibit a higher degree of environmental friendliness compared to solder tin cream, primarily due to their composition consisting predominantly of Pb-free components. Moreover, finer structures with higher resolution may be observed using these materials compared to solder tin cream. These materials can be efficiently manufactured on a wide scale for the development of flexible electronics, including roll-to-roll printing, screen printing and inkjet printing techniques [62].

Among the various novel materials used for interconnecting and interfacing purposes, silver paste distinguishes as the preferred choice due to its exceptional electrical conductivity, impressive thermal conductivity, and commendable adhesive properties. In addition, it is important to say that silver paste exhibits a lower curing temperature compared to solder tin cream. Particularly, silver paste can be effectively cured at approximately 150ºC whereas solder tin cream requires a higher temperature of over 200ºC. The difference in curing temperatures is significant as it helps to mitigate several undesirable effects, including thermal deformation of materials, thermal deterioration of electronic devices and substrates, and the generation of internal stress induced by high temperature processes. The significance of this aspect is particularly evident in the context of flexible and stretchable structures, as the majority of these systems rely on polymers as both the substrates and encapsulating layers. Consequently, silver paste has gained significant popularity as a substitute for tin-lead solder in the interconnects and soldering processes of flexible devices [62].

2.2.3 Flexible Electronics towards Wearable Health Monitoring

The utilization of wearable electronics is anticipated to have a significant impact on the field of personalized medicine, as these devices provide continuous and close monitoring of an individual's physical activity and health condition as it is shown in Figure 2.26 [38]. Due to its exceptional flexibility and compatibility, flexible electronics have the potential to function as an ideal platform for the development of future personalized wearable electronic devices [4, 63]. For instance, current personal health-monitoring systems, characterized by their portable, flexible, and wearable configurations, have been successfully introduced into the market as various wearable accessories including clothing, eyeglasses, bands, and watches. These devices have the purpose of detecting essential physiological indicators such as blood pressure, heart rate, body temperature and breathing rate [7].

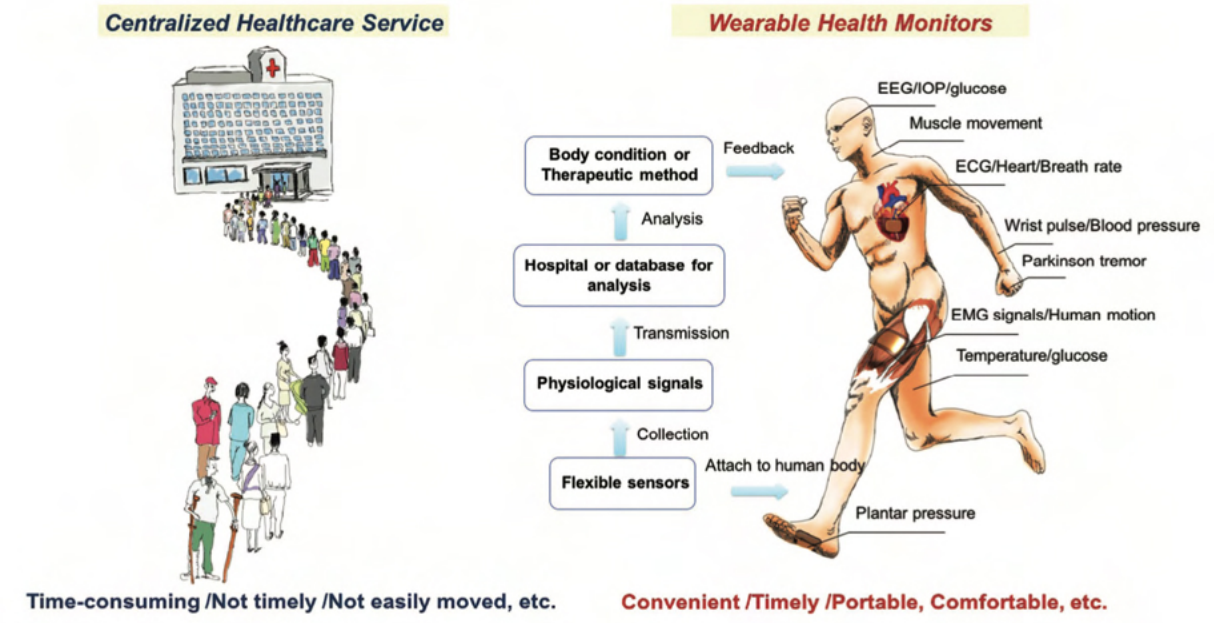

Figure 2.26. Wearable health monitors offer a convenient way of portable healthcare and facilitate the transition of conventional diagnostic approaches in clinical practice from centralized healthcare services to decentralized healthcare delivery [38].

2.2.4 Importance of Mechanical Conditions for the Fabrication of Wearable Electronics

As it was previously mentioned, wearable electronics are of significant importance in the implementation of personalized medicine, since they have the capability to consistently obtain data from the human body in order to detect significant changes in health status in a timely manner, thus allowing preventive action. Nevertheless, the presence of motion disturbances and mechanical mismatches between traditional stiff electronic materials and the flexible nature of human skin can result in significant inaccuracies in sensor readings during epidermal measurements [63, 64]. Therefore, designing an appropriate material interface is of the highest priority in order to develop flexible electronics capable of withstanding sophisticated mechanical deformation, including bending, twisting, and stretching [65]. For instance, Niu et. al. [4] presents in Figure 2.27 the mechanical conditions that each part of the human body experiences in different daily activities.

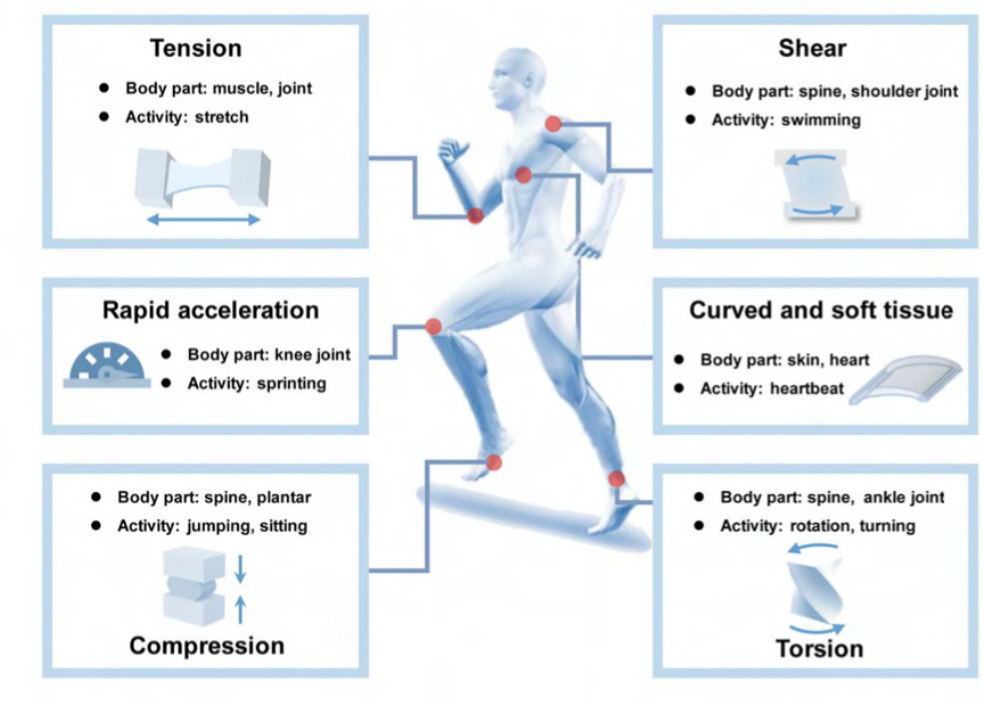

Figure 2.27. Mechanical conditions experienced by various body regions during physical activity [4].

Polymers are considered highly favorable substrates for wearable technologies because to their intrinsic property of possessing low mechanical stiffness. Indeed, there has been a growth of flexible and stretchable electronic devices that have been integrated with polymeric substrates. These devices have demonstrated the ability to convert biological signals into digital format, thus facilitating their application in healthcare monitoring [5, 66].

2.3 Additive Manufacturing

In recent years, there has been a significant use for additive manufacturing (AM), commonly referred to as three-dimensional 3D printing, across several industrial and academic fields [67, 68]. This emerging technology demonstrates the capability to efficiently fabricate complex components within a much reduced time as compared to conventional production methodologies. In simple terms, additive manufacturing is a novel technological process that involves the layer-by-layer fabrication and printing of components where these layers are sequentially built until the desired component is formed. It is important to mention that among the various current manufacturing techniques employed globally, additive manufacturing has demonstrated its capabilities and exhibits significant potential for revolutionizing the production of sensors [69, 70, 71].

2.3.1 Additive Manufacturing Process and Techniques

The initial step in the 3D-printing process involves generating a digital representation of the desired product. This objective can be accomplished by the utilization of a three-dimensional scanner, computer-aided design (CAD) software, or by employing photogrammetry techniques. After the creation of the 3D model, it is necessary to go through a conversion process to the STL file format, often known as STereoLithography. This file format is specifically designed to contain the geometric data of the model's surfaces in the form of a collection of coordinates representing triangulated sections [6].

The file format in question is well known for its universal compatibility with various 3D printer software. Subsequently, this file experienced a ”slicing” procedure to turn the data into a G-code file. The slicing process involves creating many 2D cross-sectional layers of the complete item. At the end, the printer initiates the process of material deposition by sequentially layering 2D components upon one another, culminating in the formation of the desired 3D structure. This entire process is schematically shown in Figure 2.28 [6].

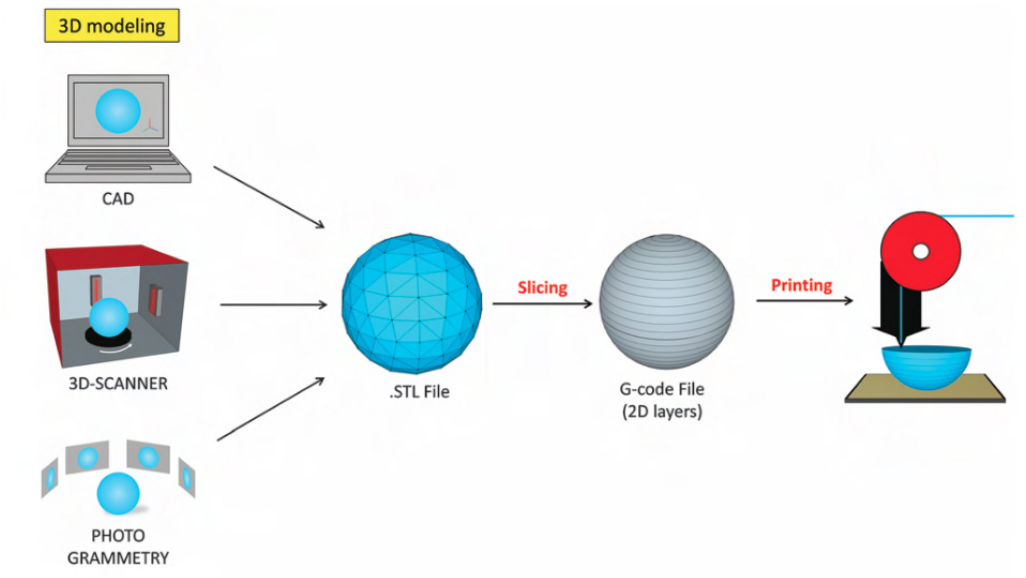

Figure 2.28. Steps for the creation of a 3D printed structure [6].

Based on the ASTM F2792 [72] and being explained by Khosravani et. al. [73], the technology of 3D printing is characterized and categorized into seven distinct classifications which are:

1. **Material extrusion (ME)**: during this procedure, the raw material is extruded through a nozzle under the action of applied pressure. Layers are formed through the process of extruding hot material onto a substrate.
2. **Binder jetting (BJ)**: this methodology involves the construction of component layers by applying an adhesive to a powder bed. Following this, the function of newly fallen powder is to create an additional layer. At the end, the manufactured product needs to go through a subsequent post-processing stage.

3. **Material jetting (MJ)**: the proposed technique involves the deposition of raw material onto a platform using a jet-propelled extrusion, resulting in the gradual solidification and formation of the model in a layer-by-layer way. Ultimately, the component must be separated from the structure's platform and the auxiliary material needs to be removed.

4. **Directed energy deposition (DED)**: in this technique a concentrated energy source is employed to induce the melting of the raw materials. After the initial layer has been deposited, the nozzle and energy source are relocated in order to proceed with the deposition of the subsequent layer.

5. **Powder bed fusion (PBF)**: this method involves the utilization of a heat source, such as a laser, to facilitate the fusion process between particles of powder. During the fabrication process, a layer of powder material is distributed equally onto the preceding layer.

6. **Vat photopolymerization (VP)**: this technology employs a liquid resin that experiences a transition to a solid state after exposure to ultraviolet light. The above-mentioned light source is employed for the purpose of selectively solidifying photosensitive resin in a sequential manner, so allowing the fabrication of a desired object according to a computer-aided design (CAD) file.

7. **Sheet lamination (SL)**: during this particular procedure, a three-dimensional structure is generated by manipulating a thin sheet of unprocessed material. The fabrication process involves the attaching of thin sheets of material in a layer-by-layer manner, followed by the cutting of the joined layers to create the desired product.

All these 3D printing technologies mentioned before are presented in Figure 2.29 [74]. Moreover, their own advantages and disadvantages are explained by Ambrosi et. al. [6] in Figure 2.30.

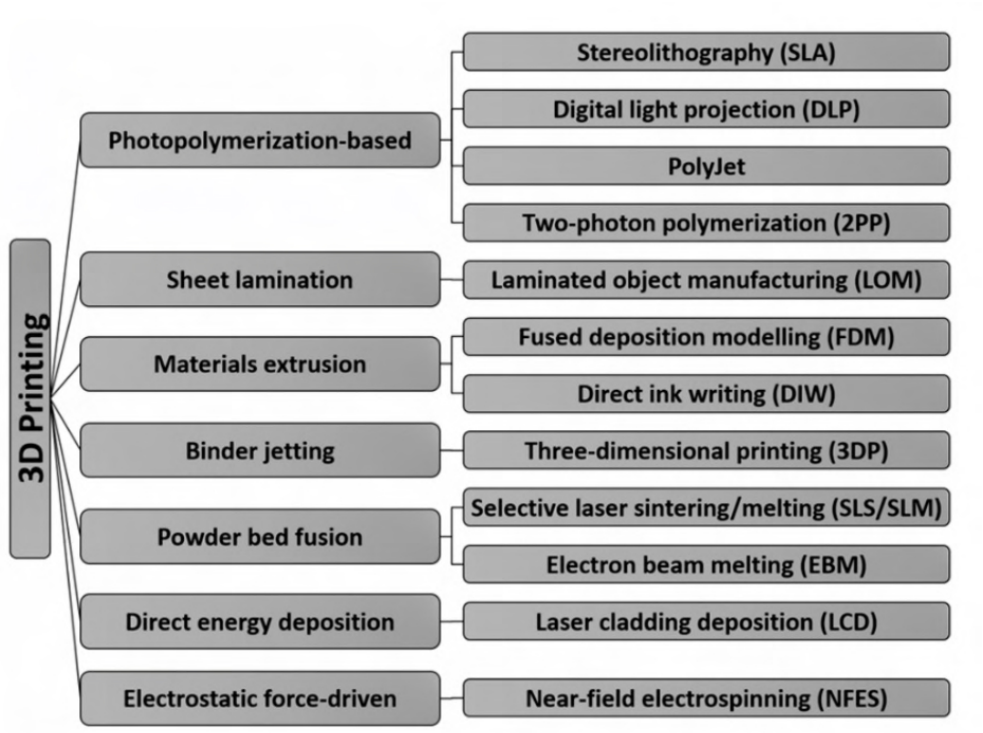

Figure 2.29. 3D printing technologies and their derivates [74].

3D-printing process	Technique	Materials	Advantages	Limitations
Photopolymerization	Stereolithography (SLA)	Photopolymers	Simple	Single material
	Material jetting	Photopolymers	Multimaterial structures	High cost
	Continuous liquid interface printing (CLIP)	UV-curable resins	High speed	Single material
	Two-photon polymerization (2PP)	UV-curable resins	Sub-100 nm resolution	Low yield of production
Extrusion	Fused deposition modeling (FDM)	Thermoplastics (ABS, PLA, PC, PA, *etc.*); glass (new); metal (new)	Simple, multimaterial structures; low cost (for thermoplastic materials)	High cost (for glass and metal)
	Robocasting (DIW)	Plastics, ceramic, food, living cells, composites	Versatile	Requires post-processing; low resolution
Powder based	Selective laser sintering (SLS)	Thermoplastics, metals	No need for support material	Limited mechanical properties of object; high cost
	Selective laser melting (SLM)	Metals	No need for support material	High cost
	Electron beam melting (EBM)	Metals	No need for support material	High cost
	Binder jetting	Any material in particulate form	No need for support material; versatile; lower cost than laser-based methods	Limited mechanical properties
	Selective inhibition sintering (SIS)/inhibitor jetting	Metal	Sintering is performed only once after printing; lower cost than laser-based methods	Low resolution; limited mechanical properties
Lamination	Laminated object manufacturing (LOM)	Paper, metal, plastic, *etc.* as laminated sheets	Versatile	Limited mechanical properties; some design limitations

Figure 2.30. Most important advantages and disadvantages for each 3D printing technology [6].

A schematic view of the process for each 3D printing process is also illustrated in Figure 2.31 [75].

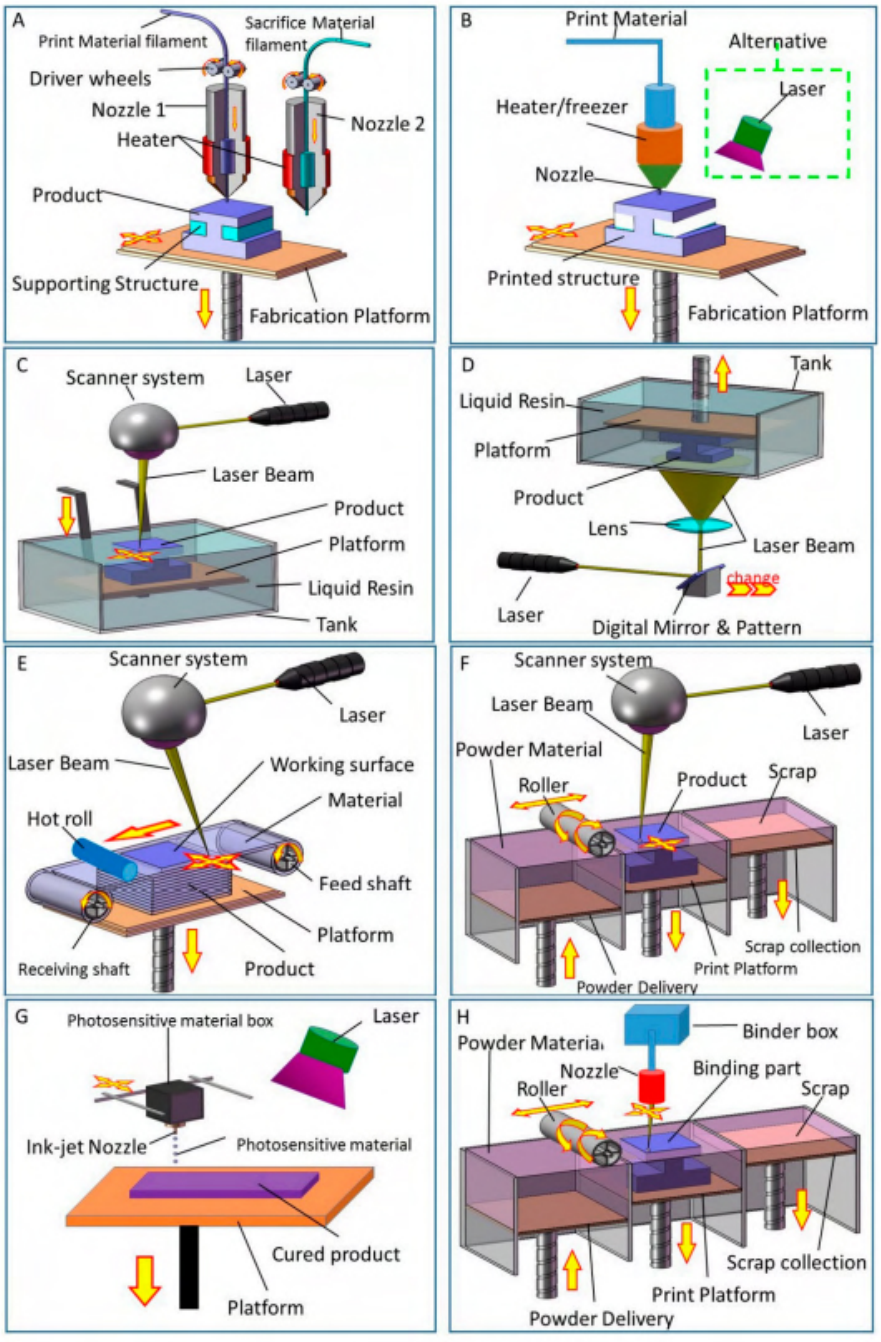

Figure 2.31. Schematic view of the process for different 3D printing technologies. (A) Fused deposition modeling (FDM); (B) Direct ink writing (DIW); (C) Stereolithography (SLA); (D) Digital light processing (DLP); (E) Lamination (LOM); (F) Selective laser sintering (SLS) and Selective laser melting (SLM); (G) Photopolymer jetting (Polyjet); (H) Binder jetting (3DP) [75].

Since there are many different additive manufacturing technologies, in the present work we will focus on stereolithography (SLA) and direct ink writing (DIW) which were the technologies used for the development of the 3D printed flexible electronic platform.

2.3.1.1 Vat Photopolymerization

Vat photopolymerization is recognized as one of the initial techniques employed for implementing the 3D printing process during the early 1980s. The present method involves exposing the photo-hardening polymer to ultraviolet (UV) light, consequently initiating the process of polymerization until the desired three dimensional object is created. This process could be better explained as the process of solidifying the liquid polymer through the application of ultraviolet (UV) radiation to its surface. By exposing the solidified layer to a controlled immersion, it becomes possible to solidify subsequent layers and assemble them in a manner that ensures strong adhesion, which results in the creation of a final three-dimensional object [6, 76].

In this 3D printing technology, the UV curing system can involve either a laser that crosses the polymer surface in accordance with the layer design (known as direct laser writing), or a digital mirror device (referred to as digital light projection (DLP)) that emits UV light for each layer based on the design. Regarding the process of polymerization, it can be performed in two configurations. The first configuration, known as the bath configuration, involves the polymerization occurring at the liquid surface. In this configuration, the stage moves downwards after each layer is solidified, as shown in Figure 2.32 A). The second configuration, known as the layer configuration or bat configuration, involves the polymerization being obtained from the bottom. In this configuration, an optically transparent window is used, and the stage moves upwards upon layer formation, as depicted in Figure 2.32 B). The utilization of this alternative method proves to be advantageous in cases where the resin polymer is available in restricted amounts, and a small volume for printing is considered [6, 76].

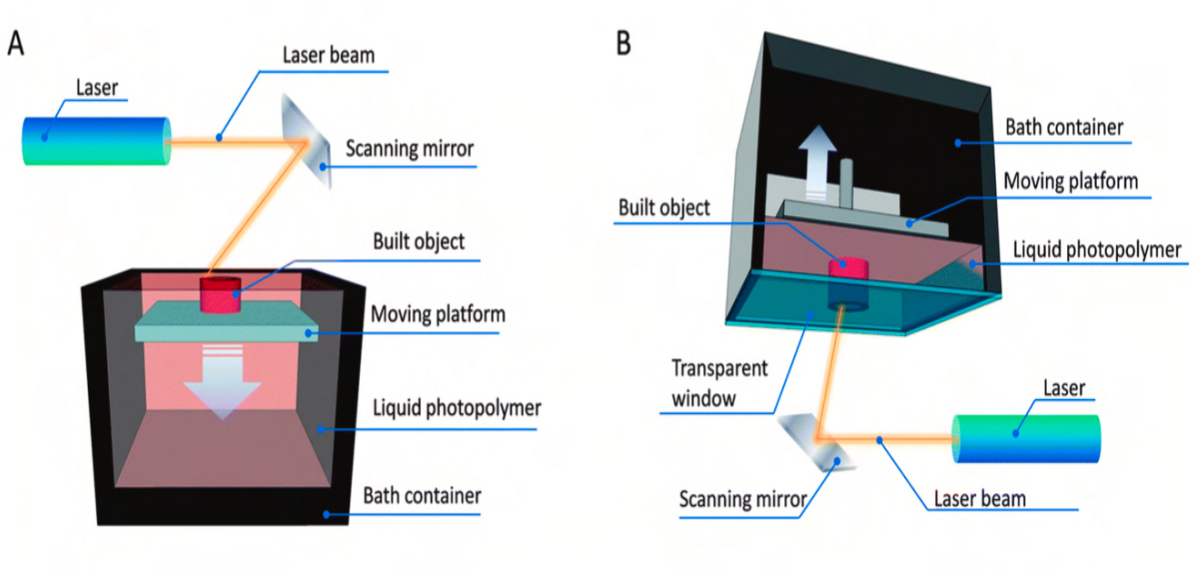

Figure 2.32. Schematic representation of 3D printing procedures based on photopolymerization. Two processes involved in stereolithography (SLA) are depicted as (A) and (B), which are categorized into two distinct configurations known as the bath configuration and the bat configuration, respectively [76].

These two techniques demonstrate enough capability in reaching a resolution of 18-20 μm, which is ideal for the fabrication of microfluidic devices. Moreover, this level of resolution is comparable to other transducing techniques utilized in the detection of biomarkers, genes, and proteins. These techniques can be effectively employed in flexible wearable applications [77, 78].

2.3.1.2 Material Extrusion

The process of material extrusion using 3D printing involves the direct deposition of material onto a substrate using a computer-controlled nozzle head, facilitated by either a mechanical or pneumatic system. Various extrusion-based 3D printing methodologies have a common operational principle, where material is continuously deposited. These techniques can be categorized into two distinct groups: the first involves the melting of material, while the second requires dispensing material without the need for melting [76].

The Fused Deposition Modeling (FDM) process, along with its variations including Precise Extrusion Manufacturing (PEM), Precise Extrusion Deposition (PED) and Multi-Phase Jet Solidification (MJS), are additive manufacturing methods that depend on the melting of materials to achieve three-dimensional printing. In contrast, solvent-based extrusion free-forming, pressure-assisted microsyringe (PAM), low-temperature deposition manufacturing (LDM) and direct ink writing (DIW) are additive manufacturing methods that do not involve the melting of materials. In the process of melting, two often utilized types of nozzles are the screw-driven and wheel-driven filament extruders. In the context of non-melting mode, it is common to employ four types of nozzles: piezoelectric actuated, pressure-driven, solenoid and volume-driven injection dispensers [79]. Figure 2.33 presents a schematic view of the processes for FDM as well as DIW 3D printing technologies.

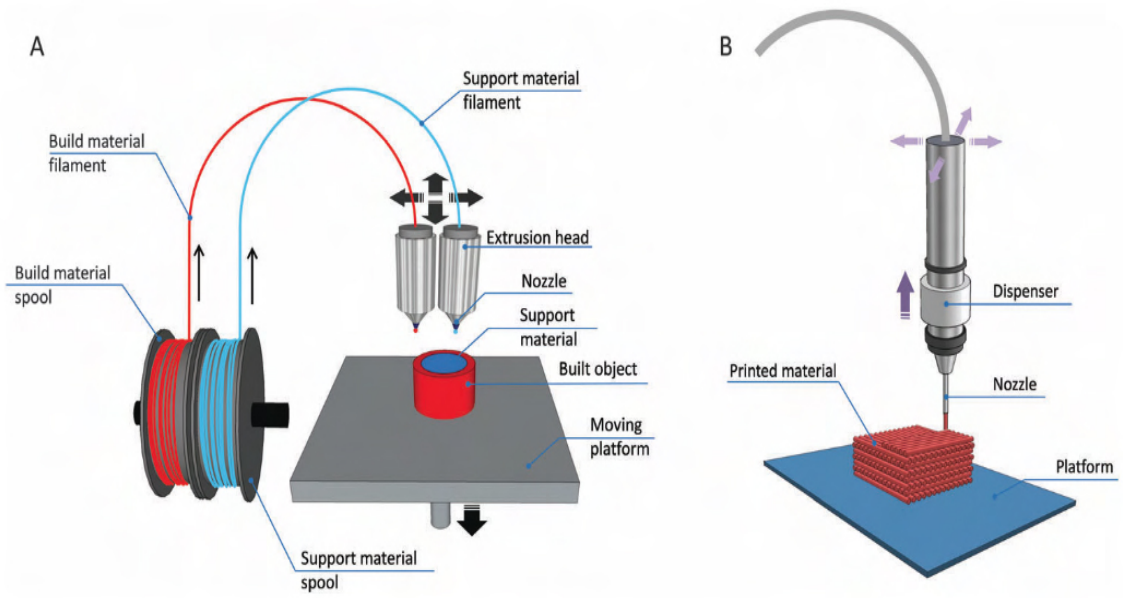

Figure 2.33. Schematic representation of 3D printing procedures based on material extrusion. Two techniques involved in this technology are shown as (A) and (B), being these fused deposition modeling (FDM) and direct ink writing (DIW), respectively [76].

Particularly, the direct ink writing (DIW) technique can be applied in situations where there is a need for extensive manufacturing of flexible LED, energy conversion devices and stretchable electrodes [80]. The DIW approach provides a method for precise and regulated deposition of individual ink materials, as well as the ability to combine several ink materials. These ink materials possess a high viscosity, ensuring that they maintain their shape and do not undergo deformation upon deposition [81]. In this particular context, a vast array of components, spanning from nanoparticles to food-grade substances and even live cells, holds the potential to be utilized for the purpose of implementing 3D printing [82].

The selection of an appropriate extruder for the production of a desired 3D model is heavily influenced by several important aspects, including the type of material, particle size, ink density, and viscosity. The strategic importance and popularity of this technology for the deposition of soft materials can be attributed to its greater rate of material utilization, diverse ink composition options, and cost-effectiveness [81]. Following the deposition of the material, the subsequent stages of the printing process involve thermal treatment, desiccation, elimination of solvents, and chemical alterations achieved via sintering or cross-linking [83]. Therefore, the utilization of this 3D printing process can potentially facilitate the production of wearable sensors, incorporating advantageous attributes such as flexibility, recyclability, self-healing capability, stretchability and conductivity, among others [81, 82].

2.4 Wearable Gas Sensors

The recognition of the necessity for gas detection originated subsequent to the observation of the harmful effects of toxic gases on the well-being of laborers in the era of industrialization. Consequently, industries in which individuals may come into contact with such gases necessitated the implementation of a mechanism to notify them of the gas's presence. Coal miners were indeed affected by this situation, causing the development of gas detection techniques as a preventative measure in the mining industry [84].

Different strategies were developed in order to detect these harmful gases at those times, and eventually sensors became part of these ones as well. In addition to their conventional utilization in coal mines, gas sensors have become more essential in a wider variety of applications. These include but are not limited to indoor and outdoor air quality monitoring, industrial manufacturing, national defense and chemical process regulation. Nowadays, there is a strong demand for sensors in industrial applications that show better responsiveness, improved safety, ease of operation, portability, cost-effectiveness, and heightened sensitivity towards specific target analytes compared to currently available technology. Apart from these characteristics, there is an increased need for miniaturization in gas sensors' applications, particularly those that may be portable and capable of being integrated into the Internet of Things (IoT). This necessitates manufacturing procedures that facilitate reduced cost and material consumption [84].

In this context, over the course of time, technological advancements have led to a diversification in the field of technology for manufacturing sensors, resulting in the evolution and progression of printed electronics in terms of techniques, applications, and materials. Current advancements in printing methodologies have facilitated the production of personalized devices, incorporation of nanoscale characteristics, and the seamless integration of many materials and functionalities at lower temperatures onto a single substrate. These developments have opened up novel possibilities for the creation of printed sensors [85]. Nevertheless, despite their small size, high sensitivity and high integration, commercial gas sensors are often produced on rigid substrates and designed to operate at elevated temperatures, making them impractical for daily use [86].

Hence, there is an urgent need to design easily operable and transportable sensors that possess the ability to sensitively and selectively monitor gases in real-time, thus allowing effective gas detection. The field of wearable devices has experienced significant growth in both research and commercialization for gas sensors due to advancements in materials science and manufacturing capabilities. Wearable devices, which are portable electronic equipment that incorporate sensors, have gained substantial attention. These devices can be found integrated into various accessories such as watches, clothes, bracelets, necklaces, and even directly attached to the human body [87]. Zhou et. al. [88] presents in Figure 2.34 the different fabrication techniques for wearable gas sensors.

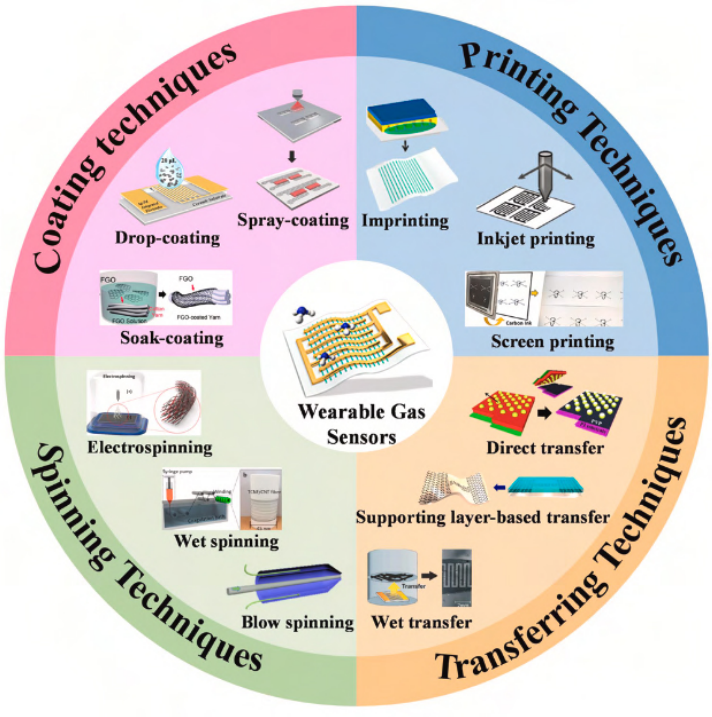

Figure 2.34. Schematic illustration showing the representative manufacturing techniques employed in the production of wearable gas sensors [88].

2.4.0.1 Electronic Techniques Utilized in Gas Sensing and Common Sensor Structures

Gas sensors can be categorized based on their method of signal transduction, which includes electrochemical, optical, acoustical, thermometric, or gravimetric sensors. Electrically-transduced gas sensors have received significant attention in research due to their inherent advantages, including compatibility, portability, simplicity with ordinary electronics, capability of continuous monitoring, non-line-of-sight detection, and possibility for wireless transmission [89].

A gas sensing device that utilizes electrical transduction typically has two primary elements: the sensing material and the transducer as it is shown in Figure 2.35 [84]. The sensing material, when exposed to the surrounding atmosphere, interacts in covalent or noncovalent interactions with the target gas. This interaction leads to alterations in one or more physical properties of the sensing material, such as changes in electrical conductivity ($\Delta\sigma$), work function ($\Delta\varphi$), and permittivity ($\Delta\varepsilon$) [90].

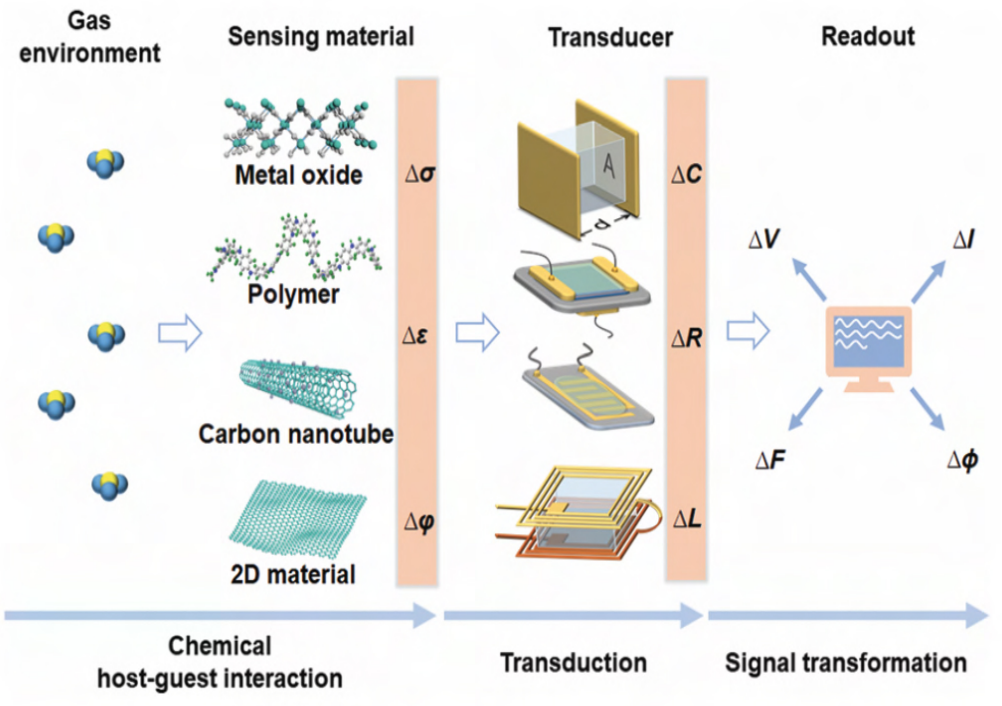

Figure 2.35. Schematic image illustrating the process of electrical gas detection [84].

After this, standard electronic components of the gas sensor, including capacitors, diodes, resistors, and field-effect transistors (FETs), experience changes in their physical properties that are subsequently translated into variations in their electrical parameters, such as capacitance (ΔC), resistance (ΔR), and inductance (ΔL). These variations are ultimately expressed as changes in device current (ΔI) or voltage (ΔV), which can be measured in terms of magnitude, frequency (ΔF), and phase ($\Delta \Phi$) [91]. Printed-enabled gas sensors utilize several device architectures to transform gas-solid interactions into electrical signals. These structures include field-effect transistors (FETs), chemiresistors, inductors and capacitors, as depicted in Figure 2.36 [84].

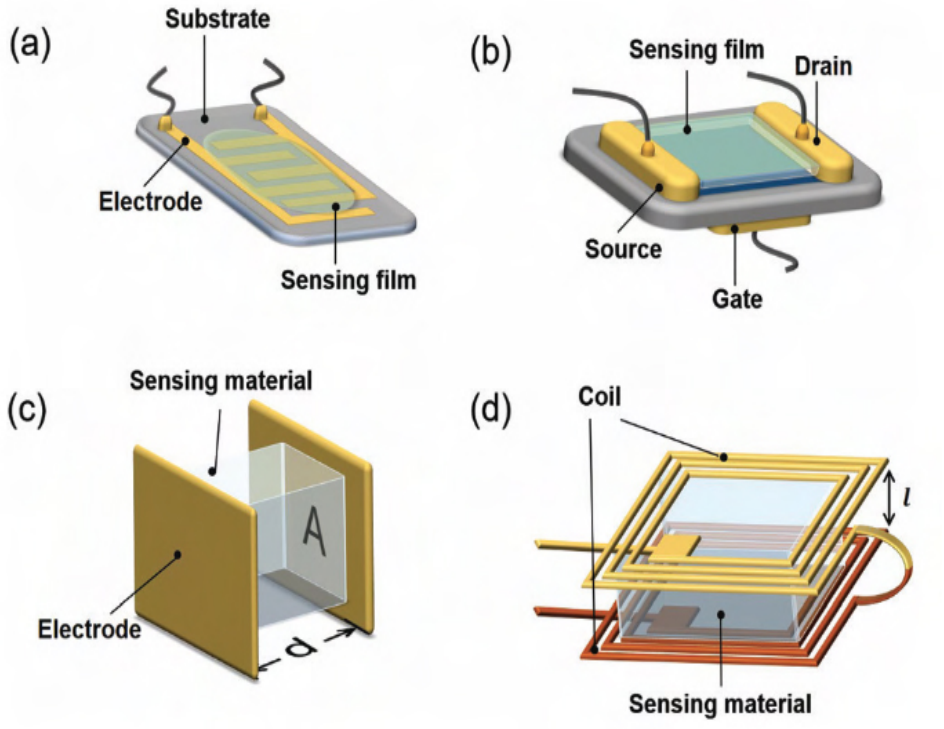

Figure 2.36. Schematic description of four types of gas sensors: chemiresistive, field-effect transistor (FET), capacitive, and inductive. In (c), the symbol A denotes the interface area between the dielectric sensing material and the electrodes, while the symbol d represents the distance separating the parallel electrodes. In (d), the variable l denotes the distance between the coils [84].

2.4.0.2 NO_2 Gas Detection

Nitrogen dioxide (NO_2) is a volatile gas characterized by its pungent odor. It possesses poisonous properties which represent a significant threat to human health and have negative impacts on the environment. Nitrogen dioxide (NO_2) is generated through various mechanisms, including the combustion of fossil fuels, car exhaust emissions, and the release of pollutants from industrial facilities. Furthermore, nitrogen dioxide (NO_2), being a volatile gas, has the ability to interact in photochemical reactions with other pollutants or water, resulting in the production of ozone or acid rain. It also has the potential to be generated as a secondary pollutant, hence increasing its harmful effects on the environment. In addition, the emission of this gas is known to induce pain in the nasal and throat regions, resulting in temporary coughing, eye irritation, exhaustion, and nausea, even at concentrations below 10 parts per million (ppm). Additionally, it can aggravate pulmonary disorders, leading to significant health implications, often without presenting any noticeable symptoms [92]. Therefore, the detection of the dangerous NO2 gas has been an important sensing technology in recent times. Particularly, the development of wearable gas sensors capable of detecting this harmful gas is really important since these devices can be worn and able to detect, prevent and avoid the negative effects that this gas represents in the environment. For instance, Wang et. al. [93] presents a gas sensor integrated into wearable electronics capable of providing sensitive, selective and real-time data for the detection of harmful gases in the environment in Figure 2.37.

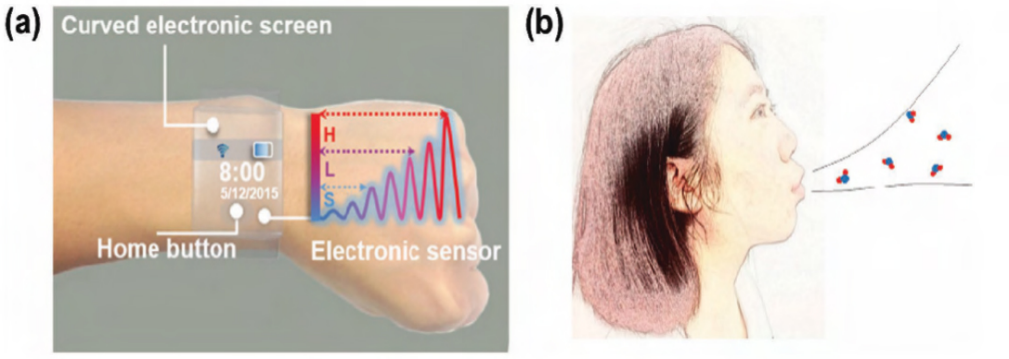

Figure 2.37. a) Image of a flexible and transparent electronic sensor that has been incorporated into wearable devices. b) The sensor can also detect exhaled gases, which can provide information on the degree of air pollution or the physiological status of the individual [93].

Experimental Approach

The present work presents the fabrication of a 3D printed flexible electronic platform capable of withstand mechanical fatigue such as bending during long periods of time. In order to fabricate this platform, various 3D printing technologies were utilized, being these ones, stereolithography (SLA) and direct ink writing (DIW). For the first part of the experiments, a platform was printed using a light-sensitive resin by SLA. Once the platform was printed, a line was printed onto the surface of this flexible platform by DIW where the material used was a stretchable conductor. After the deposition of the stretchable conductor on the surface, a post-treatment was carried out by sintering the 3D printed platform in a specific temperature and time. This was done in order to make the line conductive since the stretchable conductor was not conductive without a sintering process. Then, the flexible platform with the printed line was exposed to mechanical fatigue being this one a bending movement. This was done in order to see the change in resistance for the conductive line over a long period of time, giving insights for its use as a wearable platform for the development of a wearable gas sensor. Moreover, an embedded gas sensor fabricated by students at Youngstown State University was further utilized for the detection of NO_2 gas at different polluted environment scenarios.

3.1 Materials

Different materials were used in order to fabricate the 3D printed flexible electronic platform. The photopolymer resin Elastic 50A was purchased from Formlabs as the elastomeric material with high elongation in order to print the platform. The stretchable silver conductor SS1109 with volume resistivity of 4.5 x 10^{-5} Ω cm was purchased from ACI Materials and nothing was added to it. Non of the materials present in this work were purified or received any additional treatment apart from the sintering process that was used in order to make conductive the stretchable conductor. Moreover, two different 3D printers were used in this work. The 3D printer named Form 3+ and manufactured by Formlabs was used for printing the platform using the SLA technique while the 3D printer named Hyrel EHR was utilized for printing the conductive line and circuit onto the platform by using the DIW technique. This Hyrel EHR printer is fabricated by the company Hyrel 3D. In Figures 3.1 and 3.2, the materials and the 3D printers mentioned above are presented, respectively.

(a) Photopolymer resin Elastic 50A.

(b) Stretchable silver conductor SS1109.

Figure 3.1. Materials utilized for the fabrication of the 3D printed flexible electronic platform.

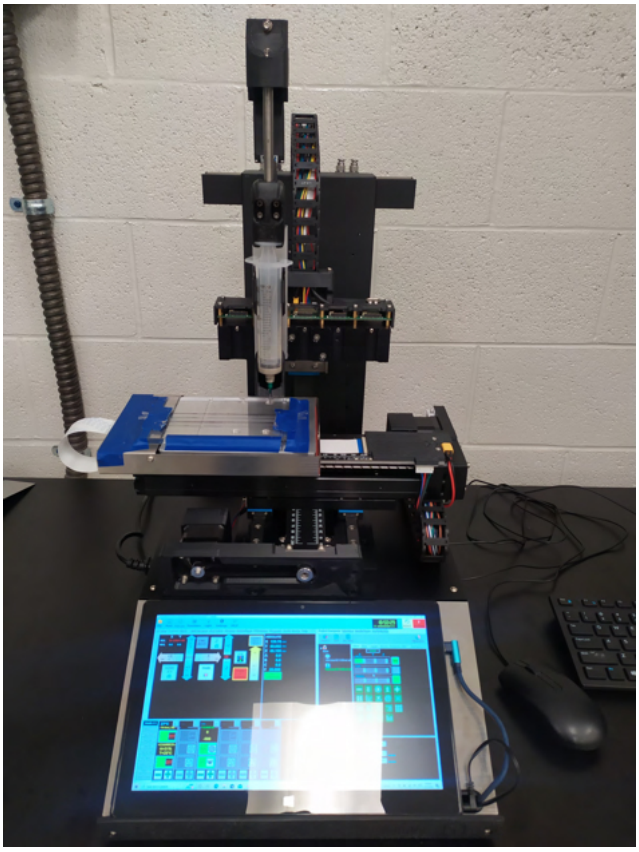

(a) Hyrel EHR.

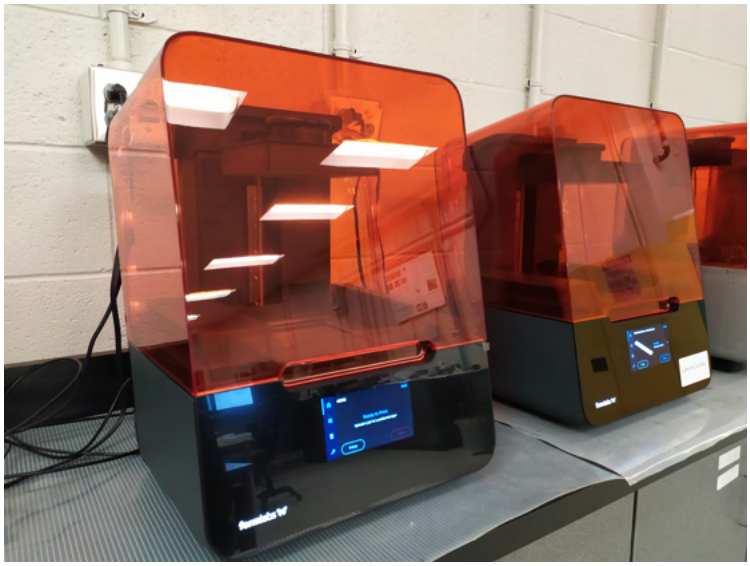

(b) Form 3+.

Figure 3.2. 3D printers used for the fabrication of the 3D printed flexible electronic platform.

3.2 Process for the Fabrication of the Platform and Circuit utilizing 3D Printing

For the first part of the experiments, the evaluation of the electrical resistance for the stretchable conductor was evaluated under bending fatigue for a period of 22.5 hr. Firstly, a platform was printed by SLA using the Formlabs 3D printer. Once printed, this platform was washed inside isopropyl alcohol for 10 minutes, and then exposed to a post-cure time of 30 minutes inside a UV curing box at a temperature of 60ºC as the Formlabs manufacturer recommends. After this process, a single line of the stretchable conductor was printed onto the surface of this printed flexible platform by using the 3D printer Hyrel EHR. Then, the flexible platform with the printed line were exposed to a sintering process for 7 minutes at 140ºC in order to make conductive the stretchable conductor. Lastly, the bending test was performed and the platform with the conductive line were exposed to a continuous bending movement for 22.5 hr while the change of the electrical resistance was collected. One important thing to mention is that the 3D designs for the platform and circuit were created by the Software Fusion 360. In Figure 3.3 is presented the design for the platform and its dimensions while in Figure 3.4 are shown the design and the dimensions of the printed conductive line as well.

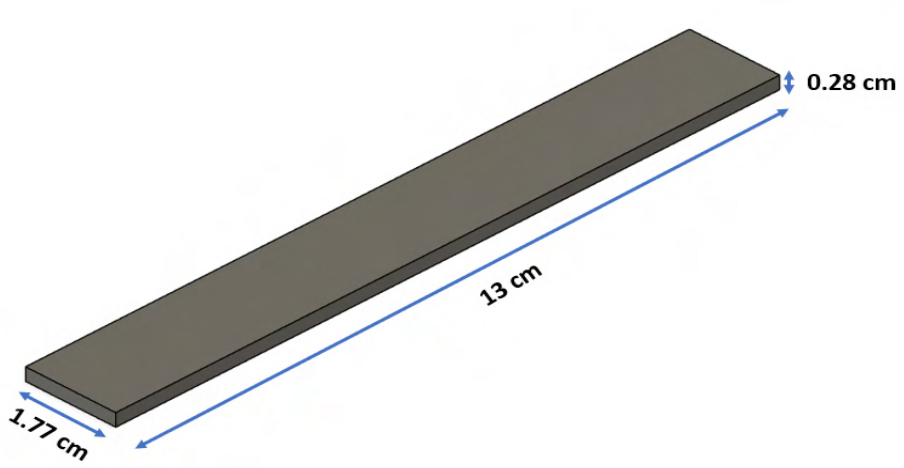

Figure 3.3. 3D design of the platform and its dimensions.

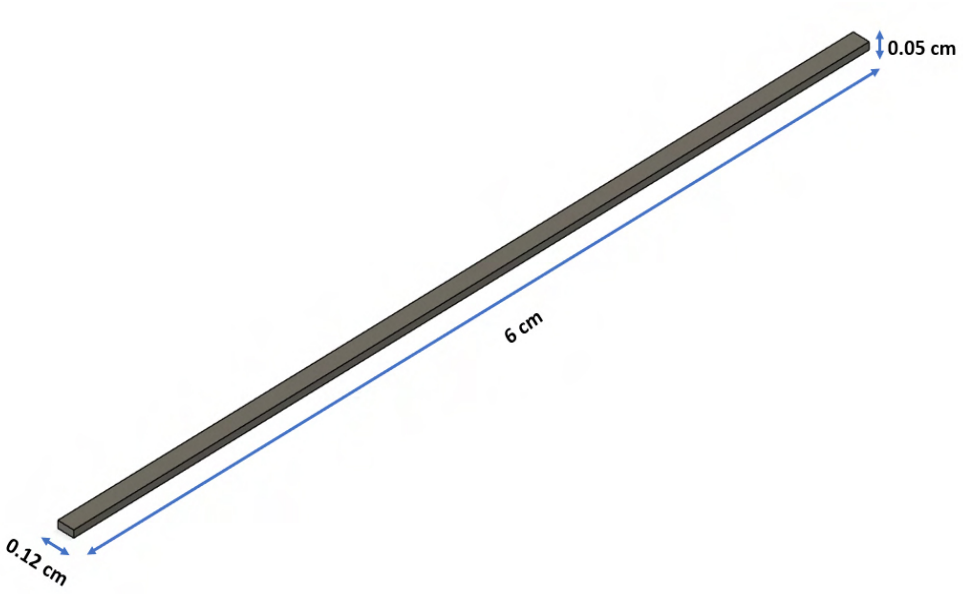

Figure 3.4. 3D design for printing the stretchable conductor line.

In Figure 3.5 are shown both the platform and the conductive line once printed. For the second part of the experiments, other two different 3D designs were produced for the development of the 3D printed flexible electronic platform. These 3D designs, also created by the software Fusion 360, include a wider platform that was printed using SLA, see Figure 3.6, and an electronic circuit made of the stretchable conductor and printed by DIW, see Figure 3.7. The printing process for each design as well as their pos-treatment process were the same as the ones previously mentioned above. Nevertheless, for these experiments, the evaluation of the voltage for this printed circuit was evaluated under bending fatigue. The electronic circuit consisted of an LED light, a resistor and a power source which are shown in Figure 3.8. It is important to mention that these components were placed by hand in each specific place in order to close the circuit. For instance, the characteristics of the resistor were a resistance value of 10,000 Ohm, tolerance of 1% and power of 1/4 Watts.

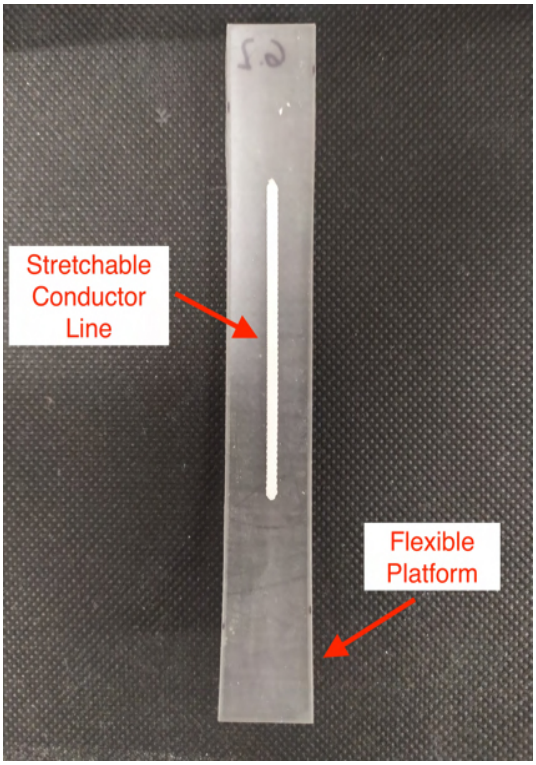

Figure 3.5. Both platform and conductive line once printed.

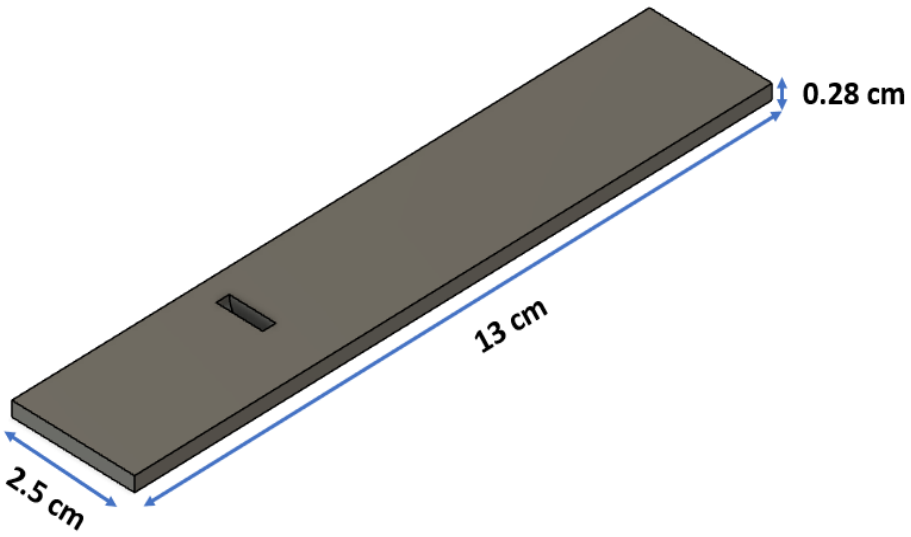

Figure 3.6. Design and dimensions of the flexible platform where the circuit is printed onto.

Regarding the specifications of the LED light, it worked with direct current values from 2 to 3 volts and 20 mA, as well as it was a 1206 SMD type of chip size. These two components were purchased from the website Amazon. In the other hand, for the power source, a direct current (DC) power supplier was used in order to provide a constant voltage of 3V to the printed circuit while the bending fatigue was carried out. The model for this power supplier was a XP-752A by the company Elenco Electronics, Inc. This device can be shown in Figure 3.9.

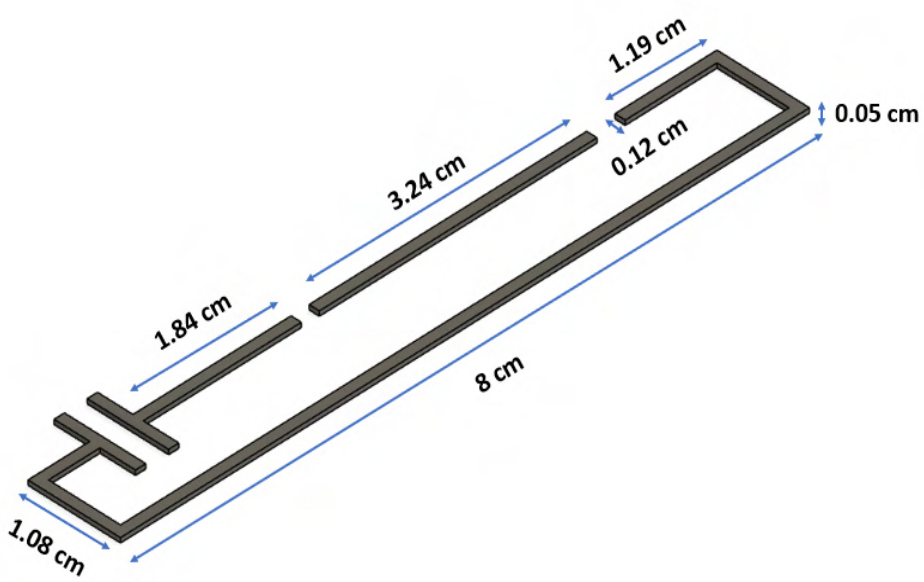

Figure 3.7. Design and dimensions of the 3D printed electronic circuit.

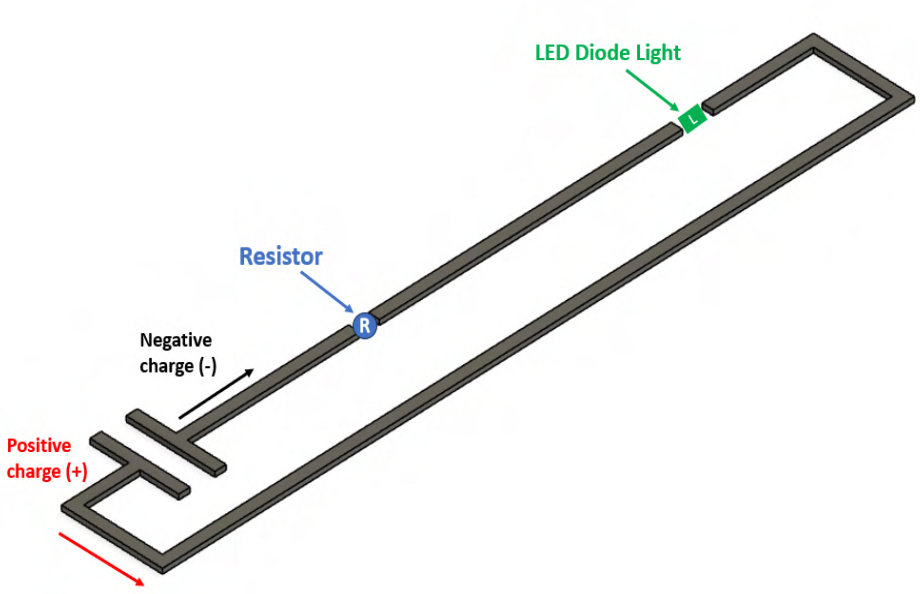

Figure 3.8. Components that constitute the electronic circuit.

Figure 3.9. Direct current (DC) power supplier.

3.3 Methodology for the Bending Test

The methodology in this work was based on previous published papers. Particularly, the methodology of the published article by Su et. al. [94] was of really importance in order to take into account different variables that were involved during the bending movement. Some of these variables are shown in Figure 3.10, where the symbol L_o represents the length of the substrate in an initial state while symbol θ represents the angle in which it is bended.

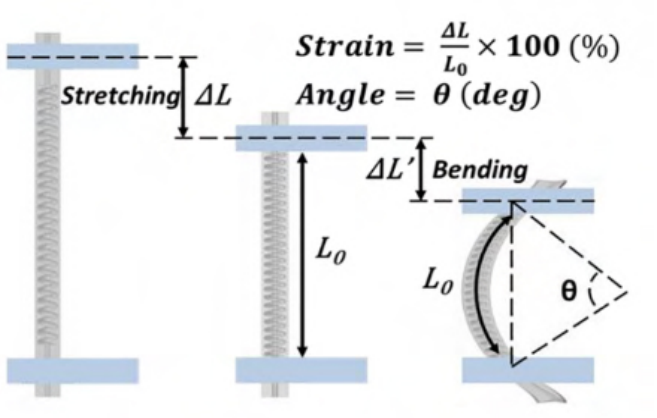

Figure 3.10. Schematic view of the bending movement [94].

In this regard, the set up for this experiment began with clamping the flexible printed platform with either the conductive circuit or the conductive line to its both ends using an instrument Mark-10 model ESM303, see Figures 3.11 and 3.12. Once the flexible platform was clamped, the crossheads speed was stablished to a value of 330 mm/min and a total number of cycles was set to 4,050 cycles. However, in order to calculate the angle θ at which the samples were bended, it was followed the methodology given by Su et. al. [94]. This one explained how to calculate this angle by two equations once the geometry in Figure 3.13 is examined.

Figure 3.11. Mark-10 Instrument. Model ESM303.

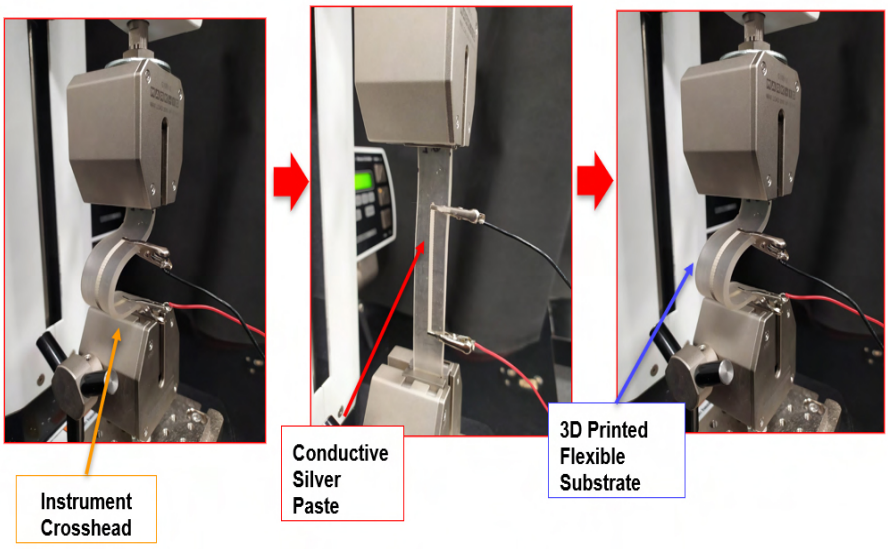

Figure 3.12. 3D printed flexible platform clamped to the Mark-10 instrument.

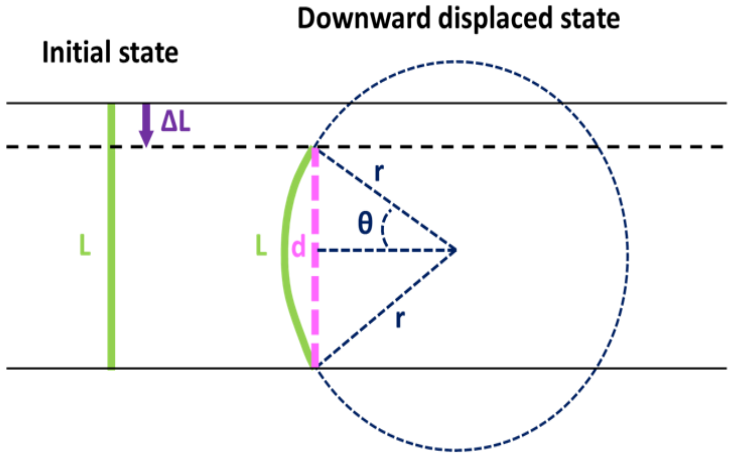

Figure 3.13. Schematic representation of the methodology employed for calculating the radius of curvature [94].

From Figure 3.13, L represents the initial length of the flexible platform while ΔL defines the downward displacement once the bending movement starts. Moreover, d represents the length of the platform once it has reached the maximum bending point at a specific angle θ. Looking at the geometry in Figure 3.13, two equations can be identified as:

$$L = r(2\theta) \tag{3.1}$$

$$sin(\theta) = \frac{d}{2r} \tag{3.2}$$

Combining equations 3.1 and 3.2 and eliminating r from them, we have:

$$\frac{d}{L} = \frac{sin(\theta)}{\theta} \tag{3.3}$$

For this equation, the values of L and d were given as 10.5 cm and 5.5 cm, respectively. Once these values were known, the equation 3.3 was solved using the MATLAB software with the command vpasolve giving a value of 105.44º for θ. After calculating the angle, the experimental set up looked like as it is shown in Figure 3.14

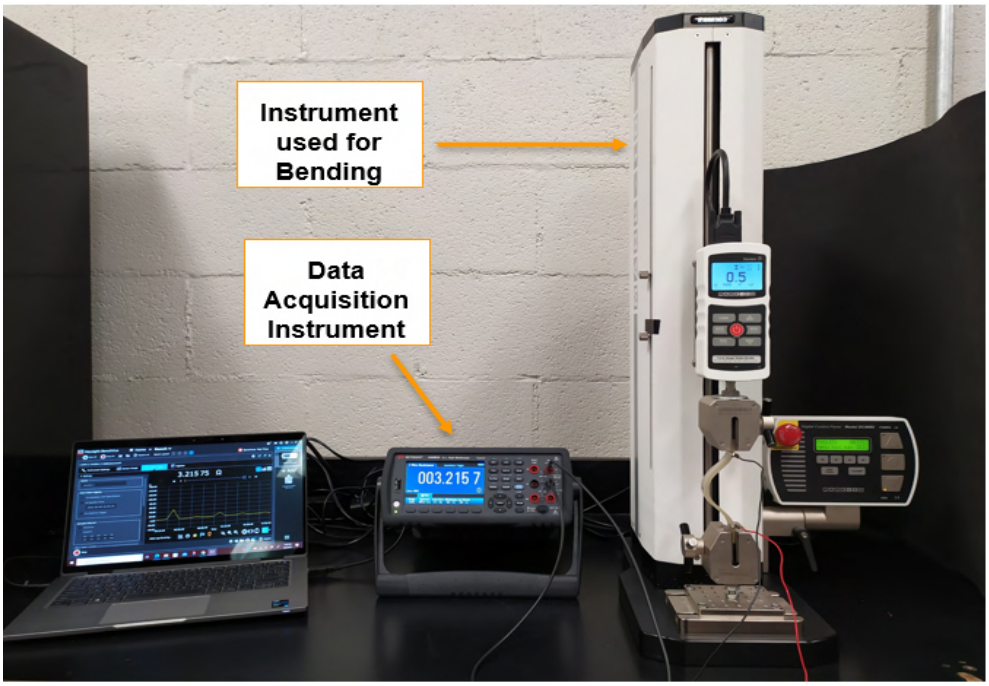

Figure 3.14. Experimental setup for the bending test.

In order to measure the change in the electrical resistance for the conductive line as well as the change in the voltage for the printed circuit, two alligator clips were clamped to both ends of the flexible platform. The collection of the data was accomplished by the utilization of a data acquisition instrument, being this one a 34465A model digit multimeter manufactured by the company Keysight. Moreover, these experimental data were plotted and saved using a software called BenchVue, also product of the company Keysight. The methodology for the collection of the data consisted of collecting each second the value of either the electrical resistance or the voltage while the bending movement was carried out. The collection of the data started at the maximum bending position (θ =105.44º) without movement for 1 minute, and after this, the bending movement started and lasted for 22.5 h. Once the bending movement finished, experimental data were still collected for one more minute at the maximum bending position in order to get a proper and constant value. It is important to mention that the duration of one bending cycle in these experiments was 20 seconds, which is 0.05 Hertz. Therefore, the complete duration of the experiment was 22.5 h for 4,050 cycles. A schematic view of the process for one bending cycle is depicted in Figure 3.15.

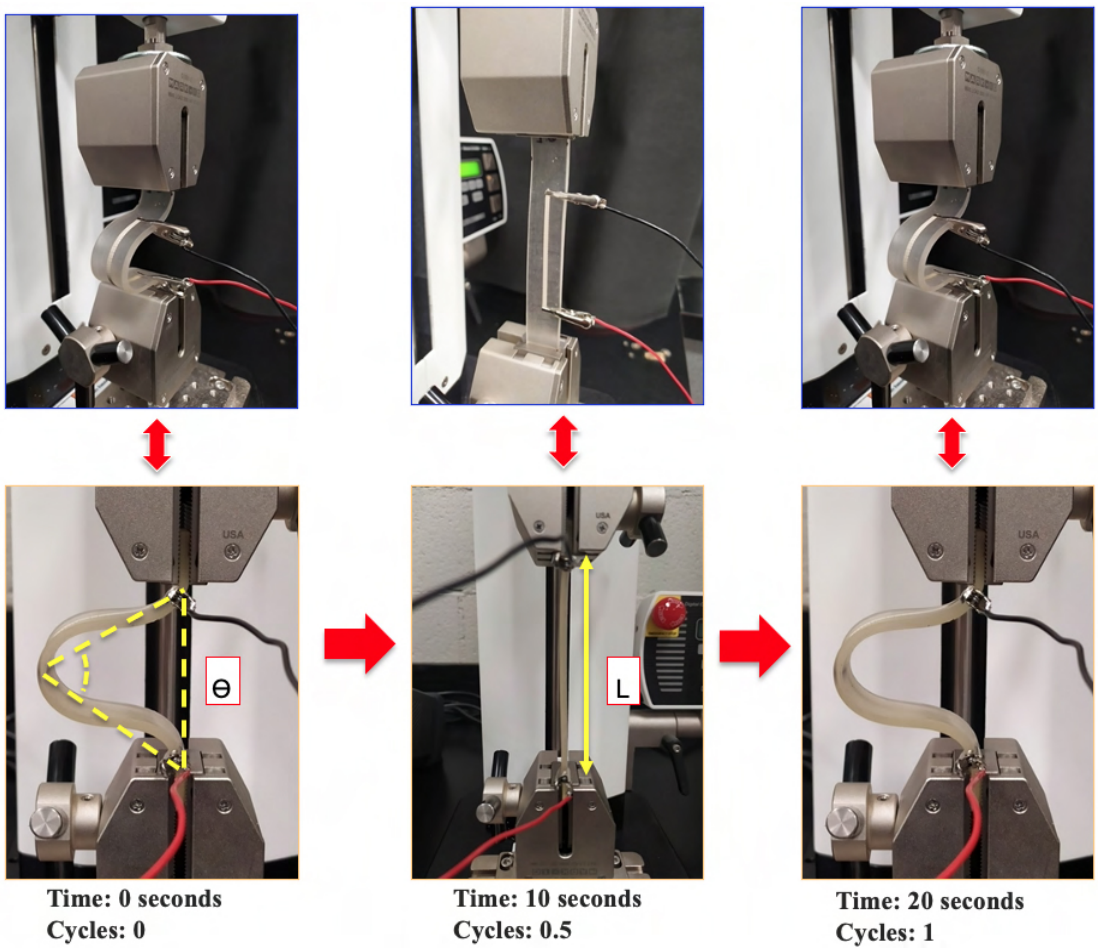

Figure 3.15. Schematic view of one bending cycle.

3.3.1 Embedded and Not-Embedded System

In the present work, the evaluation of the change in the electrical resistance for a flexible printed conductive line as well as the change in the voltage for a flexible printed circuit were investigated. Nevertheless, for the experiments related with the evaluation of the electrical resistance, two different configurations or systems were studied in order to understand their behavior under bending fatigue. These two configurations consisted of an embedded and not-embedded system. The difference between these two relied on an additional photopolymer resin layer (Resin Elastic 50A) for the embedded system in order to avoid the formation of cracks during the bending movement that could cause the lost of the conductivity for the printed line.

Indeed, the addition of this layer enhance the interaction between the flexible platform and the stretchable conductor leading to a better performance for this last one under bending fatigue. In other words, this additional layer helps keeping a constant value of electrical resistance which can be explained as a good electrical conductivity under mechanical fatigue. These two systems are shown in Figure 3.16.

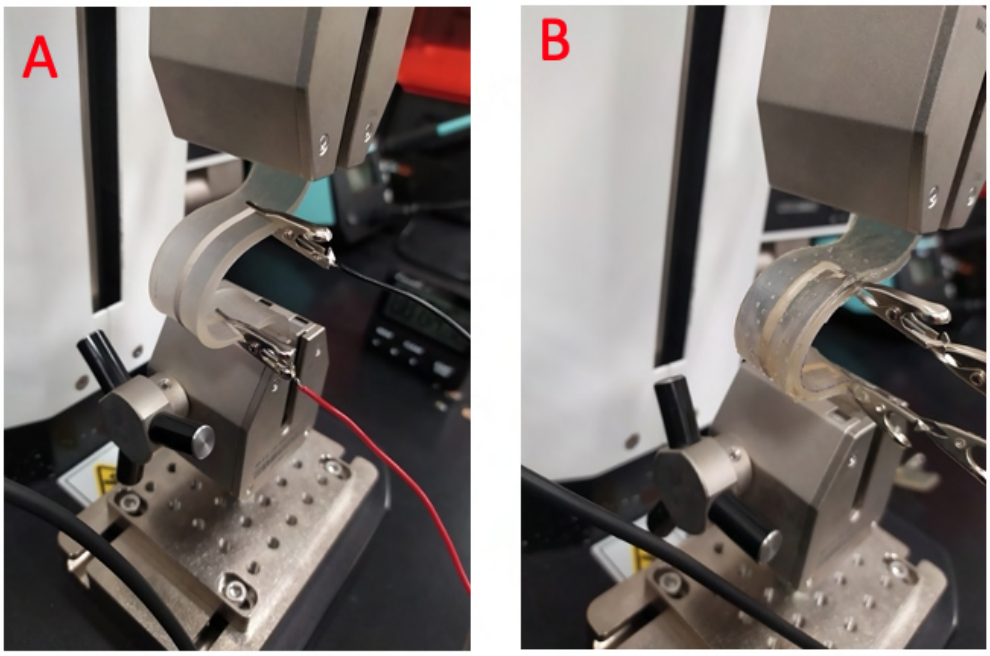

Figure 3.16. Different design strategies used in order to see how the bending movement affects the electrical conductivity. Figure A) shows the not-embedded system while Figure B) shows the embedded system.

It is important to mention that for the experiments related with the evaluation of the change in the voltage for the flexible printed circuit, the system was embedded in order to avoid the disadvantages of a not-embedded system which are the generation of cracks using this type of system, increment of the power consumption and limiting the overall performance of the stretchable conductor. Therefore, for this experiment, these drawbacks did not play a significant role for the behavior of the change in the voltage while the bending fatigue was taking place. Figure 3.17 shows the LED light on of the flexible conductive circuit once an energy potential of 3V was provided by the DC power supplier. Moreover, this figure shows the parts of this printed circuit.

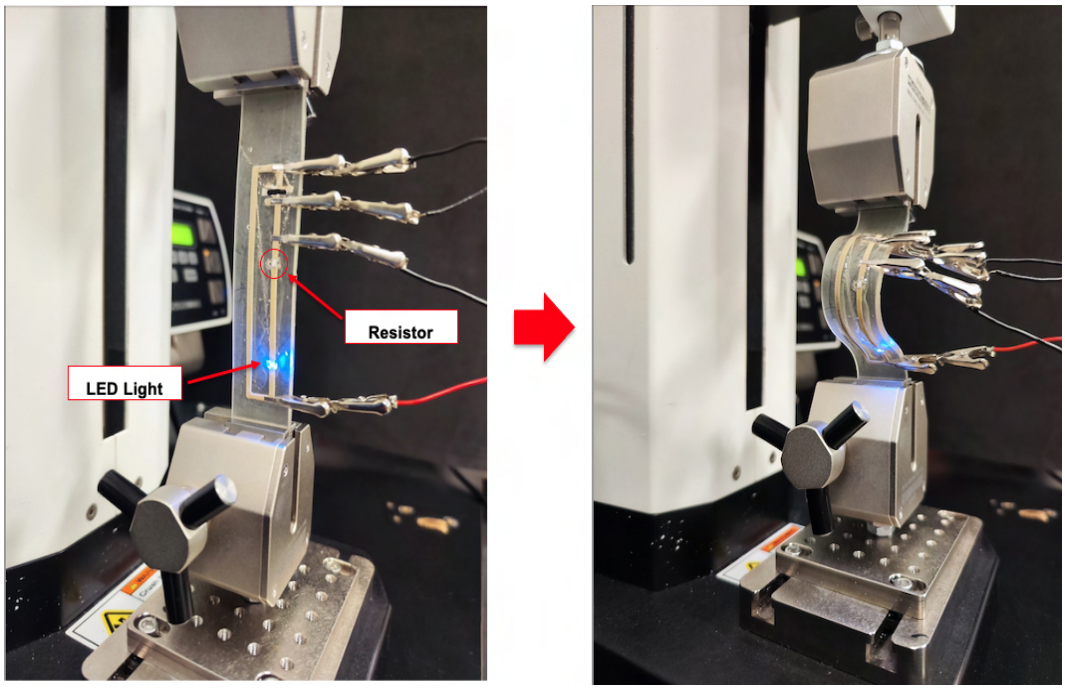

Figure 3.17. Flexible 3D printed circuit.

3.4 Adhesion Test

In order to evaluate the interaction between the flexible substrate and the stretchable conductor, an adhesion test was carried out. Indeed, the durability of a printed sample's adherence to the substrate is an important factor, which is significantly impacted by the surface characteristics of the substrate, the ink's wetting and penetration into the substrate, and the ink's composition [95]. Furthermore, the sintering process is a crucial factor that greatly influences the adherence of the ink to the substrate. The control of parameters such as the solvent evaporation rate, ink drying time, and sintering temperature is achieved through the process of sintering. It is also important to mention that the augmented roughness of the substrate can result in a decrease in adhesive strength. This occurs when the ink elements fail to penetrate the troughs, particularly when the particle size exceeds that of the troughs as it can be seen in Figure 3.18. This phenomenon leads to the creation of empty spaces in which moisture might become trapped, so compromising the adhesive's strength [95].

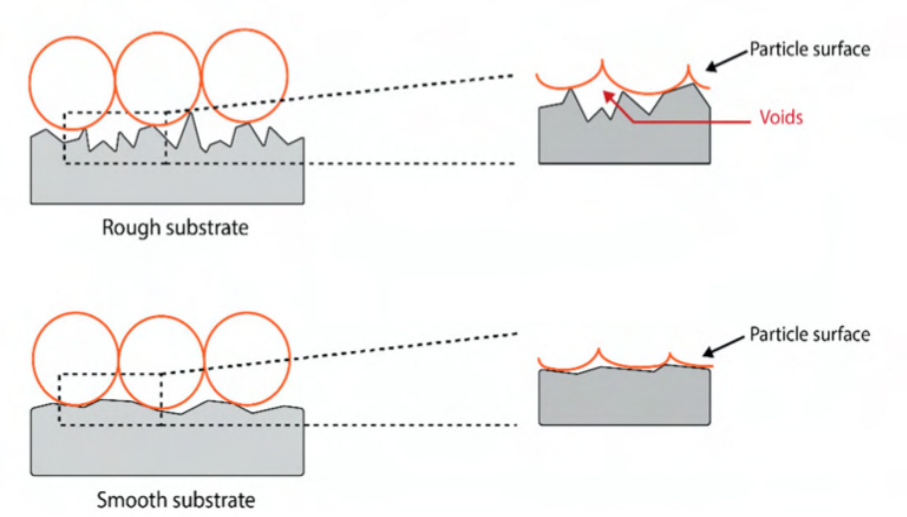

Figure 3.18. Adhesion properties of particles on surfaces with different roughness levels, specifically a rough surface and a smooth surface. The magnified observations reveal the presence of voids in the post-deposition processing stage, particularly in circumstances where the surface exhibits roughness [95].

The ASTM standard (ASTM D3359-17) [96] was firstly reviewed for its implementation in this work using the flexible substrate. The methodology of this ASTM standard consists in the application and subsequent removal of pressure-sensitive tape onto incisions created in the sintered films. Nevertheless, it is a qualitative method, meaning it offers a binary determination of either ”yes” or ”no” and provides a straightforward assessment of adhesion degree in a quick and uncomplicated manner. Even though this method might give a quick evaluation of the adhesion strength between the flexible substrate and the stretchable conductor, a slightly different methodology was used. Firstly, a stretchable conductor line of 6 cm was printed by DIW onto a flexible substrate with dimensions 0.28 cm (H) x 4.5 cm (W) x 13.0 cm (D) following the post treatment process for sintering, see Figure 3.19. The experimental setup for the adhesion test is shown in Figure 3.20. For this experiment, an Instron machine model 5967 was utilized in order to remove the adhesion test tape from the flexible substrate at a specific velocity of 5 mm per minute using a static load cell of 100 N, see Figure 3.20a. While this experiment was taking place, experimental data for the strength or load in Newtons and the extension in mm were collected.

The adhesion tape was purchased from Amazon, and it was manufactured specifically for its use for the ASTM standard D3359-17. Moreover, a total length of 3.18 cm was set as the maximum extension for the head to move upwards while the total extension of the removed tape from the flexible substrate was 5 cm.

Figure 3.19. Printed flexible platform and conductive line for the adhesion test.

(a) Instron machine model 5967.

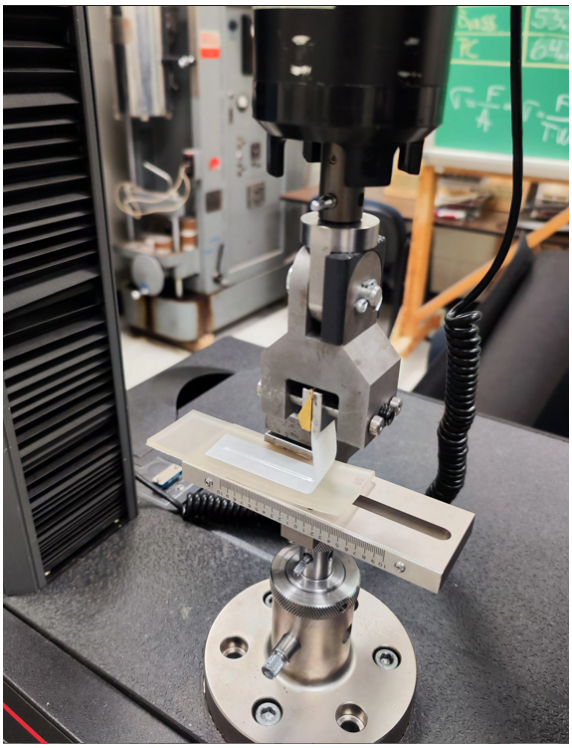

(b) Adhesion tape placed onto the stretchable conductor line.

Figure 3.20. Experimental setup for adhesion test.

It is of great importance to mention that the height of the printed line was measured before and after the adhesion test using a digital microscope in order to see how much conductive material was removed once the test was finished. This part of the experiment was able to give quantitive results of the actual change in the height of the printed line, providing a better understanding of the adhesion strength between the flexible substrate and the stretchable conductor. Regarding the digital microscope that was used for this part of the experiments, it was a model VHX 7000 manufactured by Keyence which can be shown in Figure 3.21.

Figure 3.21. VHX 7000 digital microscope.

3.5 NO_2 Gas Experiment

In the present work, a bluetooth gas sensor developed by alumni at Youngstown State University was used in order to detect the hazardous gas NO_2 at different polluted environments, being this gas sensor shown in Figure 3.22. This gas was generated by following the next chemical reaction:

$$Cu(s) + 4HNO_3(aq) \longrightarrow Cu(NO_3)_2(aq) + 2NO_2(g) + 2H_2O(l)$$

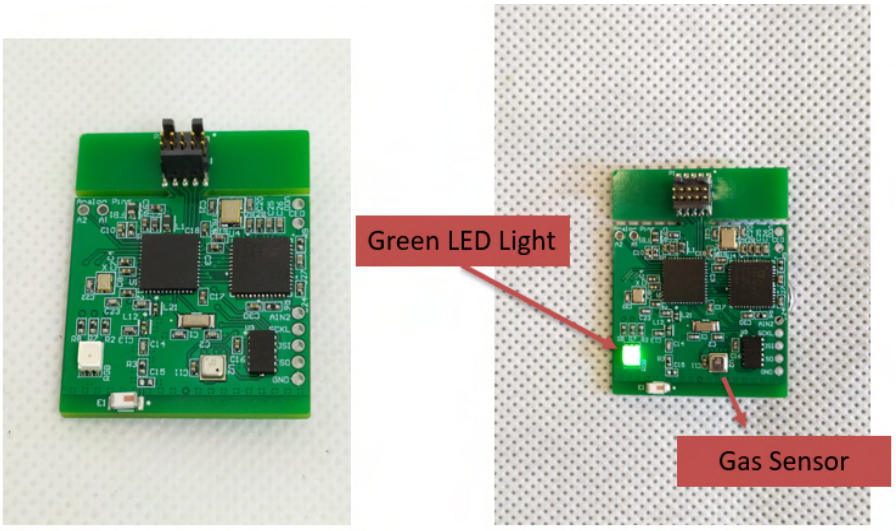

Figure 3.22. Bluetooth gas sensor developed by alumni at Youngstown State University.

The methodology for these experiments involved the utilization of specific measured volumes of nitric acid, $HNO_3(aq)$, and placing them onto copper sheets with given dimensions. By placing these different volumes, the reaction, previously stated, took place and generated different concentrations of $NO_2(g)$ depending of the added volumes. While the generation of the gas was occurring, the gas sensor was placed near the copper sheet so it could be able to detect the gas resistance. In this regard, both the copper sheets and the sensor were placed inside a vacuum desiccator which had a volume of 2.094 liters. This experimental setup is depicted in Figure 3.23. This closed container was used in order to have a specific volume where the reaction could take place and to avoid any interference related with air coming inside or going outside the container, hence collecting more representative results of the gas resistance related with only the generation of the NO_2 gas. For this experiment, proper stoichiometric calculations were done in order to obtain the parts per millon (ppm) generated for the NO_2 gas with the different added volumes of $HNO_3(aq)$. Particularly, these calculations were based on the limiting reagent which in this case was the $HNO_3(aq)$. Regarding the dimensions of the copper sheets, these were 0.008 cm (H) x 2 cm (W) x 2 cm (D), and with respect to the utilized volumes in this experiment, these were 10, 20 and 40 μl.

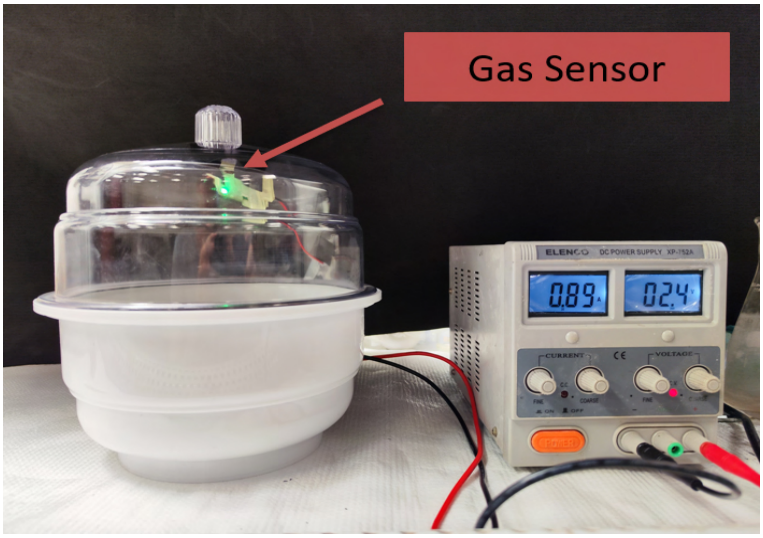

Figure 3.23. Experimental setup for the gas experiment.

One important aspect to mention is that the collection of the gas resistance was completed through the connection between the bluetooth gas sensor with a desktop application also developed by alumni at Youngstown State University. Specifically, this particular characteristic is really important for the application of this sensor as a wearable device for gas detection. Therefore, this bluetooth gas sensor represents a promising alternative for a wearable sensor capable of detecting different gases under different polluted environments.

Continuing with the followed methodology, the gas sensor was embedded using the same material as the flexible platform which was the photopolymer resin Elastic 50A, see Figure 3.24. After the sensor was embedded, the experimental setup was placed, and the different volumes were added to the copper sheets. However, before the addition of the volumes, a proper control experiment was carried out in order to analyze the gas resistance at normal conditions (1 atm, 25 ºC) without any generation of gas. This gave helpful data for the differentiation between a polluted environment and a daily life environment. Once the control experiment was done, the volumes were added and the collection of the values for the gas resistance was done for about 300 seconds. Furthermore, the same power supplier was utilized in order to provide an energy potential of 3V to the sensor so it could operate.

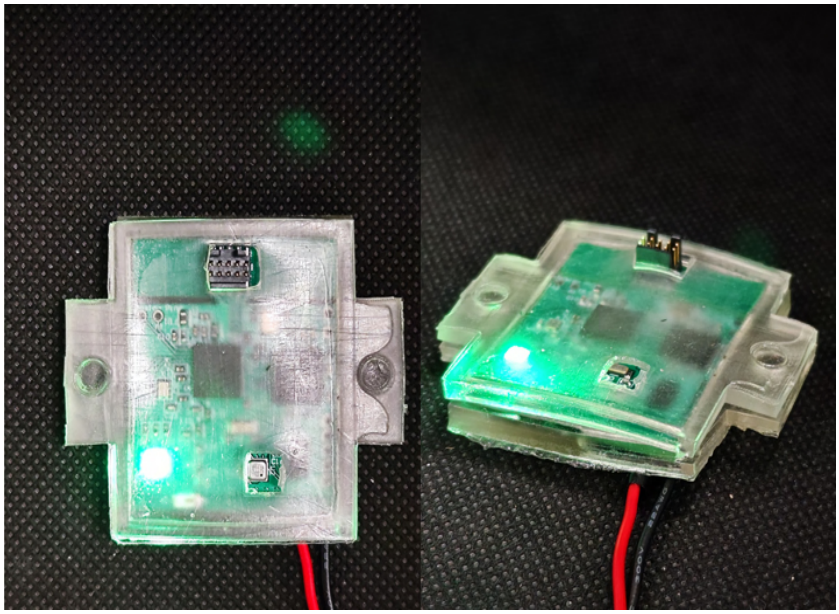

Figure 3.24. Embedded gas sensor.

In addition, the sensing part for the gas detection was a digital low power gas, pressure, temperature and humidity sensor with artificial intelligence model BME 688. This sensor is manufactured by the company Bosch and it is shown in Figure 3.25. Lastly, after the collection of the experimental data for the gas resistance, an average value was considered for each utilized volume. Then, these data were plotted against the values of the calculated ppm from the stoichiometric calculations for each volume. This was done in order to provide a graph capable of showing the relationship between the gas resistance and the concentration of the gas. In this sense, this graph would tell the user the approximate concentration of the gas in the environment depending on the given value for the gas resistance.

Figure 3.25. Sensor gas model BME 688 manufactured by Bosch.

Results and Discussion

4.1 Behavior of the Electrical Resistance under Bending Fatigue

In this section, the experimental results of the electrical resistance under the bending fatigue for the embedded and not-embedded system are presented. For each system, three experiments were carried out by collecting the change of the electrical resistance while the bending movement was taking place. After this, the experimental data were analyzed in two graphs, one representing the electrical resistance versus the time, and the second one showing the electrical resistance against the total number of cycles. For the not-embedded system, these two graphs for the first experiment are shown in Figure 4.1. In this graph, it can be seen that the maximum value for the electrical resistance was 4.95 Ω while the minimum was 0.46 Ω. Even though the electrical resistance changed through all the experiment, the maximum value for this experiment did not reach a value that could represent the total loss of the conductivity for the printed line. Nevertheless, if the experiment had continued, it would have reached bigger values than 4.95 Ω. This could represent a really important disadvantage in terms of performance along the time, however, the stretchable conductor line was exposed to this bending fatigue without interruption which is not a real scenario for a daily life application. Therefore, based on these experimental results, this flexible platform is capable of withstand mechanical fatigue under a prolonged period of time while the electrical conductivity does not change considerably.

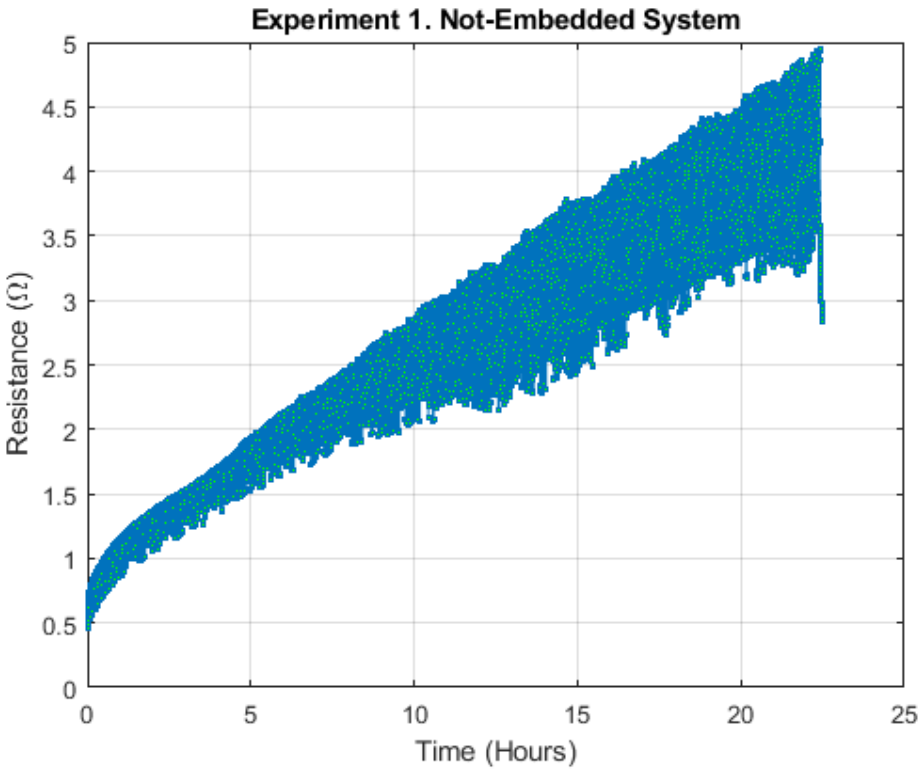

(a) Experimental values for the first experiment. Time vs Resistance.

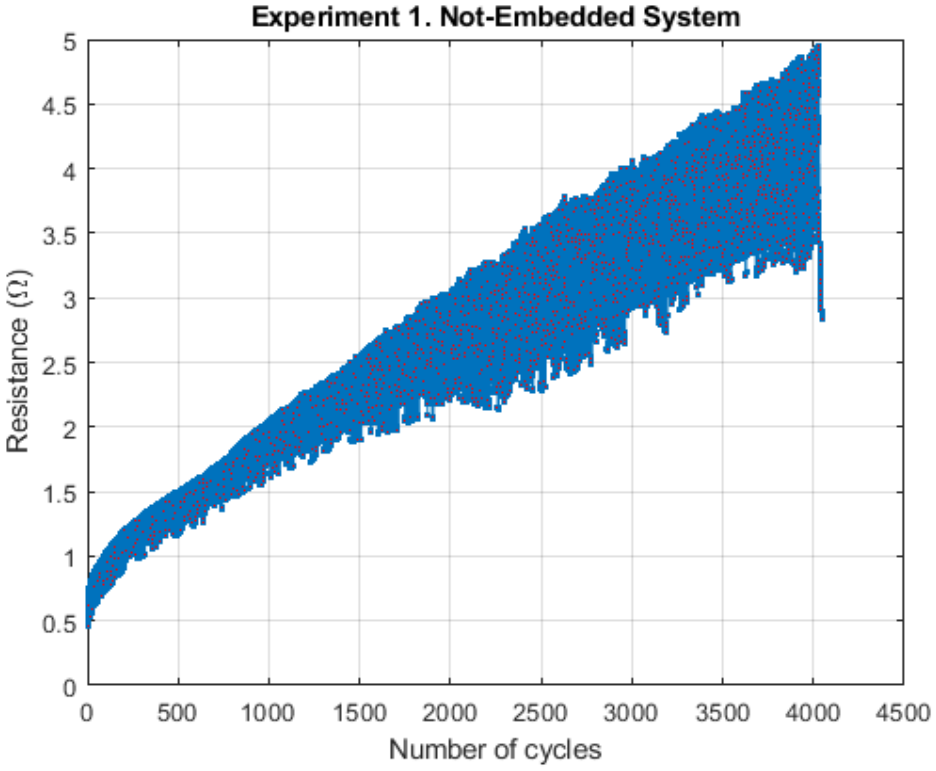

(b) Experimental values for the first experiment . Number of Cycles vs Resistance.

Figure 4.1. Experimental values of the first experiment for the not-embedded system.

The results of the second experiment for the not-embedded system are presented in Figure 4.2 and Figure 4.3 . For this experiment, the maximum and minimum values for the electrical resistance were 2.84 Ω and 0.60 Ω, respectively. As it can be seen, the maximum value for the electrical resistance in this experiment was lower than the one presented by the first experiment. Nevertheless, the behavior related with the continuous increment for the electrical resistance was still observed. As previously discussed, this behavior might not seem the best one in terms of performance, however, the maximum value in this experiment still does not represent a total loss of the conductivity for the stretchable conductor line after the 22.5 h of continuous bending fatigue. Lastly, the results of the third experiment for the not-embedded system are depicted in Figures 4.4 and 4.5. From these figures, it can be seen that the maximum value for the electrical resistance was 7.41 Ω which was the biggest value between the three experiments while the minimum value was 0.43 Ω.

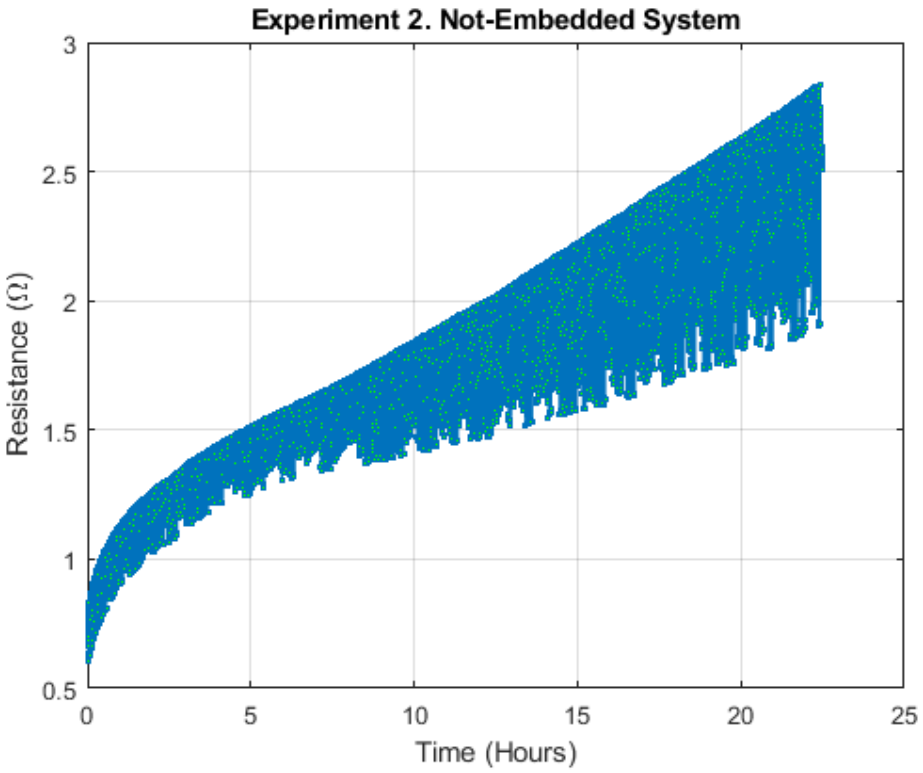

Figure 4.2. Experimental values for the second experiment. Time vs Resistance.

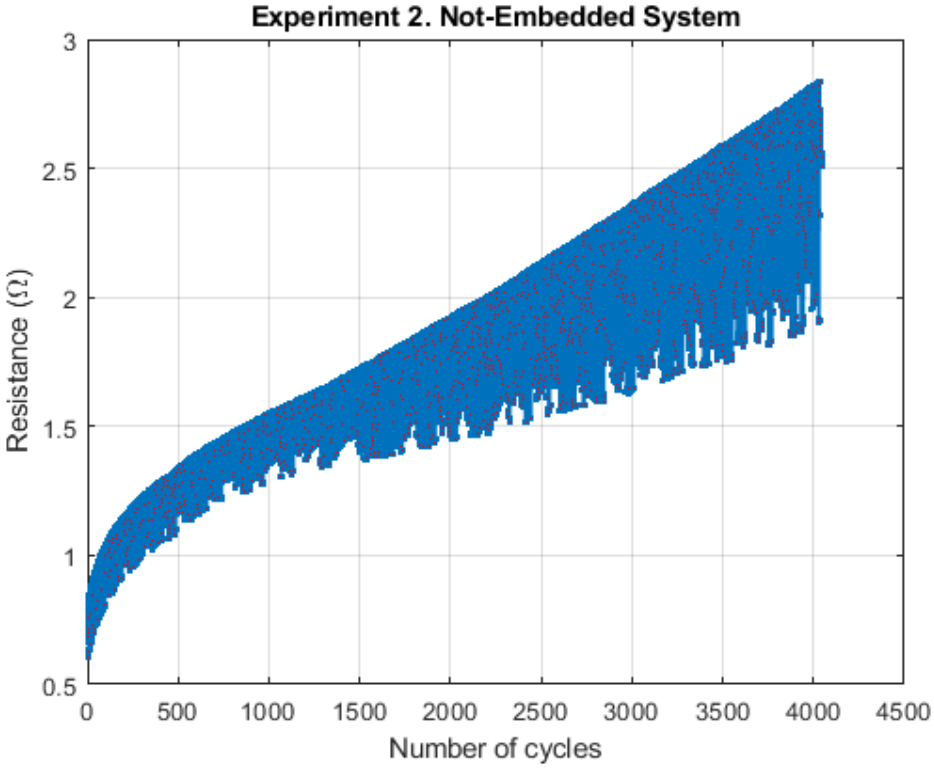

Figure 4.3. Experimental values for the second experiment. Number of Cycles vs Resistance.

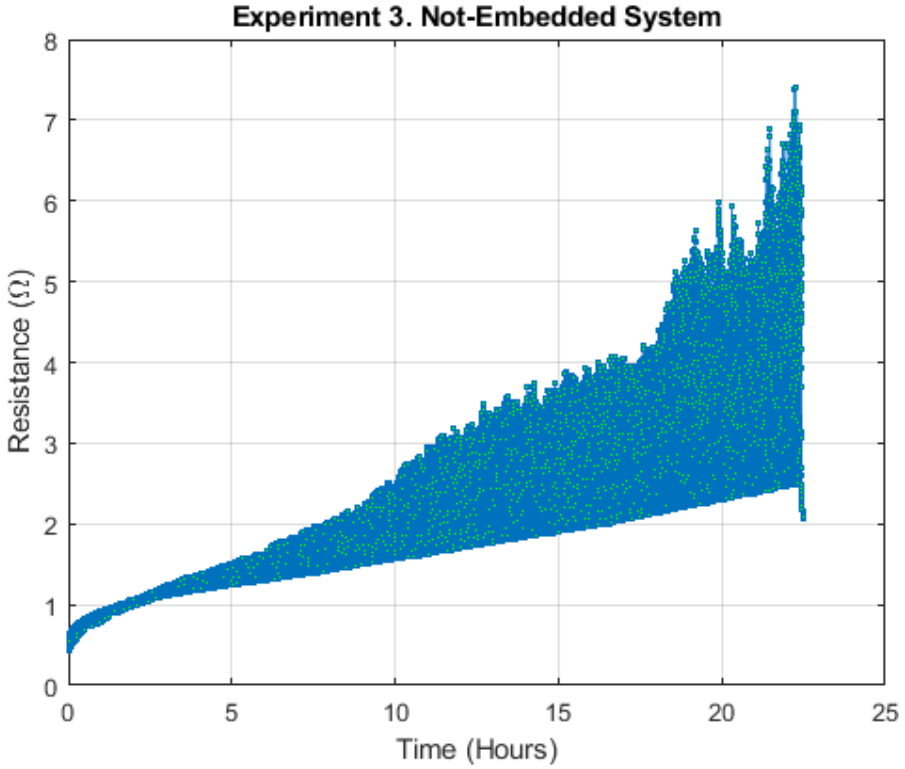

Figure 4.4. Experimental values for the third experiment. Time vs Resistance.

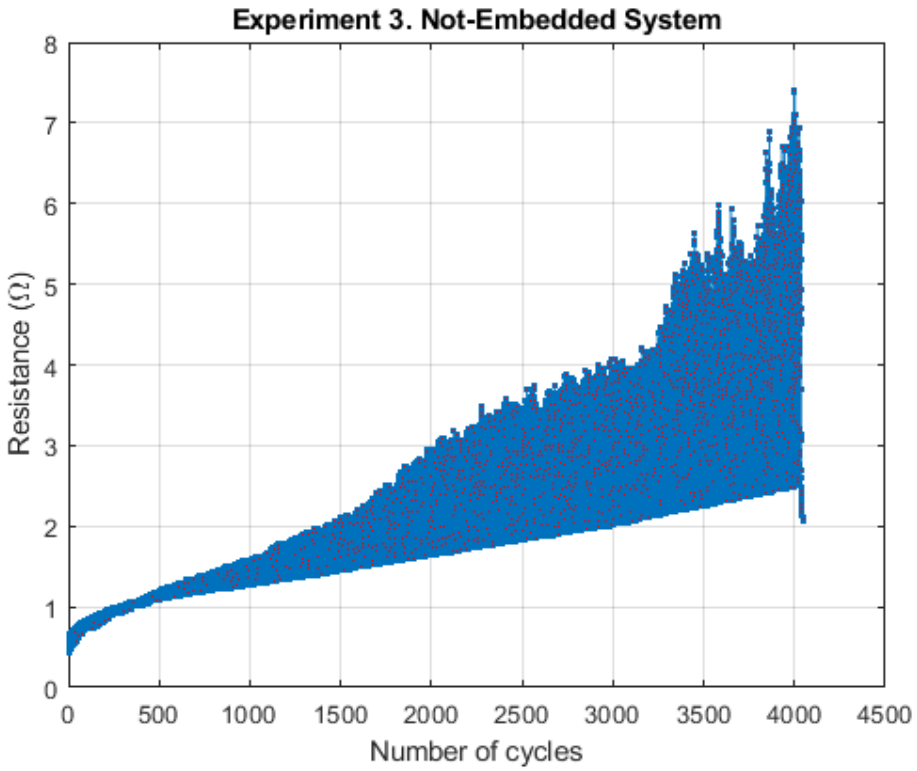

Figure 4.5. Experimental values for the third experiment. Number of Cycles vs Resistance.

Based on these results, the electrical properties of the printed conductive line onto the flexible platform represent good insights for its application as wearable electronic platform for future sensor applications. However, its implementation must be well studied since each application will have its own requirements. The experimental values of the three experiments for the not-embedded system are presented in Table 4.1.

Table 4.1. Experimental values of the electrical resistance for the not-embedded system.

Experiment	Maximum Value (Ω)	Minimum Value (Ω)
First	4.95	0.46
Second	2.84	0.60
Third	7.41	0.43

Continuing now with the experimental results for the embedded system, for the first experiment, these ones are shown in Figure 4.6.

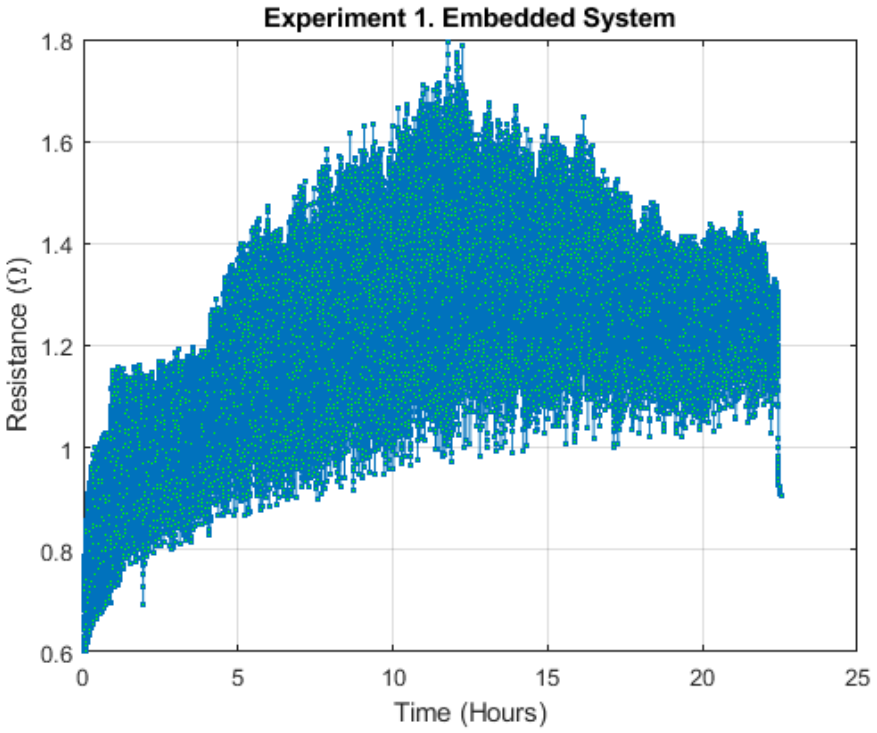

(a) Experimental values for the first experiment. Time vs Resistance.

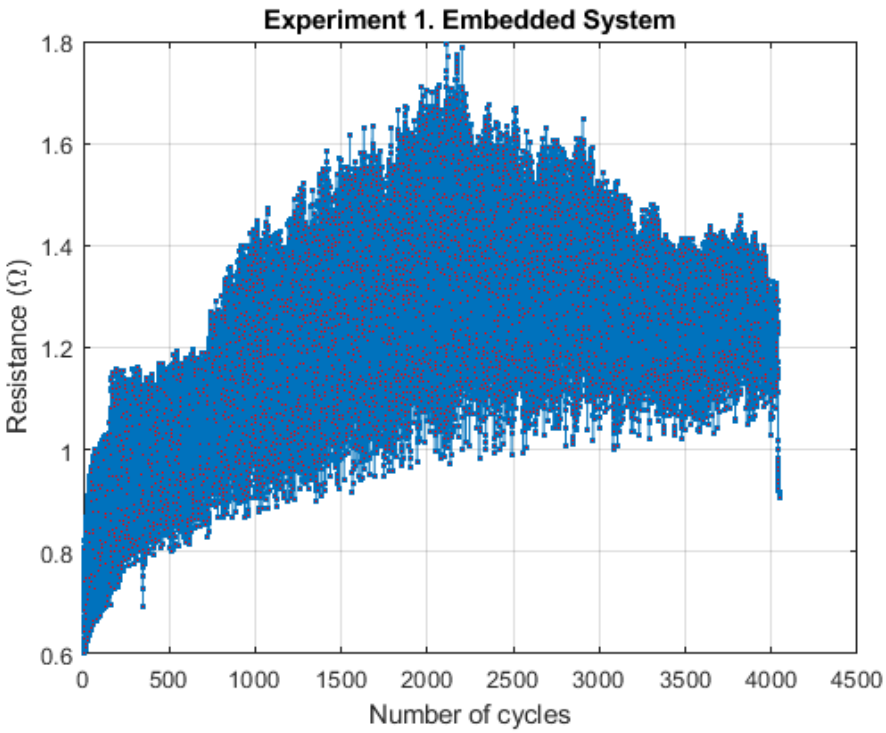

(b) Experimental values for the first experiment. Number of Cycles vs Resistance.

Figure 4.6. Experimental values of the first experiment for the embedded system.

Based on the experimental results given by Figure 4.6, there is a noticeable difference between the maximum value of this experiment with the ones presented by the not-embedded system, being this value a much lower one. In this case, the maximum value for the electrical resistance was 1.80 Ω and the minimum value was 0.60 Ω. This behavior can be explained due to the additional resin layer that protected the stretchable conductor line from the creation and propagation of cracks that eventually lead to the loss of the electrical conductivity. This layer is capable of enhance the adhesion of the printed line onto the flexible platform leading to a better performance in terms of constant conductivity under bending fatigue. Indeed, this behavior was also seen for the experimental results of the second experiment as it can be seen in Figures 4.7 and 4.8 where the maximum and minimum values were 1.92 Ω and 0.70 Ω, respectively. Nevertheless, the three experiments for the embedded system also shown the same trend regarding the increase of the electrical resistance through the bending cycles.

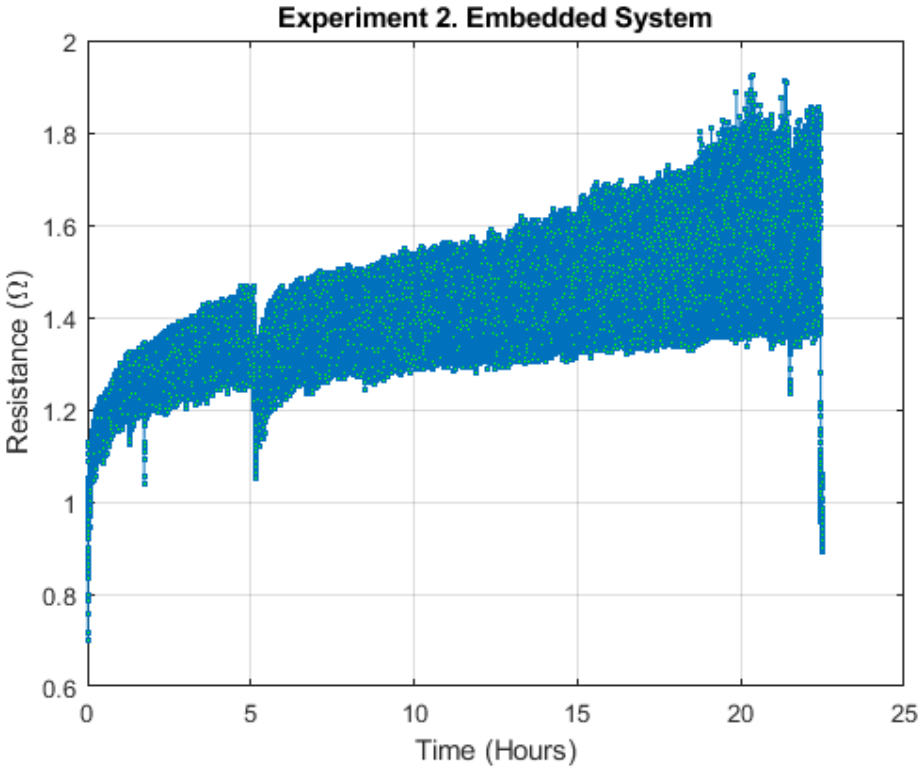

Figure 4.7. Experimental values for the second experiment. Time vs Resistance.

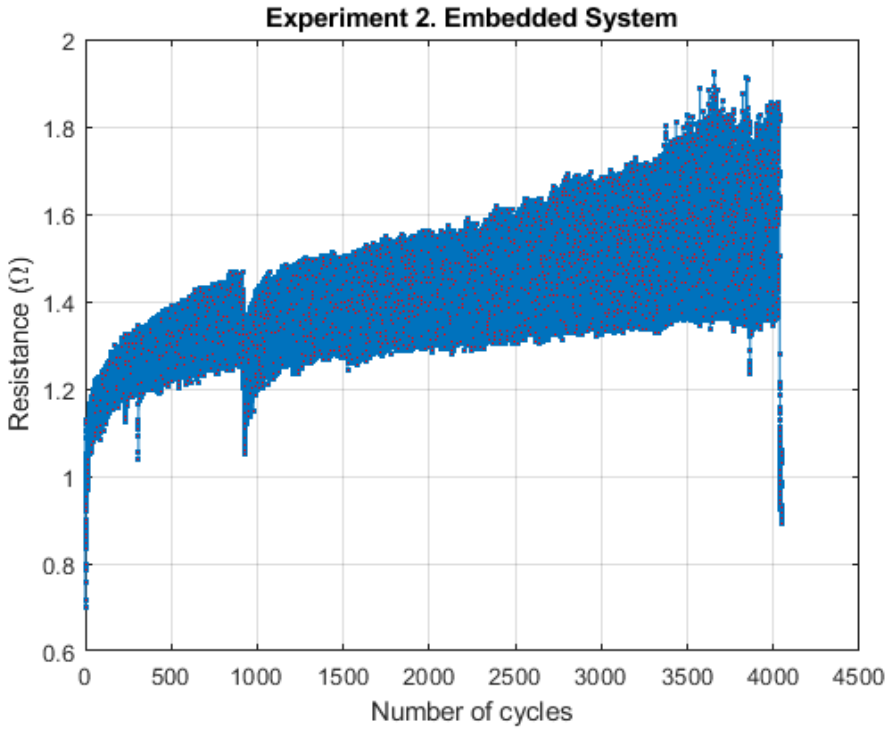

Figure 4.8. Experimental values for the second experiment. Number of Cycles vs Resistance.

Even though the previous two experiments reached lower values than the ones presented by the not-embedded system, the third experiment was not the case. This experiment reached a maximum value of 6.67 Ω and had a minimum value of 0.46 Ω (see Figure 4.9). Since this experiment was also for an embedded system, the maximum value might have happened due to the possibility that, during the bending cycle, cracks could have formed leading to an increase for the electrical resistance. However, the reached value is not considered as a one related with the total loss of conductivity. Therefore, the embedded system presented the best performance for the electrical resistance under bending fatigue, meaning that its implementation as a wearable electronic platform can be considered as a potential one. Lastly, the experimental results for the embedded system are presented in Table 4.2.

Table 4.2. Experimental values of the electrical resistance for the embedded system.

Experiment	Maximum Value (Ω)	Minimum Value (Ω)
First	1.80	0.60
Second	1.92	0.70
Third	6.67	0.46

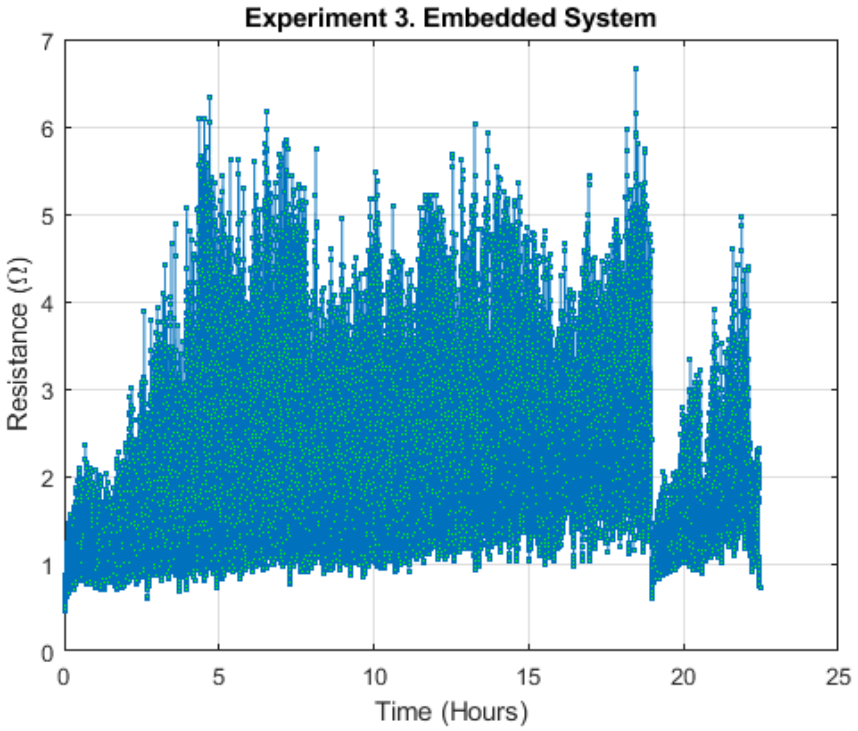

(a) Experimental values for the third experiment. Time vs Resistance.

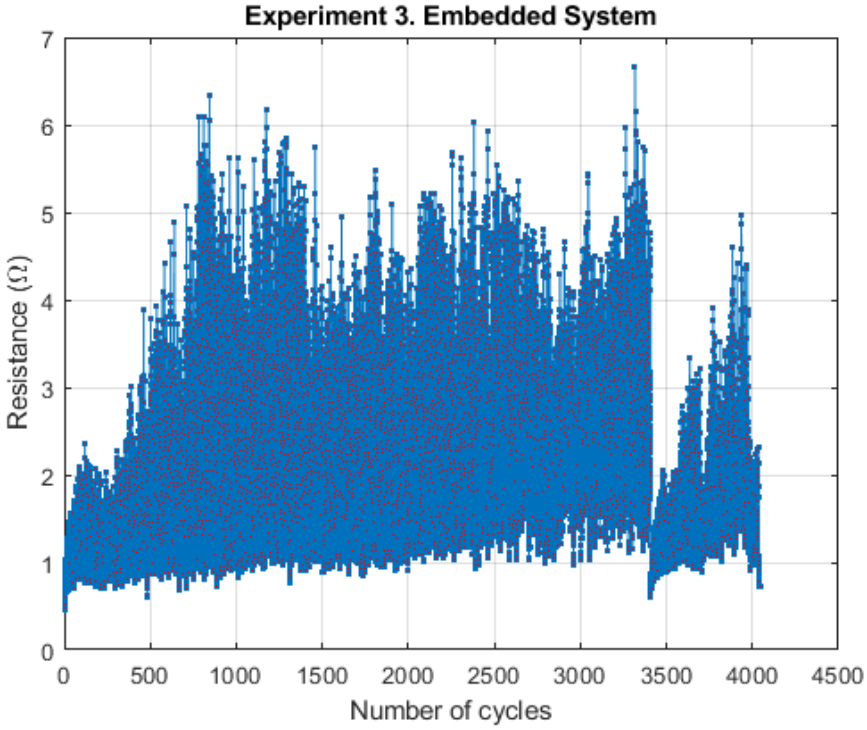

(b) Experimental values for the third experiment. Number of Cycles vs Resistance.

Figure 4.9. Experimental values of the third experiment for the embedded system.

4.2 Behavior of the Electrical Resistivity under Bending Fatigue

The electrical resistivity for the 3D printed conductive line was calculated based on the dimensions that were given by the Figure 3.4. In this case, the electrical resistivity was measured for both the not-embedded and embedded systems in the most representative experiment. Therefore, the study of this intrinsic property was done for the third experiment of the not-embedded system and the first experiment of the embedded system. It is crucial to note that a resistivity test is a definitive method for establishing the actual performance of the functional conductive ink or paste when printed. The electrical resistivity of a material is an inherent physical characteristic that represents its ability to impede the flow of electricity, regardless of the sample's geometry. Resistivity, represented by the symbol ρ, is a physical property that is quantified in units of ohm·meters (Ω·m) [95]. It is mathematically defined as:

$$\rho = \frac{A}{L} \cdot R \tag{4.1}$$

where, ρ is the volume resistivity in (Ω·m), A is the cross-sectional area in m^2, L represents the length in m and R is the electrical resistance in Ω. In the present work, the cross-sectional area was calculated based on the average thickness of the 3D printed conductive line with a value of 432.63 μm and a value of 0.12 cm for the width. Regarding the value for the length, this one was 6 cm. Once these values were obtained, the electrical resistivity was calculated by the multiplication of the fraction in equation 4.1 with the experimental values of the electrical resistance already shown in the previous section. These new experimental data for the electrical resistivity are shown in Figure 4.10 and Figure 4.11 for the not-embedded system.

The behavior of the experimental data in this section was the same as the one shown by the third experiment in the previous section for the not-embedded system, however, in this case the electrical resistivity was studied. From these two figures, it can be seen that the highest value for the electrical resistivity was 6.41 x 10^{-3} Ω·cm while the lowest value was 3.75 x 10^{-4} Ω·cm. The same conclusions can be obtained from these two figures as previously mentioned where the highest values of the electrical resistivity began almost at the end of the experiment due to the possible formation of cracks in the 3D printed conductive line. Considering now the electrical resistivity values of the first experiment for the embedded system, these ones are presented in Figures 4.12 and 4.13.

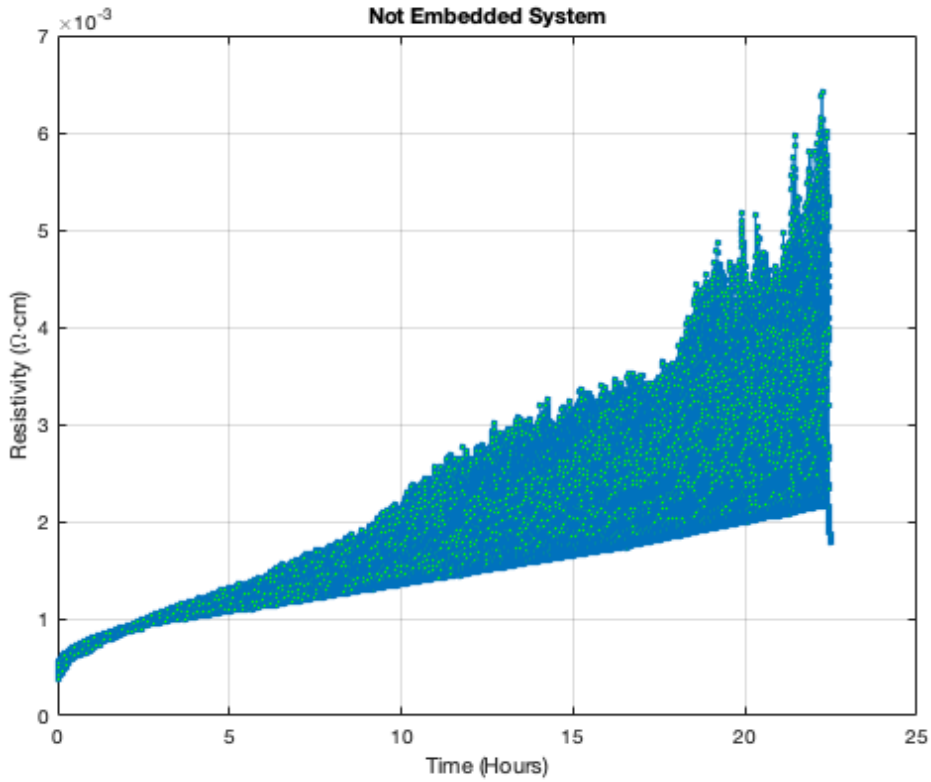

Figure 4.10. Experimental values for the third experiment. Time vs Electrical Resistivity.

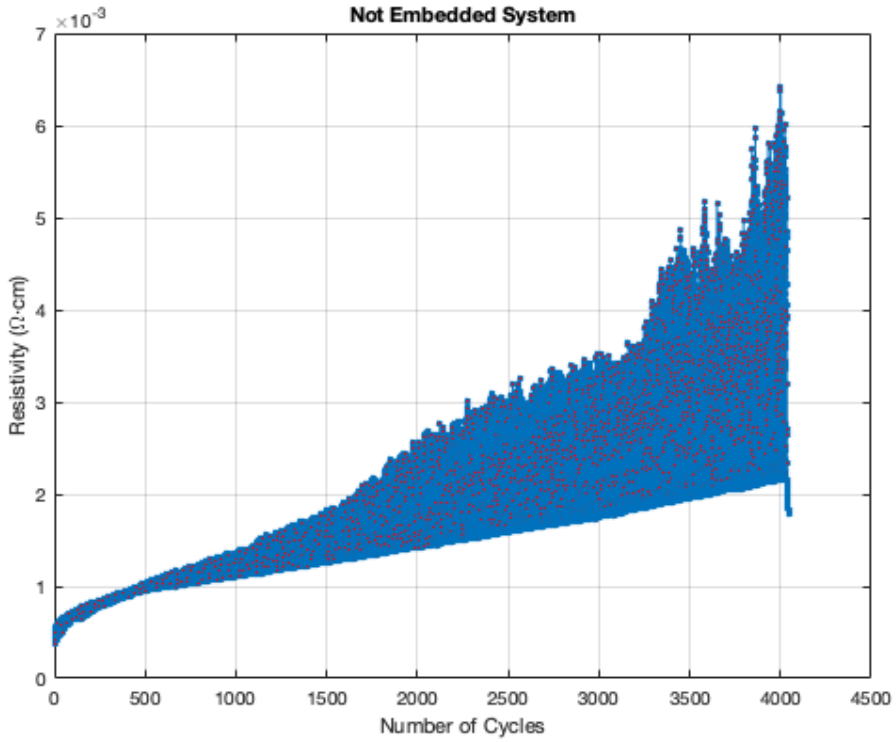

Figure 4.11. Experimental values for the third experiment. Number of Cycles vs Electrical Resistivity.

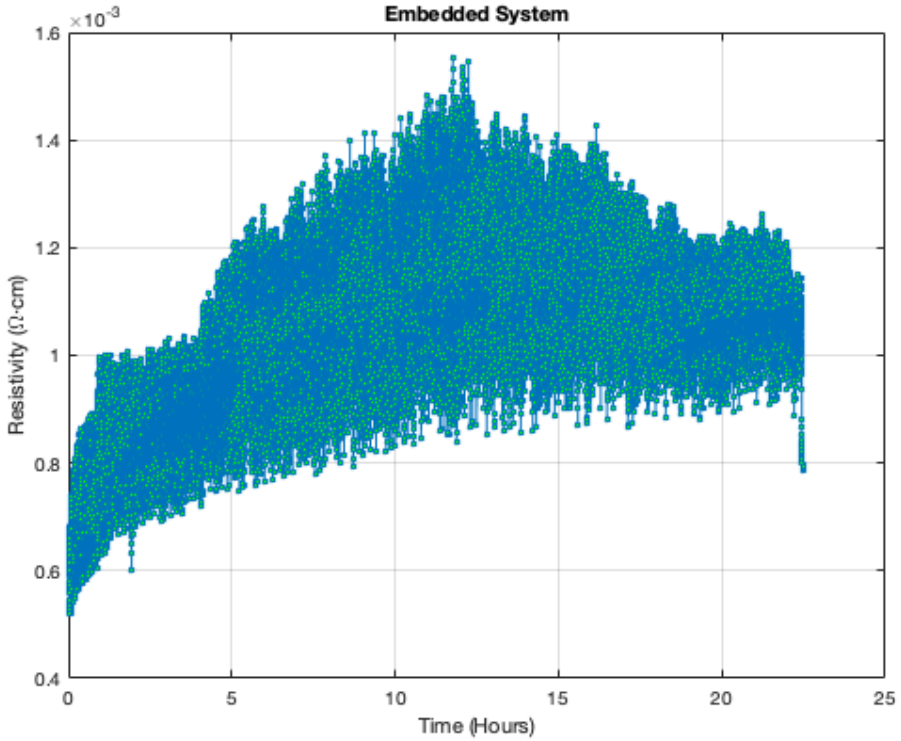

Figure 4.12. Experimental values for the first experiment. Time vs Electrical Resistivity.

In this case, it can be seen that the highest value was 1.55 x 10^{-3} Ω·cm and the lowest value was 5.20 x 10^{-4} Ω·cm. Nevertheless, it is clearly showed that by comparing the maximum values of the electrical resistivity for both systems, the embedded system presented a lower value. This behavior was also seen in the previous section, meaning that the embedded system presented once again the best electrical properties under bending fatigue due to the additional layer that was placed on the top of the 3D printed conductive line that helped avoiding the generation of cracks.

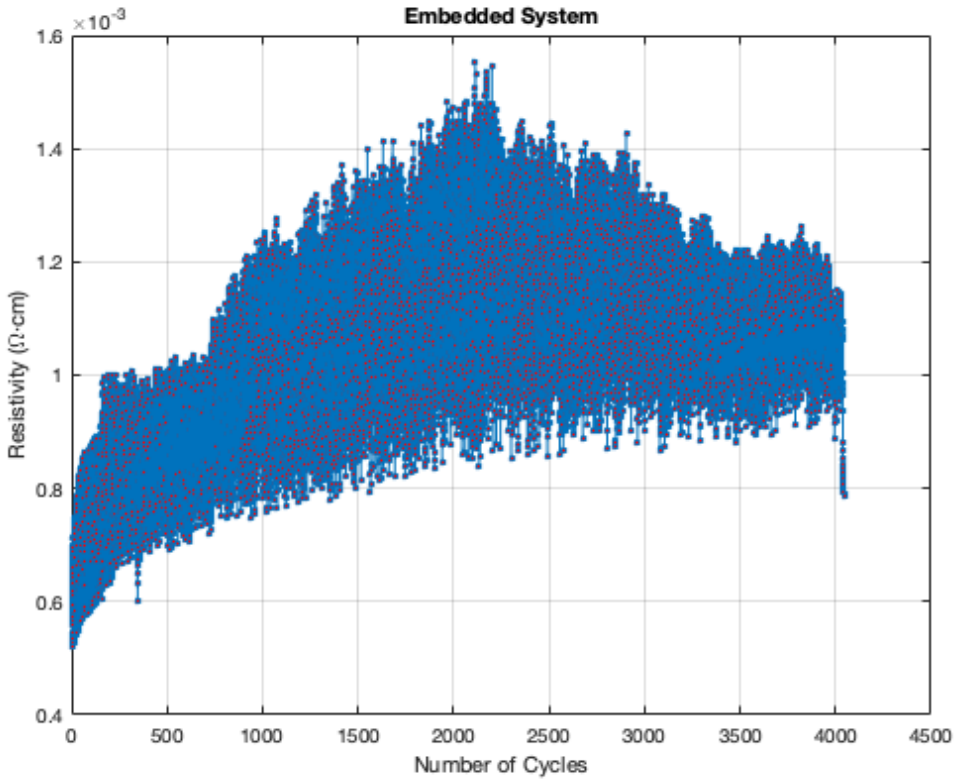

Figure 4.13. Experimental values for the first experiment. Number of Cycles vs Electrical Resistivity.

4.3 Behavior of the Voltage under Bending Fatigue

In the present section, the experimental results of the change for the voltage under bending fatigue are presented. In this experiment, an embedded 3D printed electronic circuit was exposed to bending mechanical fatigue during 22.5 hr and 4,050 cycles while a constant voltage of 3V was provided by a DC supplier. The objective of this experiment was to analyze the behavior of this circuit under mechanical fatigue for its implementation as a wearable electronic platform in the future. Moreover, the experimental data that were collected in this experiment provided a fair judgement for its possible use in more complex scenarios. In this regard, three experiments were done in order to evaluate this behavior. For each experiment, the change in voltage was collected while the bending movement was taking place as previously explained. One aspect about this experiment was the importance of the LED light on while the bending movement was happening, meaning that the electrical conductivity was constant even under mechanical fatigue, this can be seen in Figure 4.14. The experimental results for the first experiment are presented in Figure 4.15.

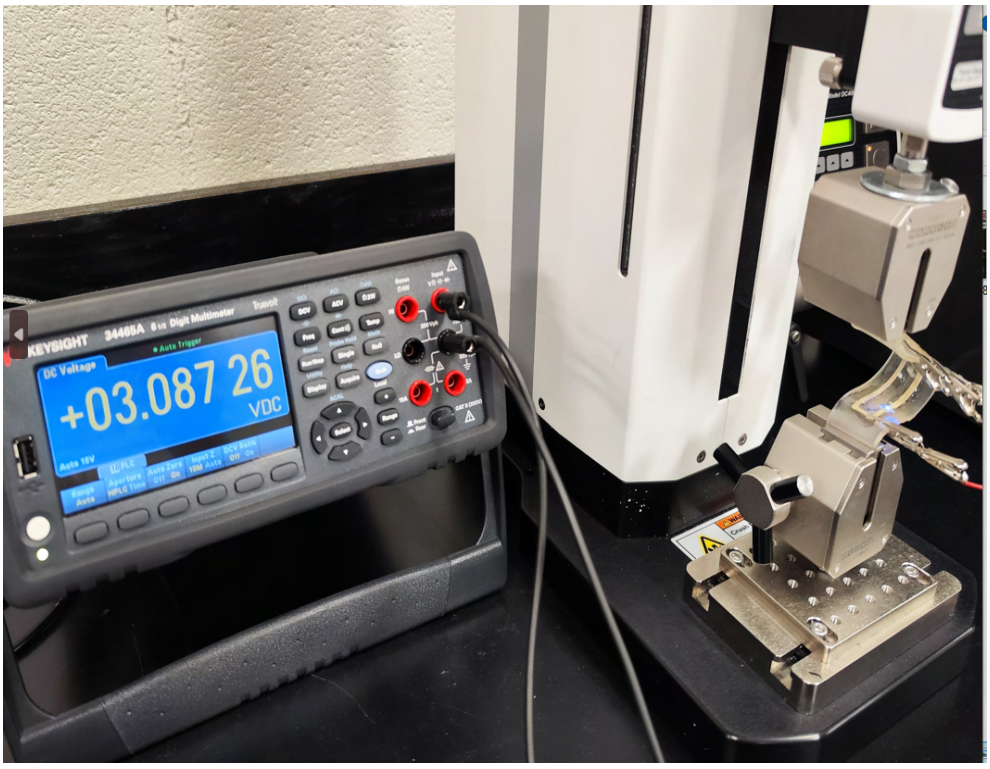

Figure 4.14. 3D printed electronic circuit with LED light on under bending fatigue.

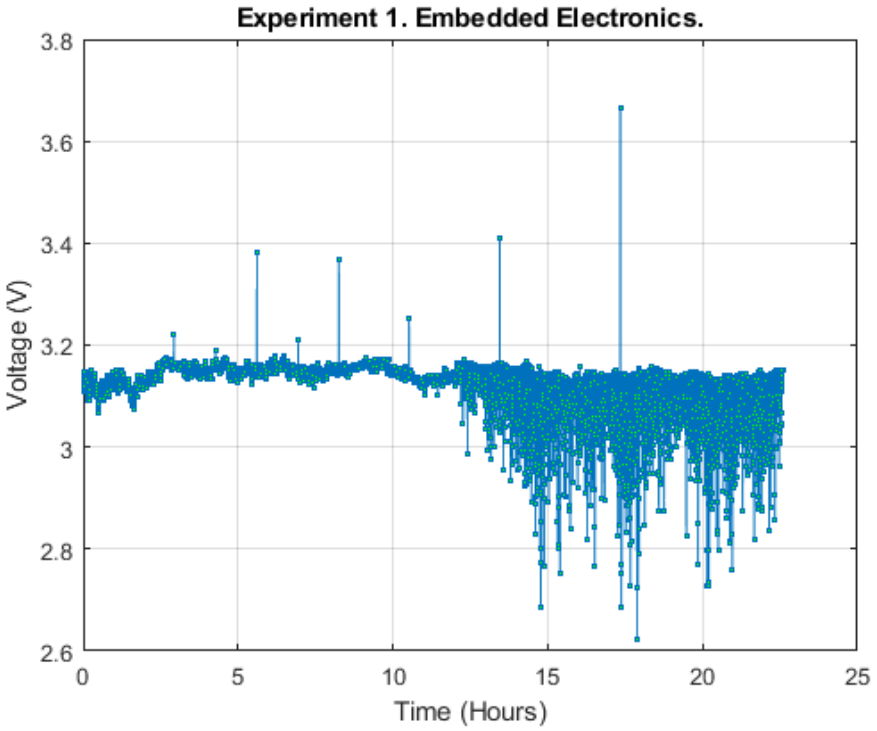

(a) Experimental values for the first experiment. Time vs Voltage.

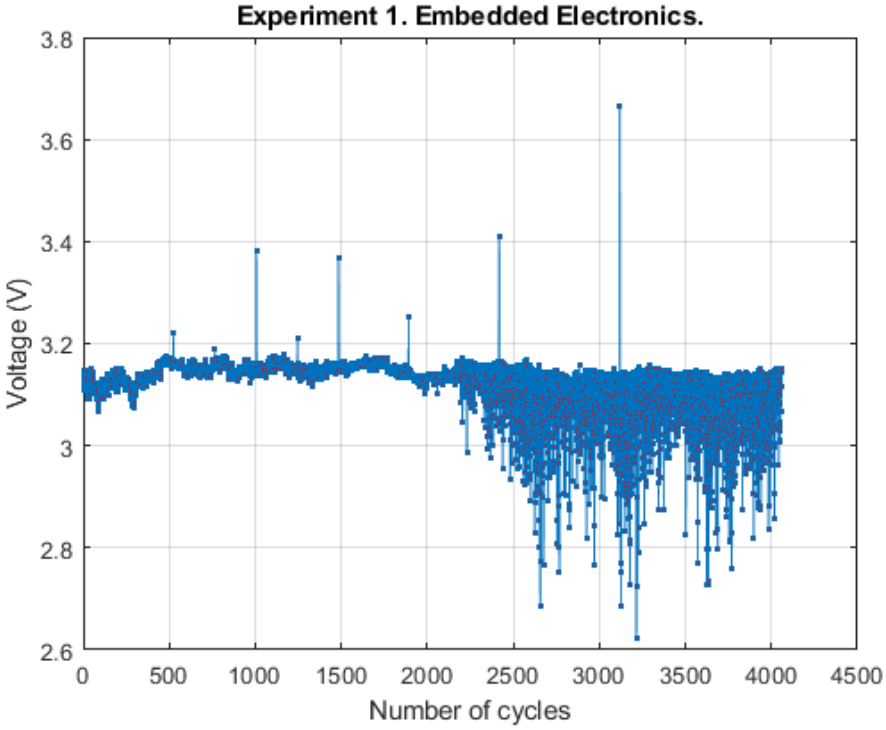

(b) Experimental values for the first experiment. Number of Cycles vs Voltage.

Figure 4.15. Experimental values of the first experiment for the embedded electronics.

As it can be seen in Figure 4.15, the change for the voltage varied from a minimum value of 2.62 volts to a maximum peak at 3.66 volts. Since 3 volts were supplied to the 3D printed circuit by the DC supplier, in an ideal case, the voltage should not have changed during the bending fatigue. However, it can be seen that after eleven hours and around 2200 bending cycles, the voltage started fluctuating. In this experiment, a decrease for the voltage is also related with the loss of conductivity that could have been caused because of the generated fractures or cracks in the stretchable conductor. Moreover, another important aspect for this experiment is the movement that the alligator clips might have suffered while the bending movement was taking place, causing bad connection between the alligator clips and the stretchable conductor and leading to unrepresentative values for the voltage. Nevertheless, the range between this two voltage values did not represent a total loss of conductivity due to non of them reached a value of zero volts and the LED light was on during all the experiment. A second experiment was carried out giving the experimental values that are presented in Figures 4.16 and 4.17. For this second experiment, the voltage varied from 3.57 to 3.47 volts providing good results in terms of electrical performance.

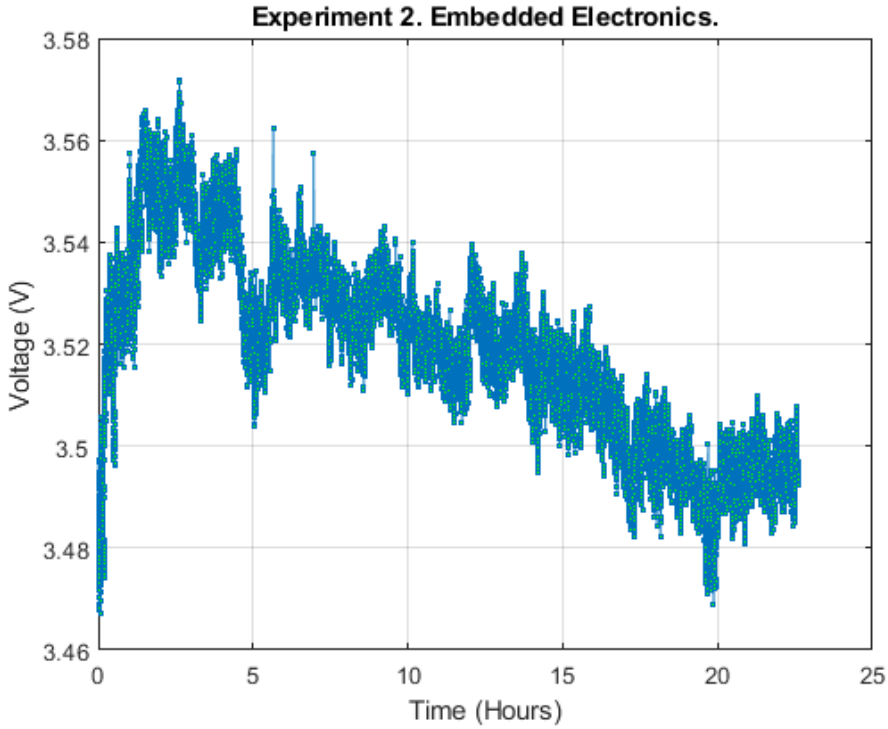

Figure 4.16. Experimental values for the second experiment. Time vs Voltage.

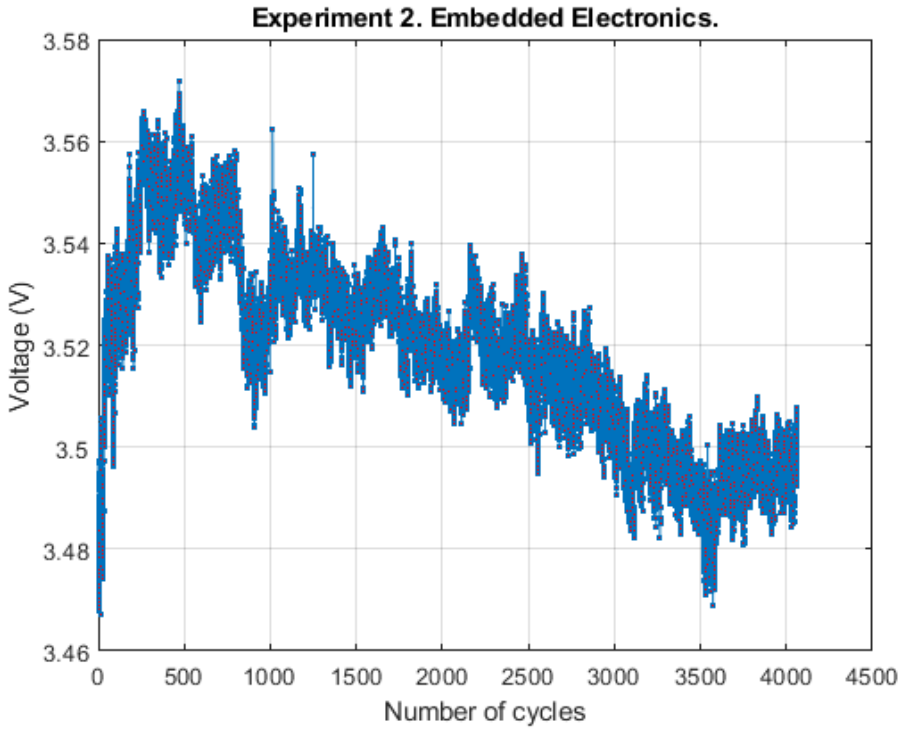

Figure 4.17. Experimental values for the second experiment. Number of Cycles vs Voltage.

For the third experiment, its experimental results are shown in Figures 4.18 and 4.19.

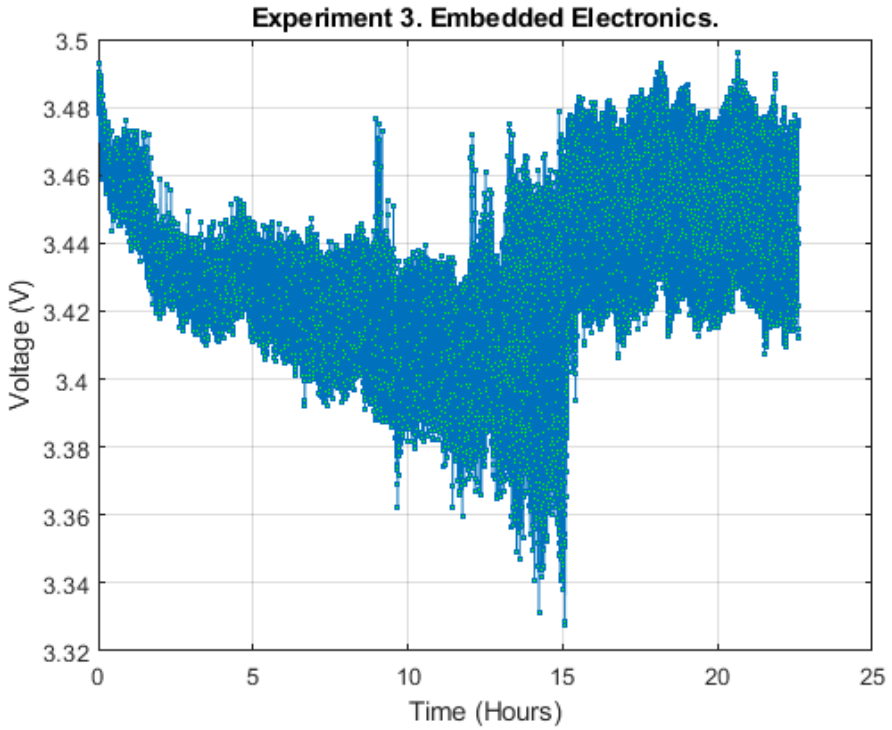

Figure 4.18. Experimental values for the third experiment. Time vs Voltage.

From these two last figures, it can be seen that for this experiment the voltage values were between 3.50 and 3.33 volts. Therefore, once again, the electrical performance remained good under mechanical fatigue. Overall, the three experiments showed that the 3D printed electronic circuit was capable of withstand bending fatigue for a prolonged period of time representing a potential strategy for its application in wearable sensors applications. Lastly, the range of the voltage values for each experiment are summarized in Table 4.3.

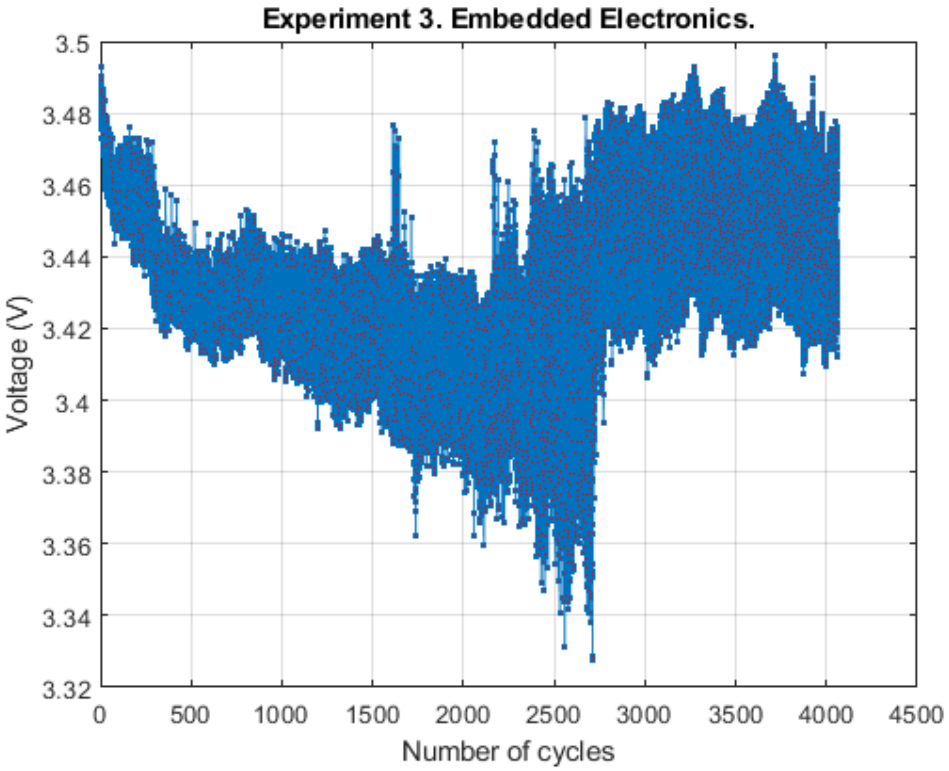

Figure 4.19. Experimental values for the third experiment. Number of Cycles vs Voltage.

Table 4.3. Experimental values of the voltage for the embedded electronics.

Experiment	Maximum Value ($Volts$)	Minimum Value ($Volts$)
First	3.66	2.62
Second	3.57	3.47
Third	3.50	3.33

4.4 Experimental Values of Adhesion Strength

In the present section, the evaluation of the adhesion strength between the flexible platform and the stretchable conductor was conducted. Three experiments were carried out as well as one control. This control consisted of evaluating the strength between the adhesion test tape and the flexible platform without any printed conductive line. Primarily, this control was helpful to differentiate the adhesion strength for the stretchable conductor line and for the flexible platform by itself. Once the experimental values for the controls were analyzed, three experiments were done by printing a conductive line onto a flexible platform with dimensions 0.28 cm (H) x 4.5 cm (W) x 13.0 cm (D). After printing it, the adhesion test provided insights regarding the interaction between the flexible platform and the stretchable conductor line. Moreover, the height of the printed line was measured before and after for each experiment in order to quantify the loss of conductive material. It is important to mention that for all the experiments in this section the experimental values for strength or load were collected in Newtons and for the extension in mm. In Figure 4.20 are shown the experimental data for the control where it can be seen that the maximum value for the strength was 6.30 N.

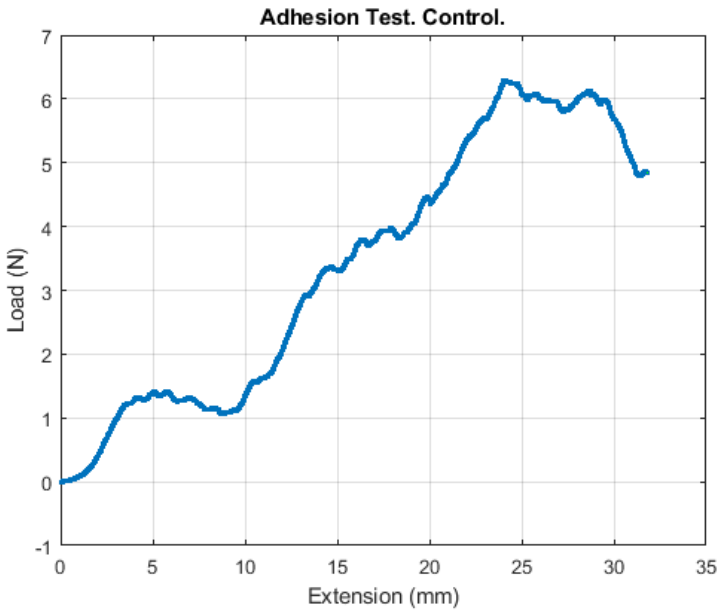

Figure 4.20. Adhesion strength of the control. Load vs Extension.

In the other hand, Figures 4.21, 4.22 and 4.23 present the experimental results for the experiments 1, 2 and 3, respectively.

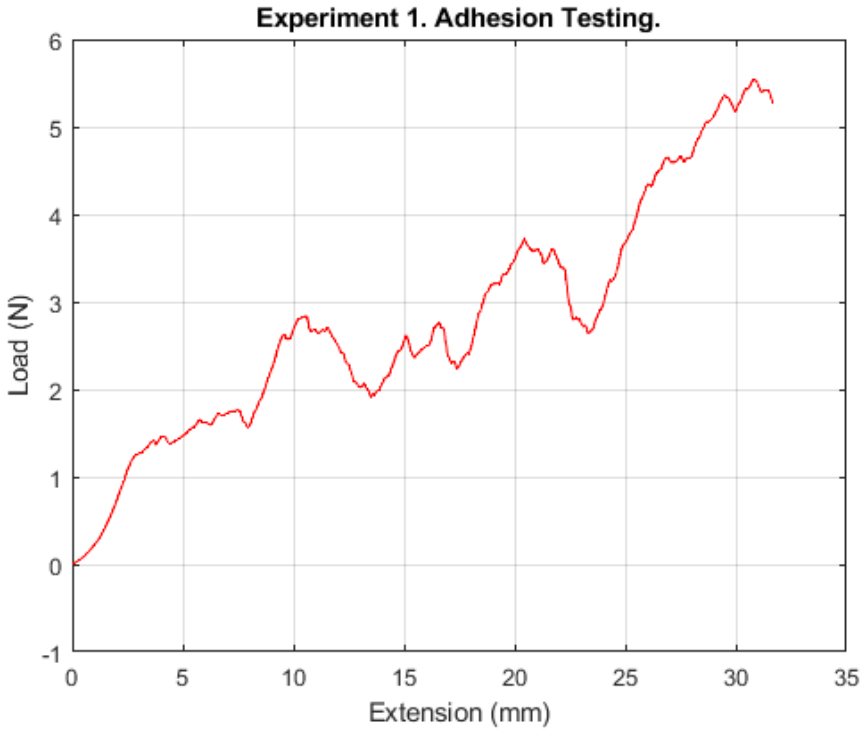

Figure 4.21. Adhesion strength for the third experiment.

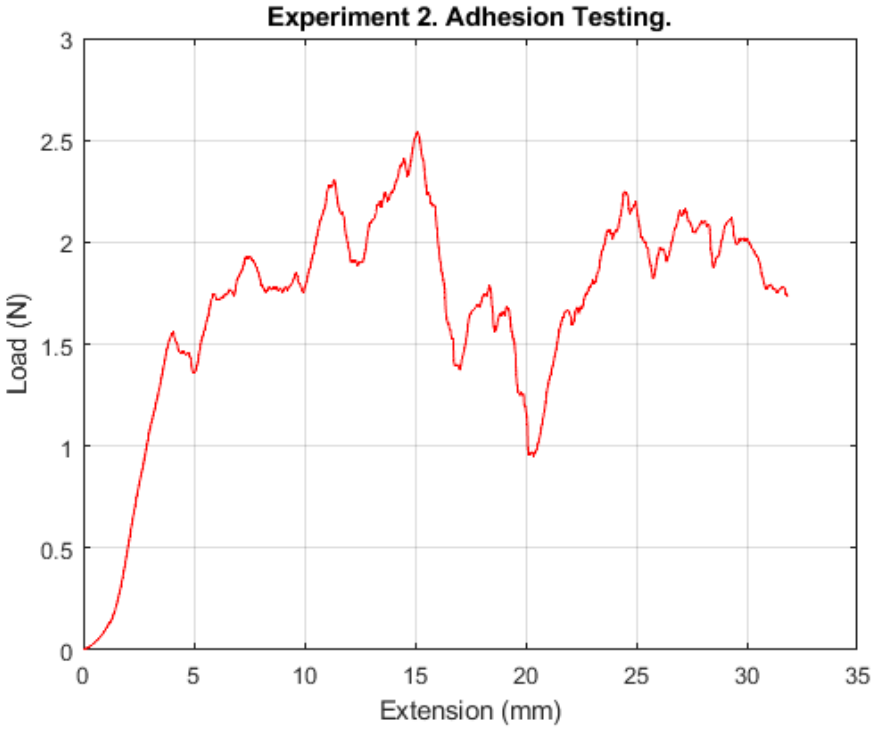

Figure 4.22. Adhesion strength for the second experiment.

From these three figures that were mentioned before, the maximum strength values were 5.54 N, 2.54 N and 4.07 N for experiments 1, 2 and 3, respectively. Nevertheless, for all the experiments a total length of 3.18 cm was set as the maximum extension for the head to move upwards providing less inaccurate results due to the different lengths of the tape that could have been removed from the flexible substrate. Even though the maximum extension for the head was set to this value, different experimental results for the adhesion strength were presented for all the experiments. For instance, the experimental data for the second experiment were not as similar as the ones presented by the first and third experiments. Particularly, for the second experiment, this low strength value can be explained as poor adhesion between the flexible substrate and the stretchable conductor that could have been aggravated for the formation of microscopic fractures capable of affecting the adhesion strength. These type of microscopic fractures or cracks are depicted in Figure 4.24. Furthermore, these ones are also related with the loss of conductivity that was explained in the previous sections.

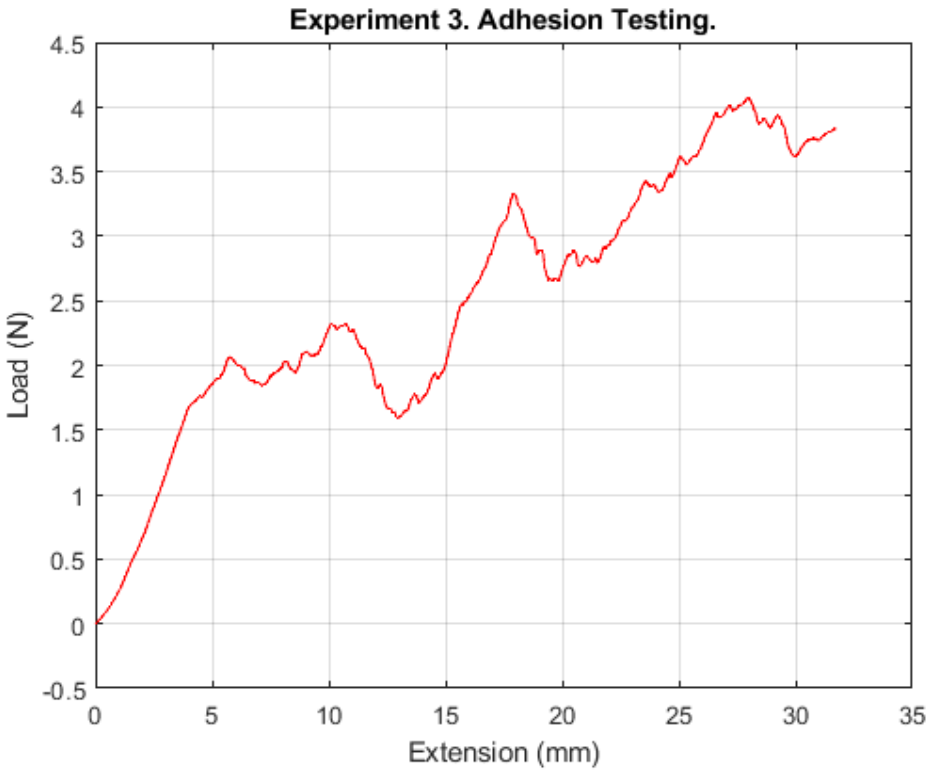

Figure 4.23. Adhesion strength for the third experiment.

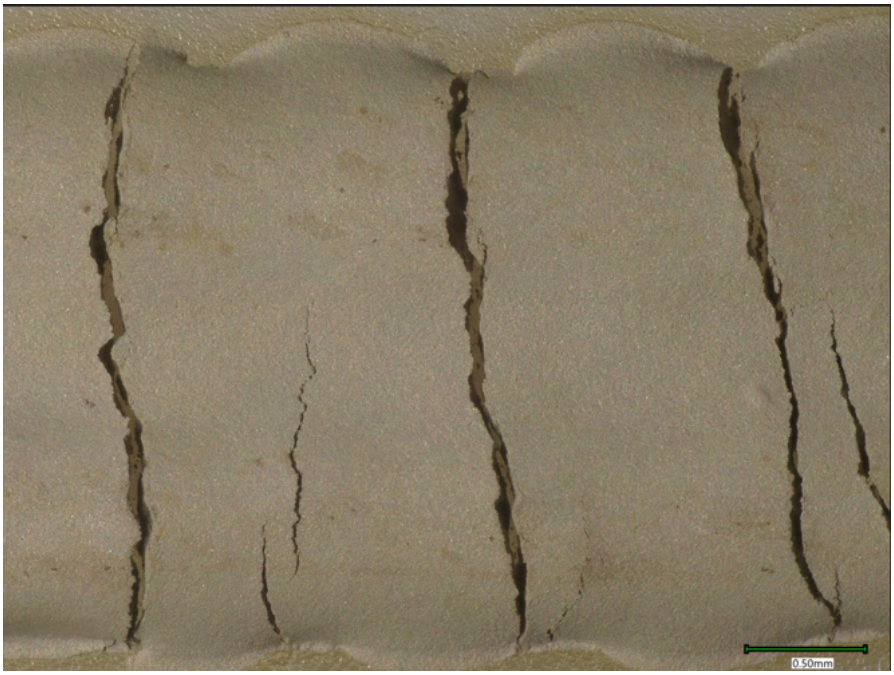

Figure 4.24. Fractures formed during the sintering process as well as the bending movement. These ones interfere with the adhesion strength as well as the conductivity for the stretchable conductor.

For the maximum values of the adhesion strength for the first and third experiments, it can be seen the difference between these ones and the one presented by the control, being the value for the control a little bigger. This situation might not be the ideal one since the adhesion strength of the stretchable conductor line should be more than the one presented by the flexible platform itself. However, the difference between these values is relatively small that it is not significantly important for the overall adhesion strength. Indeed, even though the biggest adhesion strength value for the first experiment was lower than the one presented by the control, this force was not enough in order to completely remove the stretchable conductor line from the flexible platform, meaning that the force that is required for this to happen is way bigger than the actual force showed by the control. This explanation can be supported by analyzing the height of the conductive line before and after the adhesion test. In this case, Figures 4.25 and 4.26 present the values of the height for the printed line in the first experiment before and after this adhesion test. These results were obtained using the VHX7000 digital microscope. It is important to mention that the height of the stretchable conductor was measured in each experiment using the same methodology. Therefore, the remaining results for the second and third experiment are presented in Table 4.4.

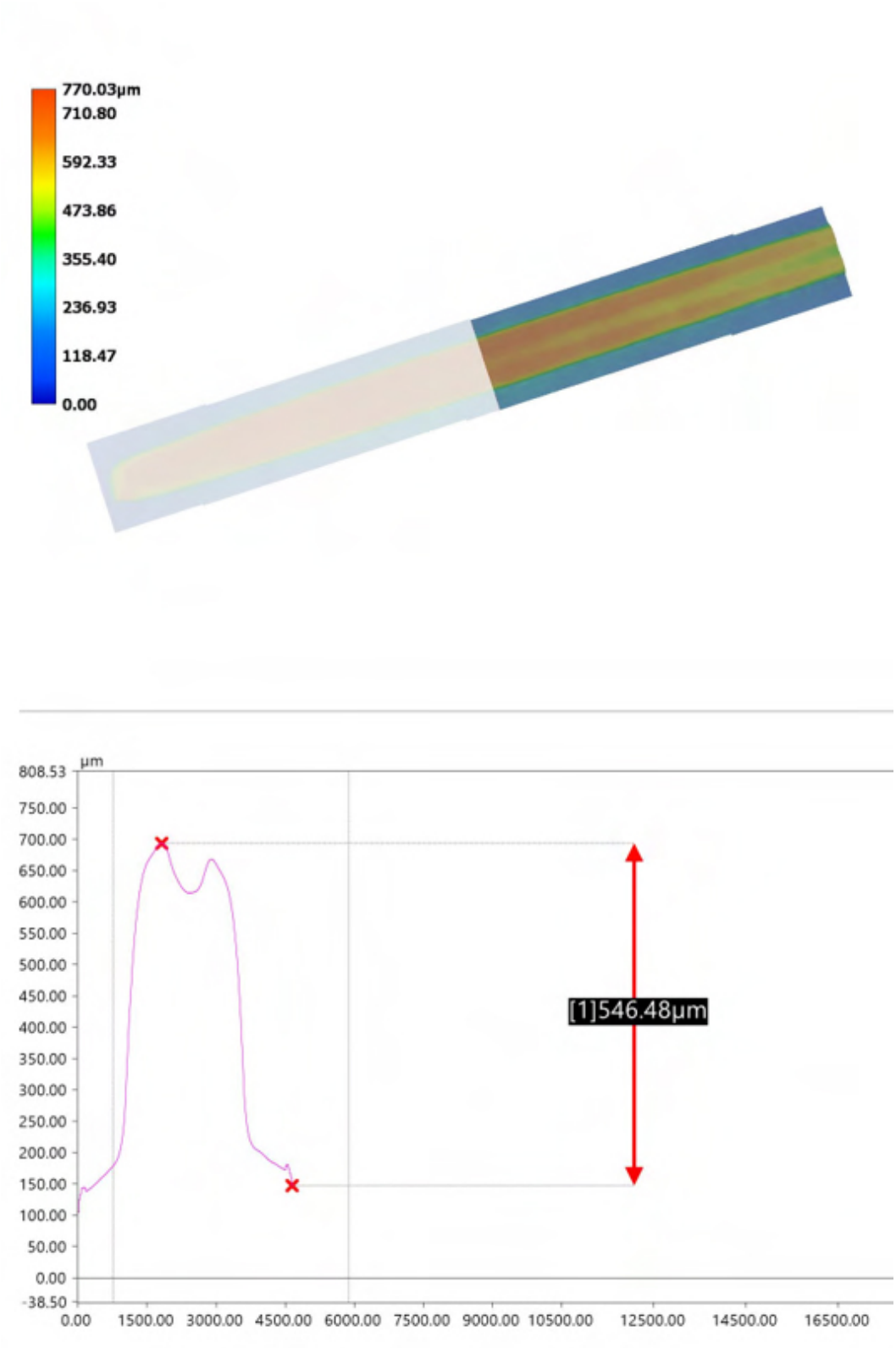

Figure 4.25. Height of the stretchable conductor line before the adhesion test.

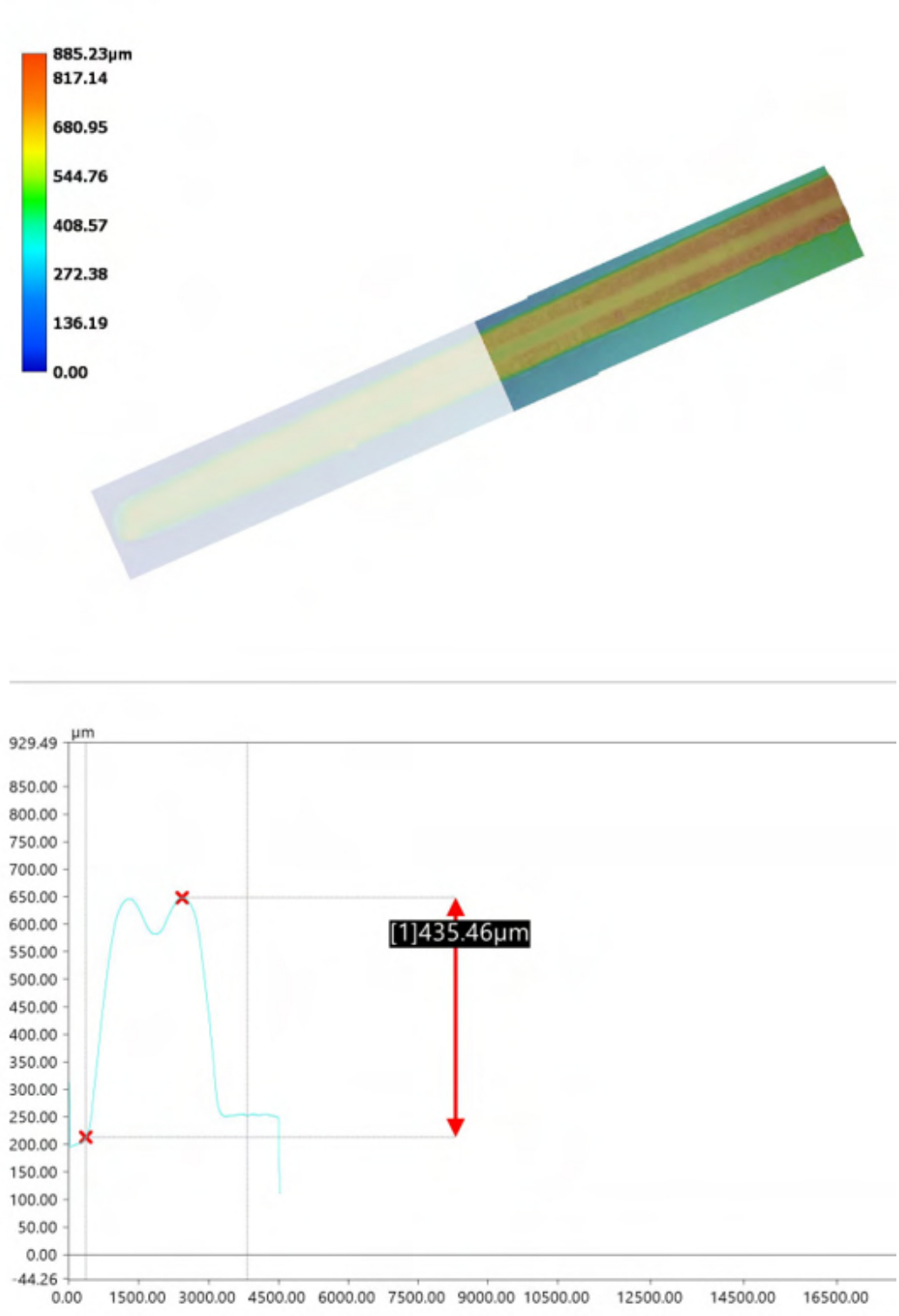

Figure 4.26. Height of the stretchable conductor line after the adhesion test.

Table 4.4. Height of the printed line before and after the adhesion test.

Experiment	Before Test (μm)	After Test (μm)	Difference (μm)
First	546.48	435.46	111.02
Second	332.58	271.71	60.87
Third	418.83	374.76	44.07

By analyzing the values in the previous table, it can be seen that the loss of the conductive material was not significantly representative after the adhesion test was carried out. This could be explained since the largest difference of the height for all the experiments was 111.02 μm or 0.111 mm which represented a really small change. Therefore, the adhesion strength between the stretchable conductor and the flexible substrate can be considered acceptable and relevant for its application in flexible electronics as well as wearable sensors. Moreover, in order to see how the electrical properties of the 3D printed conductive line were affected by removing this small amount of conductive material because of the adhesion test, the electrical resistance for the three samples was measured after this test. These values are shown in Table 4.5 for each experiment. Comparing these experimental values with the values given by Table 4.1, it can be seen that the electrical resistance values for the samples of the adhesion test were lower than the ones for the bending test. This could be explained since the samples for the adhesion test were not exposed to any mechanical fatigue, meaning that there was not generation of cracks that could possibly affect the electrical conductivity of the 3D printed conductive line. Moreover, the loss of the conductive material due to the adhesion test did not represent a big change for the conductivity of the material since the 3D printed conductive line was barely removed from the flexible platform.

Table 4.5. Electrical resistance values for each experiment after the adhesion test.

Experiment	Electrical Resistance (Ω)
First	0.320
Second	0.158
Third	0.160

4.5 NO_2 Gas Resistance Values for Different Polluted Scenarios

Lastly, in this section, the experimental values of gas resistance for different polluted scenarios with NO_2 (g) are presented. In these experiments, three control experiments were carried out in order evaluate the gas resistance under normal air conditions which were at 25ºC and 1 atm. These experimental results provided the average value of gas resistance that the gas sensor was capable to detect under these normal room conditions, being this value 20.15 Ω. The collected experimental data for each control are shown in Figure 4.27. As previously mentioned, the collection of the experimental data was accomplished by using a bluetooth gas sensor and a software application developed by alumni at Youngstown State University. Once the control tests were carried out, the volumes of HNO_3(aq) were added to the copper sheets in order to start the generation of the NO_2 gas. While the generation of the gas was taking place, the gas resistance was collected each second during an approximate time of 300 seconds.

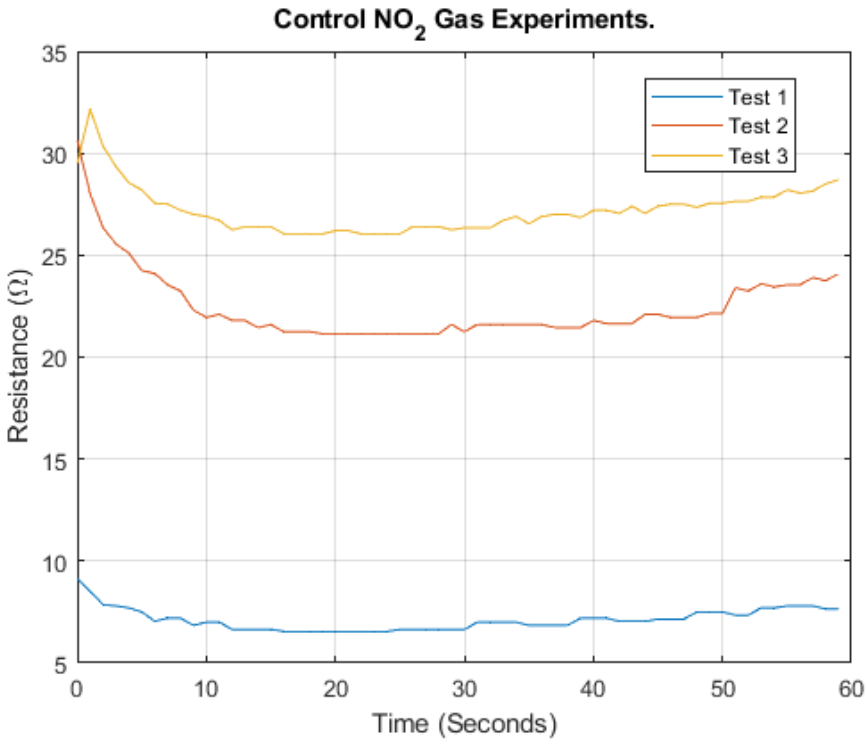

Figure 4.27. Experimental gas resistance values for the three control tests.

Regarding the volumes used for HNO_3 (aq), these were 10, 20 and 40 μl. For each volume, three experiments were carried out in order to obtain their maximum gas resistance value. Once obtained, an average between these three values was calculated in order to plot it against its respective value of the calculated ppm from the stoichiometric calculations. In this regard, Figure 4.28 presents the experimental results of gas resistance for a used volume of 10 μl. By analyzing this figure, it can be seen that the maximum values were 859, 884.60 and 883.50 Ω for experiment 1, 2, and 3, respectively. Calculating the average, this one was 875.70 Ω. Furthermore, the three experiments presented a similar behavior where the main change in gas resistance was detected by the sensor after 100 seconds since the experiment had started. Regarding the collected experimental data using 20 μl, these ones are shown in Figure 4.29. In this case, the gas resistance values were bigger than the ones that were presented by using 10 μl, being these values 813.24, 1186.90 and 1453.24 Ω for experiment 1, 2 and 3, respectively. The average was also calculated, being 1151.13 Ω.

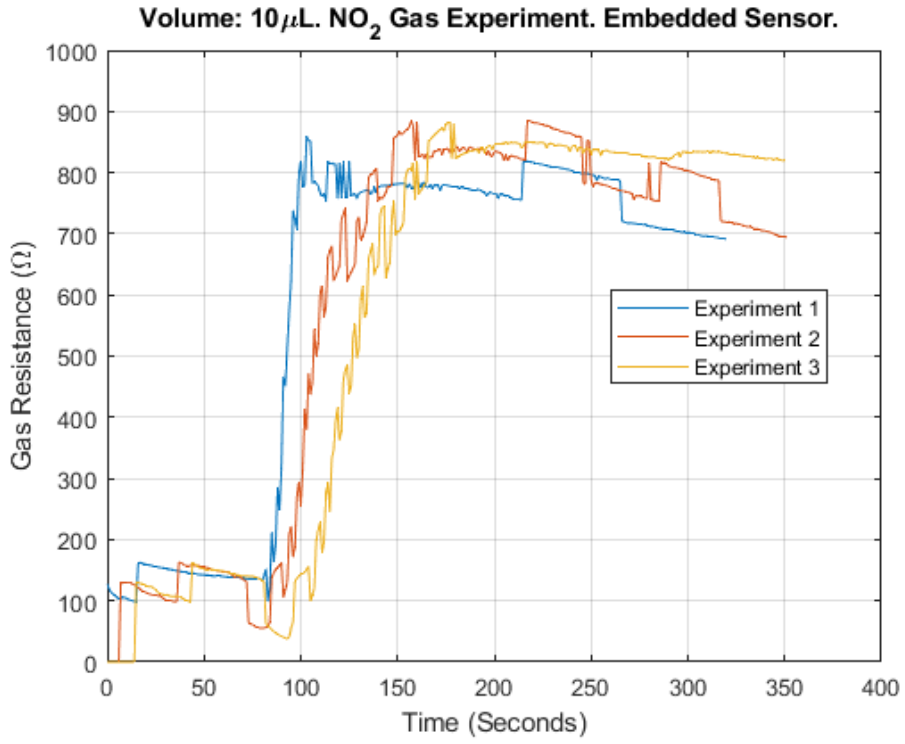

Figure 4.28. Experimental gas resistance values after adding a HNO_3(aq) volume of 10 μl to the copper sheets.

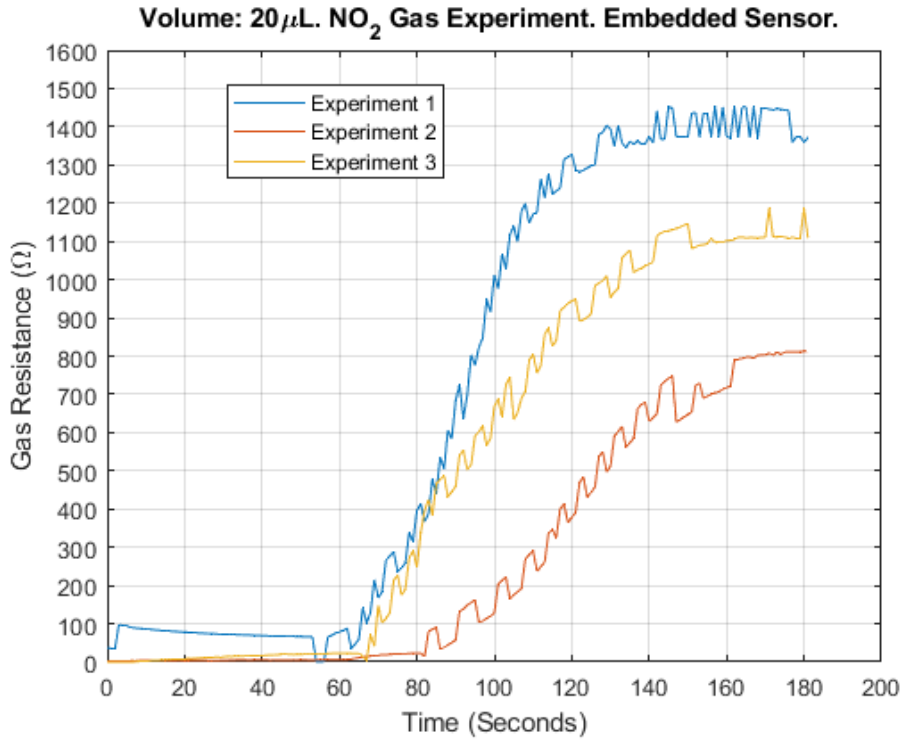

Figure 4.29. Experimental gas resistance values after using a HNO_3(aq) volume of 20 μl.

The increment for the gas resistance in these experiments was due to the increment of the concentration in ppm for the NO_2 that was produced by the chemical reaction. In fact, the more volume is added, the more concentration of the NO_2 gas will be generated, hence, the gas resistance will increase as well. Based on this, the relationship between the detected gas resistance by the sensor and the added volumes to the copper sheets is proportional. Similarly, the results of the gas resistance utilizing a volume of 40 μl are presented in Figure 4.30. The same trend regarding the increment of the gas resistance while incrementing the volume was observed again. Indeed, the increment in the gas resistance by adding 40 μl was the biggest compared with the ones showed by adding the previously mentioned volumes. Particularly, using this volume, the maximum gas resistance values for the experiment 1, 2 and 3 were 3618.04, 4658.5 and 4523.14 Ω, respectively. The maximum gas resistance value for each experiment as well as the calculated average for each utilized volume are presented in Table 4.6.

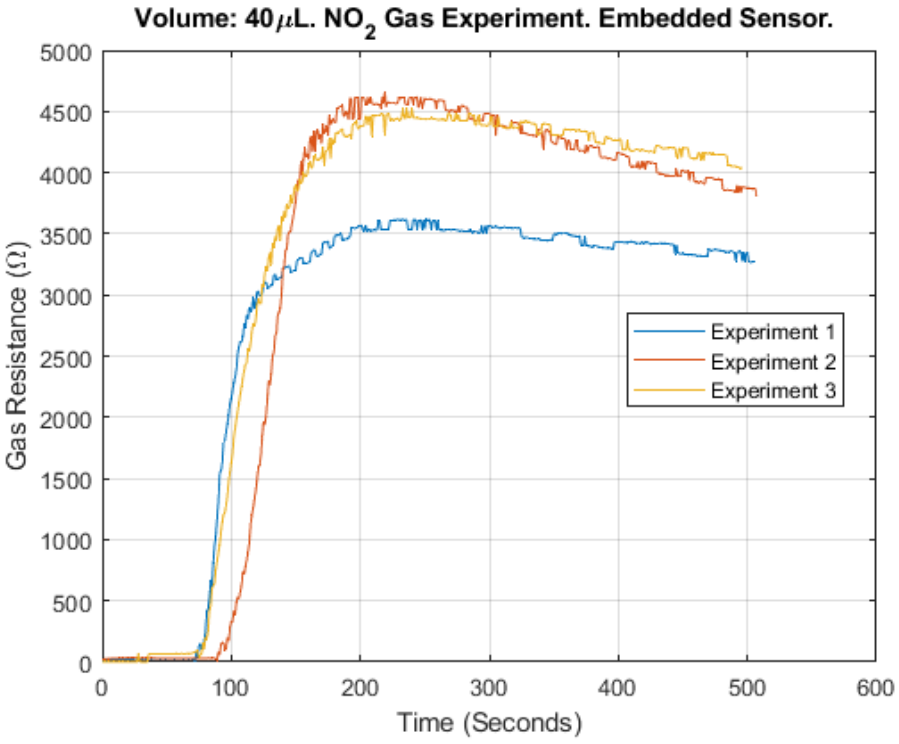

Figure 4.30. Experimental gas resistance values after using a HNO_3 (aq) volume of 40 μl.

Table 4.6. Maximum gas resistance values for the different utilized volumes of HNO_3. The present results are in ohms (Ω).

Experiment	Volume: 10 μl	Volume: 20 μl	Volume: 40 μl
First	859.00	813.24	3,618.04
Second	884.60	1,186.90	4,658.50
Third	883.50	1,453.24	4,523.14
Average	**875.70**	**1,151.13**	**4,266.56**

Based on the previous results, the sensor was sensitive enough for detecting the change in the gas resistance under different polluted environments. Indeed, its sensitivity was appropriate for measuring the air quality of the surroundings, specifically, when these ones might be polluted by different hazardous gases. However, one important aspect to mention is that even though the sensor was capable of detecting the change for the gas resistance, its selectivity for targeted gases needs to be further investigated. In this regard, the present sensor is not only capable of measuring the gas resistance produced by the generation of the NO_2 gas, but also for other different gases. Consequently, the present sensor needs to be upgraded in order to be more selective for a specific targeted gas. Moreover, this sensor is not capable of giving any concentration of the polluted gas in the environment, for this reason, stoichiometric calculations were done in order to know the concentration of the generated NO_2 gas. These concentrations in ppm are depicted in Table 4.7. In particular, Figure 4.31 provides the user with a proper approach for knowing the concentration of the NO_2 gas in the environment with a given gas resistance value.

Table 4.7. Generation of NO_2 gas for the different utilized volumes of HNO_3.

Volume (μl)	Generation of NO_2 (g) (ppm)	Average Gas Resistance (Ω)
10	2,057.38	875.70
20	4,106.30	1,151.13
40	8,179.020	4,266.56

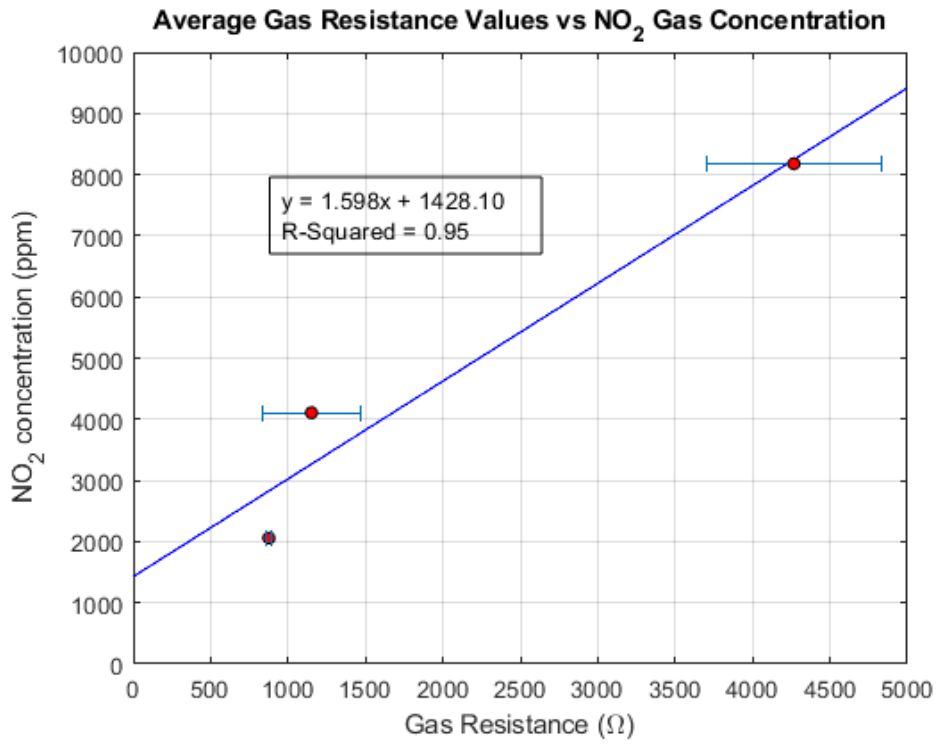

Figure 4.31. The generated concentration in ppm for the NO_2 gas can be calculated using this graph by knowing a gas resistance value.

Based on these results, the gas sensor developed by alumni at Youngstown State University represents an alternative as a wearable sensor capable of detecting different hazardous gases in the environment. Even though proper changes need to be applied to this device in order to make it more selective to targeted gases, the sensor is capable of providing the user with real-time data acquisition for the quality of the air while the user is wearing it in a daily basis. Therefore, its application in the area of wearable sensors represents a promising one.

Conclusions

In the present work, the electrical and mechanical properties were investigated for a 3D printed flexible electronic platform capable of withstand mechanical fatigue for prolonged periods of time. This flexible platform with embedded electronics could maintain the electrical resistance as well as the electrical voltage while the bending movement was being carried out. Moreover, the adhesion strength between the flexible substrate and the printed stretchable conductor was examined due to the importance that this interaction represents for the development of flexible electronics. These experiments were really important in order to evaluate the potential application of this platform using the 3D printing technologies, stereolithography (STL) and Direct ink writing (DIW), in the field of flexible electronics.

Particularly, the implementation of this 3D printed flexible electronic platform for the fabrication of wearable sensors holds a promising approach. Based on the results of this work, the embedded system represented the best configuration for withstanding the bending fatigue while the electrical resistance remained constant through all the experiment. In this case, the maximum electrical resistance value for the best experiment was 1.80 Ω while the minimum was 0.60 Ω which is a small change after 22.5 h of bending fatigue without stopping. Despite the results that were presented by the embedded system, the not-embedded system showed reasonable results since non of the experiments showed a total loss of electrical resistance. However, a difference for the electrical resistance values between these two systems was easily appreciated where the not-embedded system showed the biggest ones.

As previously mentioned, this difference was related with the added resin layer for the embedded system that protected the stretchable conductor from the creation and propagation of cracks or fractures that eventually lead to the increase or total loss of the electrical resistance. Once the best system was selected, this one was used for the addition of electronics components onto the platform. For this experiment, the change in the voltage was analyzed under bending mechanical fatigue for the same period of time which was 22.5 h. The final purpose of this one was the evaluation of the voltage for an embedded circuit under this mechanical fatigue. In this case, the voltage of the 3D printed circuit remained constant despite the mechanical conditions that it was exposed to. It is important to mention that the applications of wearable sensors require consistent operation under diverse conditions of mechanics, temperature, and hydration. In this sense, for the mechanics conditions, the type of experiments that were done in this work could assess this type of circumstances. Having this said, the voltage of these experiments did not vary that much, being the maximum and minimum values, 3.66 and 2.62 volts, respectively. Moreover, regarding the results for the adhesion strength between the flexible platform and the stretchable conductor, these ones showed a good adhesion interaction between these two since the results of the change in the height for the conductive printed line did not represent a significant difference. For instance, the maximum difference was 0.111 mm for the first experiment and the force that is needed in order to remove the stretchable conductor from the platform has to be more than 6 N.

Lastly, the experiments regarding the detection of the NO_2 gas using the sensor developed by alumni at Youngstown State University showed that this sensor is capable of being utilized as a wearable gas sensor. Particularly, this sensor has the capacity to offer the user with real-time data collection regarding the air quality when it is being worn on a daily basis. Nevertheless, it is crucial to acknowledge that while the sensor demonstrated the ability to detect variations in gas resistance, additional research needs to be done to determine its selectivity towards specific gases. In this context, the current sensor exhibits the ability to measure the gas resistance resulting from the production of NO_2 gas, as well as its applicability to many other gases.

References

[1] Alejandro H. Espera, John Ryan C. Dizon, Qiyi Chen, and Rigoberto C. Advincula. 3d-printing and advanced manufacturing for electronics. *Progress in Additive Manufacturing*, 4:245–267, 9 2019.

[2] Hui Yang, Wan Ru Leow, and Xiaodong Chen. 3d printing of flexible electronic devices. *Small Methods*, 2, 1 2018.

[3] Meng Gao, Lihong Li, and Yanlin Song. Inkjet printing wearable electronic devices. *Journal of Materials Chemistry C*, 5:2971–2993, 2017.

[4] Yan Niu, Hao Liu, Rongyan He, Zedong Li, Hui Ren, Bin Gao, Hui Guo, Guy M. Genin, and Feng Xu. The new generation of soft and wearable electronics for health monitoring in varying environment: From normal to extreme conditions. *Materials Today*, 41:219–242, 12 2020.

[5] Yuhao Liu, Matt Pharr, and Giovanni Antonio Salvatore. Lab-on-skin: A review of flexible and stretchable electronics for wearable health monitoring. *ACS Nano*, 11:9614–9635, 10 2017.

[6] Adriano Ambrosi and Martin Pumera. 3d-printing technologies for electrochemical applications. *Chemical Society Reviews*, 45:2740–2755, 5 2016.

[7] Minjeong Ha, Seongdong Lim, and Hyunhyub Ko. Wearable and flexible sensors for user-interactive health-monitoring devices. *Journal of Materials Chemistry B*, 6:4043–4064, 2018.

[8] Bo Peng, Fengnian Zhao, Jianfeng Ping, and Yibin Ying. Recent advances in nanomaterial-enabled wearable sensors: Material synthesis, sensor design, and personal health monitoring. *Small*, 16, 11 2020.

[9] Blake Herren, Mrinal C. Saha, M. Cengiz Altan, and Yingtao Liu. Development of ultrastretchable and skin attachable nanocomposites for human motion monitoring via embedded 3d printing. *Composites Part B: Engineering*, 200, 11 2020.

[10] Nadtinan Promphet, Sarute Ummartyotin, Wittaya Ngeontae, Pumidech Puthongkham, and Nadnudda Rodthongkum. Non-invasive wearable chemical sensors in real-life applications. *Analytica Chimica Acta*, 1179, 9 2021.

[11] C Hanumanth Rao, Kothuru Avinash, BKSVL Varaprasad, and Sanket Goel. A review on printed electronics with digital 3d printing: fabrication techniques, materials, challenges and future opportunities. *Journal of Electronic Materials*, 51(6):2747–2765, 2022.

[12] Qijin Huang and Yong Zhu. Printing conductive nanomaterials for flexible and stretchable electronics: A review of materials, processes, and applications. *Advanced Materials Technologies*, 4(5):1800546, 2019.

[13] Esa Kunnari, Jani Valkama, Marika Keskinen, and Pauliina Mansikkamäki. Environmental evaluation of new technology: printed electronics case study. *Journal of Cleaner Production*, 17(9):791–799, 2009.

[14] Rokas Šakalys, Bita Soltan Mohammadlou, and Ramesh Raghavendra. Fabrication of multi-material electronic components applying non-contact printing technologies: a review. *Results in Engineering*, page 100578, 2022.

[15] Yue Dong, Chao Bao, and Woo Soo Kim. Sustainable additive manufacturing of printed circuit boards. *Joule*, 2(4):579–582, 2018.

[16] Tong Ge, Jia Zhou, Yang Kang, and Joseph S Chang. A fully-additive printed electronics process with very-low process variations (bent and unbent substrates) and pdk. In *2017 IEEE International Symposium on Circuits and Systems (ISCAS)*, pages 1–4. IEEE, 2017.

[17] Eric Macdonald, Rudy Salas, David Espalin, Mireya Perez, Efrain Aguilera, Dan Muse, and Ryan B Wicker. 3d printing for the rapid prototyping of structural electronics. *IEEE access*, 2:234–242, 2014.

[18] Saleem Khan, Leandro Lorenzelli, and Ravinder S Dahiya. Technologies for printing sensors and electronics over large flexible substrates: A review. *IEEE Sensors Journal*, 15(6):3164–3185, 2014.

[19] Serena Laschi, Ilaria Palchetti, and Marco Mascini. Gold-based screen-printed sensor for detection of trace lead. *Sensors and Actuators B: Chemical*, 114(1):460–465, 2006.

[20] Hanna M Haverinen, Risto A Myllyla, and Ghassan E Jabbour. Inkjet printed rgb quantum dot-hybrid led. *Journal of display technology*, 6(3):87–89, 2010.

[21] Chao Wu and Xiao Feng Jin. Optimization design and fabrication of annular field emitter for field emission display panel. *Key Engineering Materials*, 467:1520–1523, 2011.

[22] Pälvi Kopola, Tom Aernouts, S Guillerez, H Jin, Markus Tuomikoski, Arto Maaninen, and Jukka Hast. High efficient plastic solar cells fabricated with a high-throughput gravure printing method. *Solar Energy Materials and Solar Cells*, 94(10):1673–1680, 2010.

[23] Yuji Gao, Hiroki Ota, Ethan W Schaler, Kevin Chen, Allan Zhao, Wei Gao, Hossain M Fahad, Yonggang Leng, Anzong Zheng, Furui Xiong, et al. Wearable microfluidic diaphragm pressure sensor for health and tactile touch monitoring. *Advanced Materials*, 29(39):1701985, 2017.

[24] Xuan Cao, Haitian Chen, Xiaofei Gu, Bilu Liu, Wenli Wang, Yu Cao, Fanqi Wu, and Chongwu Zhou. Screen printing as a scalable and low-cost approach for rigid and flexible thin-film transistors using separated carbon nanotubes. *ACS nano*, 8(12):12769–12776, 2014.

[25] Hong Hong, Hu Jiyong, Kyoung-Sik Moon, Xiong Yan, and Ching-ping Wong. Rheological properties and screen printability of uv curable conductive ink for flexible and washable e-textiles. *Journal of Materials Science & Technology*, 67:145–155, 2021.

[26] Ghassan E Jabbour, Rachel Radspinner, and Nasser Peyghambarian. Screen printing for the fabrication of organic light-emitting devices. *IEEE Journal of selected topics in quantum electronics*, 7(5):769–773, 2001.

[27] Roar R Søndergaard, Markus Hösel, and Frederik C Krebs. Roll-to-roll fabrication of large area functional organic materials. *Journal of Polymer Science Part B: Polymer Physics*, 51(1):16–34, 2013.

[28] Saleem Khan, Shawkat Ali, and Amine Bermak. Smart manufacturing technologies for printed electronics. *Hybrid Nanomaterials-Flexible Electronics Materials*, 18, 2019.

[29] Taewoong Lim, Jungkeun Yang, Seungmi Lee, Jaewon Chung, and Daehie Hong. Deposit pattern of inkjet printed pico-liter droplet. *International Journal of Precision Engineering and Manufacturing*, 13(827–833), 2012.

[30] Shweta Agarwala, Guo Liang Goh, and Wai Yee Yeong. *Optimizing aerosol jet printing process of silver ink for printed electronics*, volume 191. IOP Conference Series: Materials Science and Engineering, 2017.

[31] David Jahn, Ralph Eckstein, Lorenz Maximilian Schneider, Norman Born, Gerardo Hernandez-Sosa, Jan C Balzer, Ibraheem Al-Naib, Uli Lemmer, and Martin Koch. Digital aerosol jet printing for the fabrication of terahertz metamaterials. *Advanced Materials Technologies*, 3(2):1700236, 2018.

[32] Jaewook Nam. *Automatic Generation of Process Operating Window-Tracking Vortex Birth Inside Coating Flow*, volume 33. Elsevier, 2014.

[33] Doojin Vak, Kyeongil Hwang, Andrew Faulks, Yen-Sook Jung, Noel Clark, Dong-Yu Kim, Gerard J Wilson, and Scott E Watkins. 3d printer based slot-die coater as a lab-to-fab translation tool for solution-processed solar cells. *Advanced Energy Materials*, 5(4):1401539, 2015.

[34] Rahul Patidar, Daniel Burkitt, Katherine Hooper, David Richards, and Trystan Watson. Slot-die coating of perovskite solar cells: An overview. *Materials Today Communications*, 22:100808, 2020.

[35] Andreas Sandström, Henrik F Dam, Frederik C Krebs, and Ludvig Edman. Ambient fabrication of flexible and large-area organic light-emitting devices using slot-die coating. *Nature communications*, 3(1):1002, 2012.

[36] Daniel Corzo, Guillermo Tostado-Blázquez, and Derya Baran. Flexible electronics: status, challenges and opportunities. *Frontiers in Electronics*, 1:594003, 2020.

[37] Arokia Nathan, Arman Ahnood, Matthew T Cole, Sungsik Lee, Yuji Suzuki, Pritesh Hiralal, Francesco Bonaccorso, Tawfique Hasan, Luis Garcia-Gancedo, Andriy Dyadyusha, et al. Flexible electronics: the next ubiquitous platform. *Proceedings of the IEEE*, 100(Special Centennial Issue):1486–1517, 2012.

[38] Xuewen Wang, Zheng Liu, and Ting Zhang. Flexible sensing electronics for wearable/attachable health monitoring. *Small*, 13(25):1602790, 2017.

[39] Wei Gao, Sam Emaminejad, Hnin Yin Yin Nyein, Samyuktha Challa, Kevin Chen, Austin Peck, Hossain M. Fahad, Hiroki Ota, Hiroshi Shiraki, Daisuke Kiriya, Der Hsien Lien, George A. Brooks, Ronald W. Davis, and Ali Javey. Fully integrated wearable sensor arrays for multiplexed in situ perspiration analysis. *Nature*, 529:509–514, 1 2016.

[40] Joseph T Muth, Daniel M Vogt, Ryan L Truby, Yiğit Mengüç, David B Kolesky, Robert J Wood, and Jennifer A Lewis. Embedded 3d printing of strain sensors within highly stretchable elastomers. *Advanced materials*, 26(36):6307–6312, 2014.

[41] Abhinav M Gaikwad, Gregory L Whiting, Daniel A Steingart, and Ana Claudia Arias. Highly flexible, printed alkaline batteries based on mesh-embedded electrodes. *Advanced materials*, 23(29):3251–3255, 2011.

[42] J Torkel Wallmark and Hardwick Johnson. Field-effect transistors: physics, technology and applications. *(No Title)*, 1966.

[43] Nurdan Demirci Sankir. *Flexible electronics: materials and device fabrication*. Virginia Polytechnic Institute and State University, 2005.

[44] Daniel R Gamota, Paul Brazis, Krishna Kalyanasundaram, and Jie Zhang. *Printed organic and molecular electronics*. Springer Science & Business Media, 2013.

[45] Dae-Hyeong Kim, Roozbeh Ghaffari, Nanshu Lu, and John A Rogers. Flexible and stretchable electronics for biointegrated devices. *Annual review of biomedical engineering*, 14:113–128, 2012.

[46] Jin Young Oh, Simon Rondeau-Gagné, Yu-Cheng Chiu, Alex Chortos, Franziska Lissel, Ging-Ji Nathan Wang, Bob C Schroeder, Tadanori Kurosawa, Jeffrey Lopez, Toru Katsumata, et al. Intrinsically stretchable and healable semiconducting polymer for organic transistors. *Nature*, 539(7629):411–415, 2016.

[47] Chunfeng Wang, Chonghe Wang, Zhenlong Huang, and Sheng Xu. Materials and structures toward soft electronics. *Advanced Materials*, 30, 12 2018.

[48] Sangkil Kim. Inkjet-printed electronics on paper for rf identification (rfid) and sensing. *Electronics*, 9(10):1636, 2020.

[49] Stergios Logothetidis. Flexible organic electronic devices: Materials, process and applications. *Materials Science and Engineering: B*, 152(1-3):96–104, 2008.

[50] Joong Tark Han, Bo Hwa Jeong, Seon Hee Seo, Kwang Chul Roh, Sumi Kim, Sua Choi, Jong Seok Woo, Ho Young Kim, Jeong In Jang, Du-Chul Shin, et al. Dispersant-free conducting pastes for flexible and printed nanocarbon electrodes. *Nature communications*, 4(1):2491, 2013.

[51] Rikio Yokota, Syougo Yamamoto, Shoichiro Yano, Takashi Sawaguchi, Masatoshi Hasegawa, Hiroaki Yamaguchi, Hideki Ozawa, and Ryouichi Sato. Molecular design of heat resistant polyimides having excellent processability and high glass transition temperature. *High Performance Polymers*, 13(2):S61–S72, 2001.

[52] Su Yang, Su Liu, Xujiao Ding, Bo Zhu, Jidong Shi, Bao Yang, Shirui Liu, Wei Chen, and Xiaoming Tao. Permeable and washable electronics based on polyamide fibrous membrane for wearable applications. *Composites Science and Technology*, 207:108729, 2021.

[53] Kenji Nomura, Hiromichi Ohta, Akihiro Takagi, Toshio Kamiya, Masahiro Hirano, and Hideo Hosono. Room-temperature fabrication of transparent flexible thin-film transistors using amorphous oxide semiconductors. *nature*, 432(7016):488–492, 2004.

[54] Stefan CB Mannsfeld, Benjamin CK Tee, Randall M Stoltenberg, Christopher V HH Chen, Soumendra Barman, Beinn VO Muir, Anatoliy N Sokolov, Colin Reese, and Zhenan Bao. Highly sensitive flexible pressure sensors with microstructured rubber dielectric layers. *Nature materials*, 9(10):859–864, 2010.

[55] Jianwei Wu, Ridong Wang, Haixia Yu, Guijun Li, Kexin Xu, Norman C Tien, Robert C Roberts, and Dachao Li. Inkjet-printed microelectrodes on pdms as biosensors for functionalized microfluidic systems. *Lab on a Chip*, 15(3):690–695, 2015.

[56] Mauro Serpelloni, Edoardo Cantù, Michela Borghetti, and Emilio Sardini. Printed smart devices on cellulose-based materials by means of aerosol-jet printing and photonic curing. *Sensors*, 20(3):841, 2020.

[57] Liisa Hakola, Elina Jansson, Romain Futsch, Tuomas Happonen, Victor Thenot, Gael Depres, Aline Rougier, and Maria Smolander. Sustainable roll-to-roll manufactured multi-layer smart label. *The International Journal of Advanced Manufacturing Technology*, 117(9-10):2921–2934, 2021.

[58] Ahmed Barhoum, Pieter Samyn, Thomas Öhlund, and Alain Dufresne. Review of recent research on flexible multifunctional nanopapers. *Nanoscale*, 9(40):15181–15205, 2017.

[59] Wei Wu. Inorganic nanomaterials for printed electronics: a review. *Nanoscale*, 9(22):7342–7372, 2017.

[60] Tian Carey, Adrees Arbab, Luca Anzi, Helen Bristow, Fei Hui, Sivasambu Bohm, Gwenhivir Wyatt-Moon, Andrew Flewitt, Andrew Wadsworth, Nicola Gasparini, et al. Inkjet printed circuits with 2d semiconductor inks for high-performance electronics. *Advanced Electronic Materials*, 7(7):2100112, 2021.

[61] Jolke Perelaer, Patrick J Smith, Dario Mager, Daniel Soltman, Steven K Volkman, Vivek Subramanian, Jan G Korvink, and Ulrich S Schubert. Printed electronics: the challenges involved in printing devices, interconnects, and contacts based on inorganic materials. *Journal of Materials Chemistry*, 20(39):8446–8453, 2010.

[62] Menglu Li, Yongzhi Wu, Liang Zhang, Hualei Wo, Shuyi Huang, Wei Li, Xiangyu Zeng, Qikai Ye, Tianbai Xu, Jikui Luo, et al. Liquid metal-based electrical interconnects and interfaces with excellent stability and reliability for flexible electronics. *Nanoscale*, 11(12):5441–5449, 2019.

[63] Wei Gao, Hiroki Ota, Daisuke Kiriya, Kuniharu Takei, and Ali Javey. Flexible electronics toward wearable sensing. *Accounts of chemical research*, 52(3):523–533, 2019.

[64] KD Harris, AL Elias, and H-J Chung. Flexible electronics under strain: a review of mechanical characterization and durability enhancement strategies. *Journal of materials science*, 51:2771–2805, 2016.

[65] Shu Gong, Lim Wei Yap, Bowen Zhu, and Wenlong Cheng. Multiscale soft–hard interface design for flexible hybrid electronics. *Advanced Materials*, 32, 4 2020.

[66] Martin Kaltenbrunner, Tsuyoshi Sekitani, Jonathan Reeder, Tomoyuki Yokota, Kazunori Kuribara, Takeyoshi Tokuhara, Michael Drack, Reinhard Schwödiauer, Ingrid Graz, Simona Bauer-Gogonea, Siegfried Bauer, and Takao Someya. An ultra-lightweight design for imperceptible plastic electronics. *Nature*, 499:458–463, 2013.

[67] Shweta Agarwala, Guo Liang Goh, Yee Ling Yap, Guo Dong Goh, Hao Yu, Wai Yee Yeong, and Tuan Tran. Development of bendable strain sensor

with embedded microchannels using 3d printing. *Sensors and Actuators A: Physical*, 263:593–599, 2017.

[68] Changyong Liu, Ninggui Huang, Feng Xu, Junda Tong, Zhangwei Chen, Xuchun Gui, Yuelong Fu, and Changshi Lao. 3d printing technologies for flexible tactile sensors toward wearable electronics and electronic skin. *Polymers*, 10(6):629, 2018.

[69] Md Taibur Rahman, Arya Rahimi, Subhanshu Gupta, and Rahul Panat. Microscale additive manufacturing and modeling of interdigitated capacitive touch sensors. *Sensors and Actuators A: Physical*, 248:94–103, 2016.

[70] Tao Han, Sudip Kundu, Anindya Nag, and Yongzhao Xu. 3d printed sensors for biomedical applications: A review. *Sensors (Switzerland)*, 19, 4 2019.

[71] Josef F Christ, Nahal Aliheidari, Amir Ameli, and Petra Pötschke. 3d printed highly elastic strain sensors of multiwalled carbon nanotube/thermoplastic polyurethane nanocomposites. *Materials & Design*, 131:394–401, 2017.

[72] ASTM Committee F42 on Additive Manufacturing Technologies and ASTM Committee F42 on Additive Manufacturing Technologies. Subcommittee F42. 91 on Terminology. *Standard terminology for additive manufacturing technologies*. Astm International, 2012.

[73] Mohammad Reza Khosravani and Tamara Reinicke. 3d-printed sensors: Current progress and future challenges. *Sensors and Actuators, A: Physical*, 305, 4 2020.

[74] Changyong Liu, Ninggui Huang, Feng Xu, Junda Tong, Zhangwei Chen, Xuchun Gui, Yuelong Fu, and Changshi Lao. 3d printing technologies for flexible tactile sensors toward wearable electronics and electronic skin. *Polymers*, 10, 6 2018.

[75] Yuanyuan Xu, Xiaoyue Wu, Xiao Guo, Bin Kong, Min Zhang, Xiang Qian, Shengli Mi, and Wei Sun. The boom in 3d-printed sensor technology. *Sensors (Basel, Switzerland)*, 17, 5 2017.

[76] Ashish Kalkal, Sumit Kumar, Pramod Kumar, Rangadhar Pradhan, Magnus Willander, Gopinath Packirisamy, Saurabh Kumar, and Bansi Dhar Malhotra. Recent advances in 3d printing technologies for wearable (bio)sensors. *Additive Manufacturing*, 46, 10 2021.

[77] Hua Gong, Bryce P Bickham, Adam T Woolley, and Gregory P Nordin. Custom 3d printer and resin for 18 μm$\times$ 20 μm microfluidic flow channels. *Lab on a Chip*, 17(17):2899–2909, 2017.

[78] Mahshid Padash, Christian Enz, and Sandro Carrara. Microfluidics by additive manufacturing for wearable biosensors: A review. *Sensors*, 20(15):4236, 2020.

[79] Nabeel Ahmad, P Gopinath, Alexandr Vinogradov, et al. 3d printing in medicine: Current challenges and potential applications. In *3D Printing Technology in Nanomedicine*, pages 1–22. 2019.

[80] Jun Hyuk Song, Young-Tae Kim, Sunghwan Cho, Woo-Jin Song, Sungmin Moon, Chan-Gyung Park, Soojin Park, Jae Min Myoung, and Unyong Jeong. Surface-embedded stretchable electrodes by direct printing and their uses to fabricate ultrathin vibration sensors and circuits for 3d structures. *Advanced materials*, 29(43):1702625, 2017.

[81] Peiran Wei, Houming Leng, Qiyi Chen, Rigoberto C Advincula, and Emily B Pentzer. Reprocessable 3d-printed conductive elastomeric composite foams for strain and gas sensing. *ACS Applied Polymer Materials*, 1(4):885–892, 2019.

[82] Yubai Zhang, Ge Shi, Jiadong Qin, Sean E Lowe, Shanqing Zhang, Huijun Zhao, and Yu Lin Zhong. Recent progress of direct ink writing of electronic components for advanced wearable devices. *ACS Applied Electronic Materials*, 1(9):1718–1734, 2019.

[83] Swetha Chandrasekaran, Bin Yao, Tianyu Liu, Wang Xiao, Yu Song, Fang Qian, Cheng Zhu, Eric B Duoss, Christopher M Spadaccini, Yat Li, et al. Direct ink writing of organic and carbon aerogels. *Materials Horizons*, 5(6):1166–1175, 2018.

[84] Jie Dai, Osarenkhoe Ogbeide, Nasiruddin Macadam, Qian Sun, Wenbei Yu, Yu Li, Bao-Lian Su, Tawfique Hasan, Xiao Huang, and Wei Huang. Printed gas sensors. *Chemical Society Reviews*, 49(6):1756–1789, 2020.

[85] Alexander Kamyshny and Shlomo Magdassi. Conductive nanomaterials for 2d and 3d printed flexible electronics. *Chemical Society Reviews*, 48(6):1712–1740, 2019.

[86] Wenwen Hu, Liangtian Wan, Yingying Jian, Cong Ren, Ke Jin, Xinghua Su, Xiaoxia Bai, Hossam Haick, Mingshui Yao, and Weiwei Wu. Electronic noses: from advanced materials to sensors aided with data processing. *Advanced Materials Technologies*, 4(2):1800488, 2019.

[87] Yuji Gao, Longteng Yu, Joo Chuan Yeo, and Chwee Teck Lim. Flexible hybrid sensors for health monitoring: materials and mechanisms to render wearability. *Advanced Materials*, 32(15):1902133, 2020.

[88] Cheng Zhou, Nanqing Shi, Xue Jiang, Mingrui Chen, Jinlei Jiang, Youbin Zheng, Weiwei Wu, Daxiang Cui, Hossam Haick, and Ning Tang. Techniques for wearable gas sensors fabrication. *Sensors and Actuators B: Chemical*, 353:131133, 2022.

[89] Zheng Meng, Robert M Stolz, Lukasz Mendecki, and Katherine A Mirica. Electrically-transduced chemical sensors based on two-dimensional nanomaterials. *Chemical reviews*, 119(1):478–598, 2019.

[90] Roberto Paolesse, Sara Nardis, Donato Monti, Manuela Stefanelli, and Corrado Di Natale. Porphyrinoids for chemical sensor applications. *Chemical reviews*, 117(4):2517–2583, 2017.

[91] Eric Bakker and Martin Telting-Diaz. Electrochemical sensors. *Analytical chemistry*, 74(12):2781–2800, 2002.

[92] Sang Won Lee, Wonseok Lee, Yoochan Hong, Gyudo Lee, and Dae Sung Yoon. Recent advances in carbon material-based no2 gas sensors. *Sensors and Actuators B: Chemical*, 255(1788–1804), 2018.

[93] Ting Wang, Yunlong Guo, Pengbo Wan, Han Zhang, Xiaodong Chen, and Xiaoming Sun. Flexible transparent electronic gas sensors. *Small*, 12(28):3748–3756, 2016.

[94] Xinran Su, Ramadan Borayek, Xinwei Li, Tun Seng Herng, Dan Tian, Gwendolyn Jia Hao Lim, Yanqing Wang, Jishan Wu, and Jun Ding. Integrated wearable sensors with bending/stretching selectivity and extremely enhanced sensitivity derived from agarose-based ionic conductor and its 3d-shaping. *Chemical Engineering Journal*, 389:124503, 2020.

[95] Vimanyu Beedasy and Patrick J. Smith. Printed electronics as prepared by inkjet printing. *Materials*, 13, 2 2020.

[96] ASTM ASTM. D3359-17 standard test methods for rating adhesion by tape test. *West Conshohocken, PA: ASTM International*, 2017.

Appendix

A.1 Stoichiometric Calculations for the Generation of the NO_2 gas

In order to calculate the ppm of the NO_2 gas generated, the following calculations were made. Firstly, the total moles of air were calculated using the formula of the ideal gases while considering the volume of the vacuum desiccator which was 2.094 liters. Hence, we have:

$$n_{air} = \frac{P \cdot V}{R \cdot T} = \frac{(1atm) \cdot (2.094l)}{0.08205 \frac{l \cdot atm}{K \cdot mol} \cdot 298.15K} = 0.08560\, mol$$

Calculating the generated moles of NO_2 gas using the stoichiometric equation, and the different utilized volumes which were 10 μl, 20 μl, 40 μl, we have:

$$10\mu l\ HNO_3 \cdot \left(\frac{0.001ml}{1\mu l}\right) \cdot \left(\frac{1.40g}{1cm^3}\right) \cdot \left(\frac{1\, mol\ HNO_3}{63.012g\ HNO_3}\right) \cdot \left(\frac{2\, mol\ NO_2}{4\, mol\ HNO3}\right) = 111.09\, x\, 10^{-6}\, mol\ NO_2$$

$$20\mu l\ HNO_3 \cdot \left(\frac{0.001ml}{1\mu l}\right) \cdot \left(\frac{1.40g}{1cm^3}\right) \cdot \left(\frac{1\, mol\ HNO_3}{63.012g\ HNO_3}\right) \cdot \left(\frac{2\, mol\ NO_2}{4\, mol\ HNO3}\right) = 222.180\, x\, 10^{-6}\, mol\ NO_2$$

$$40\mu l\ HNO_3 \cdot \left(\frac{0.001ml}{1\mu l}\right) \cdot \left(\frac{1.40g}{1cm^3}\right) \cdot \left(\frac{1\,mol\,HNO_3}{63.012g\,HNO_3}\right) \cdot \left(\frac{2\,mol\,NO_2}{4\,mol\,HNO3}\right) = 444.360\,x\,10^{-6}\,mol\,NO_2$$

Calculating the concentration of NO_2 gas in ppm by taking into account the total number of moles of air already in the vacuum desiccator. For 10 μ l of HNO_3, the total concentration of NO_2 in ppm is:

$$111.09\ \text{x}\ 10^{-6}\,mol\,NO_2 \cdot \left(\frac{\frac{46.0055g}{1\,mol\,NO_2}}{0.08560\,mol\,air \cdot \frac{28.96g}{1\,mol\,air} + 111.09\,x\,10^{-6}\,mol\,NO_2 \cdot \frac{46.005g}{1\,mol\,NO_2}}\right) = 2,057.38\,ppm\,NO_2$$

Following the same procedure for the other utilized volumes which are 20 μl and 40 μl, we have:

$$222.180\ \text{x}\ 10^{-6}\,mol\,NO_2 \cdot \left(\frac{\frac{46.0055g}{1\,mol\,NO_2}}{0.08560\,mol\,air \cdot \frac{28.96g}{1\,mol\,air} + 222.180\,x\,10^{-6}\,mol\,NO_2 \cdot \frac{46.005g}{1\,mol\,NO_2}}\right) = 4,106.30\,ppm\,NO_2$$

$$444.360\ \text{x}\ 10^{-6}\,mol\,NO_2 \cdot \left(\frac{\frac{46.0055g}{1\,mol\,NO_2}}{0.08560\,mol\,air \cdot \frac{28.96g}{1\,mol\,air} + 444.360\,x\,10^{-6}\,mol\,NO_2 \cdot \frac{46.005g}{1\,mol\,NO_2}}\right) = 8,179.02\,ppm\,NO_2$$